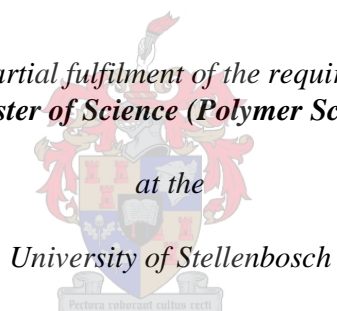


# Identification and characterization of additives in colourants by advanced analytical techniques

by

**Lebogang Jennifer Maku**

*Thesis presented in partial fulfilment of the requirements for the degree  
of **Master of Science (Polymer Science)***



Supervisor: Professor Harald Pasch

December 2015

## Declaration

### **Declaration**

By submitting this thesis electronically, I declare that the entirety of the work contained therein is my own, original work, that I am the sole author thereof (save to the extent explicitly otherwise stated), that reproduction and publication thereof by Stellenbosch University will not infringe any third party rights and that I have not previously in its entirety or in part submitted it for obtaining any qualification.

Lebogang Jennifer Maku

December 2015

Copyright © 2015 Stellenbosch University

All rights reserved

## Abstract

**Abstract**

Various types of anionic, non-ionic, cationic and zwitterionic additives are used in the coatings industry for the production of paints and colourants. These additives are added to enhance properties such as stabilization of pigment dispersions, wetting of pigments and improvement of open time and freeze/thaw stability. Very often the exact chemistry of these commercial additives is unknown and this is a limitation for new product developments. The identification and characterization of these multi-component polymeric materials continues to be a challenging task. This research presents the use of various advanced analytical techniques to identify and characterize commercial additives that are used in a multi-component colourant formulation. The focus of the present study is on additives that are based on poly(ethylene glycol) (PEG). The molar mass distribution of PEG-based additives was determined with liquid chromatography coupled to mass spectrometry (LC-MS) using solvent gradient elution and at critical conditions of adsorption (LCCC) of PEG. Using the combination of LC-MS, proton nuclear magnetic resonance spectroscopy ( $^1\text{H}$  NMR), pyrolysis gas chromatography (py-GC-MS) and Fourier transform infrared spectroscopy in attenuated total reflectance mode (FTIR-ATR), different additives were identified in terms of the number and type of polymer end groups. The efficiency of the extraction and identification protocol was demonstrated for a blend of additives in a colourant formulation.

## Opsomming

**Opsomming**

Verskeie tipes anioniese, nie-ioniese, kationiese en zwitterioniese bymiddels word gebruik in die bedekking nywerheid vir die vervaardiging van verwe en kleurmiddels. Hierdie bymiddels word bygevoeg om sekere eienskappe, soos die stabilisering van pigment dispersie, benatting van pigmente en die verbetering van ope tyd en vries/dooi stabiliteit te versterk. Dikwels is die presiese chemie van hierdie kommersiële bymiddels onbekend en het dit 'n beperking vir nuwe produk ontwikkeling tot gevolg. Die identifisering en karakterisering van hierdie meer-komponent polimeriese materiaal duur voort om 'n uitdagings te wees. Hierdie navorsingstudie stel voor die gebruik van verskeie tegnieke om kommersiële bymiddels te identifiseer en karakteriseer wat in meer-komponent kleurmiddel formulasies gebruik word. Die fokus is geplaas op bymiddels wat gebaseer is op poli(etileen glikol) (PEG). The molêre massa verdeling van PEG-gebaseerde bymiddels was bepaal met vloeistofchromatografie gekoppel tot massaspektrometrie (VC-MS) met die gebruik van oplosmiddel gradient eluasie en by kritiese toestande van adsorpsie (VCKT) van PEG. Deur die kombinasie van VC-MS, proton kern magnetiese resonansie spektroskopie ( $^1\text{H}$  KMR), pirolisegaschromatografie (pir-GC-MS) en Fourier-transformasie infrarooi spektroskopie in verswakking totale refleksie modus (FTIR-VTR), is verskillende bymiddels geïdentifiseer in terme van die hoeveelheid en tipe polimeer eindgroep teenwoordig. Die doeltreffendheid van die ekstrahering en identifisering protokol is gedemonstreer vir 'n mengsel van bymiddels in 'n kleurmiddel formulering.

## Acknowledgements

**Acknowledgements**

Firstly, I thank Dr. Siphilisiwe Ndlovu from Kansai Plascon for putting the idea of studying towards MSc in my head. I appreciate that you believed in me and convinced me that it was a wise decision. To Dr. Cor Beyers, Yolandé Inglis and Kobie Bisschoff, thank you so much for giving me the opportunity to work at the Research Centre and offering me a research project. Thank you to Kansai Plascon for the funding and a special gratitude goes to Carlos Costa for his support and approval of my bursary. I also thank Eugene Britz and Bobby Bhugwandin for the encouragement of furthering my studies.

To my supervisor Professor Harald Pasch, I am so grateful for your guidance and support throughout my research project. Due to your immense experience, I have acquired more skills and knowledge that I will apply throughout my career life.

Thank you to everyone at Kansai Plascon Research Centre who made a contribution to my studies. In particular, to Yolandé Inglis, I will never forget your continuous motivation and guidance throughout my project. You were always patient and understanding to share my frustrations and often emotional moments. Thank you to Kobie Bisschoff, Pieter Murray and Marehette Liprini for providing me with the additives and colourants as well as for sharing your knowledge. To Ashwell Makan and Webster Gova, I appreciate all the brainstorming and knowledge sharing sessions we had. They certainly helped me to have a broader mind-set of interpreting my results.

I thank Dr. Nadine Makan and Dr Khumo Maiko for helping me get in the right direction when I was once in the dark during my initial experimental runs. To Dr. Helen Pfukwa, thank you for all your guidance and assistance with NMR interpretations. I would like to express my gratitude to every past and present member of Prof. Pasch's postgraduate group for their contribution as well as Paul Reader for assistance with the NMR software.

From the Department of Chemistry and Polymer Science, I thank Erinda Cooper and Aneli Fourie for the administrative support as well as Jim Motshweni and Kevin Maart for providing chemicals for the experimental work. I also thank Dr. Jaco Brand and Mrs Elsa Malherbe for NMR analyses.

To my number one supporters: My mother Bonolo Maku and my best friend Refilwe Mothiba: I appreciate the love and encouragement you have given me. I also thank all my other friends and family for their incredible support.

Finally, I thank God for all the blessings in my life. I cherish every moment that You have given me and will always praise You.

## Table of contents

**Table of contents**

<b>Declaration.....</b>	<b>i</b>
<b>Abstract.....</b>	<b>ii</b>
<b>Opsomming.....</b>	<b>iii</b>
<b>Acknowledgements.....</b>	<b>iv</b>
<b>Table of contents .....</b>	<b>v</b>
<b>List of figures.....</b>	<b>viii</b>
<b>List of tables.....</b>	<b>xi</b>
<b>List of abbreviations .....</b>	<b>xii</b>
<b>List of symbols.....</b>	<b>xiv</b>
<b>Chapter 1 Introduction and objectives .....</b>	<b>1</b>
1.1. Introduction .....	1
1.1.1. Theoretical background of colourants.....	1
1.1.2. Identification and characterization of additives .....	2
1.2. Aims and objectives .....	3
1.2.1. Aim of the research .....	3
1.2.2. Objectives.....	3
1.3. Layout of the thesis .....	3
1.4. References .....	4
<b>Chapter 2 Theoretical and historical background.....</b>	<b>6</b>
2.1. Theory .....	6
2.1.1. Liquid Chromatography .....	6
2.1.2. Evaporative light scattering detector.....	8
2.1.3. Liquid chromatography coupled to mass spectrometry .....	9
2.1.4. Nuclear magnetic resonance spectroscopy .....	11
2.1.5. Pyrolysis gas chromatography .....	11
2.1.6. Fourier transform infrared spectroscopy .....	11
2.2. Literature review .....	11

## Table of contents

2.2.1. The types of chemical structures in additives .....	12
2.2.2. Identification and characterization of complex polymers .....	13
2.3. Conclusions .....	16
2.4. References .....	16
<b>Chapter 3 Experimental methodology .....</b>	<b>20</b>
3.1. Introduction .....	20
3.2. Experimental design .....	20
3.2.1. Materials.....	20
3.2.1. List of samples .....	20
3.2.2. Analytical techniques .....	22
<b>Chapter 4 Results and discussion .....</b>	<b>26</b>
4.1. Introduction .....	26
4.2. The search for critical conditions of adsorption for PEG.....	26
4.3. Characterization of the colourant additives.....	27
4.3.1. Characterization of type A additives.....	28
4.3.2. Characterization of type B additives .....	35
4.3.3. Characterization of type C additives .....	54
4.4. Identification of additives in colourants .....	88
4.5. Conclusions .....	93
4.6. References .....	96
<b>Chapter 5 Summary, conclusions and recommendations .....</b>	<b>97</b>
5.1. Summary .....	97
5.2. Overall conclusions .....	97
5.3. Recommendations for future work.....	99

## List of figures

**List of figures**

Figure 2.1: The modes of separation in liquid chromatography .....	7
Figure 2.2: Principles of the ELS detection system. ....	9
Figure 2.3: Schematics of the API-ES ion source.....	10
Figure 4.1 Plot of log $M_p$ versus retention time of PEG standards at various methanol/water (v/v) mobile phase compositions. ....	27
Figure 4.2: LC-ELSD (A) and positive scan TIC (B) of additive A1.....	28
Figure 4.3: Positive scan mass spectrum of additive A1. ....	29
Figure 4.4: $^1\text{H}$ NMR spectrum of additive A1 in DMSO, 25°C and 600 MHz. ....	30
Figure 4.5: LC-ELSD (A) and positive TIC scan (B) of additive A2.....	32
Figure 4.6: Positive scan mass spectrum of additive A2. ....	33
Figure 4.7: $^1\text{H}$ NMR spectrum of additive A2 in DMSO, 25°C and 600 MHz. ....	33
Figure 4.8: Positive (A) and negative (B) TIC scans of additive B1 acquired at critical conditions of PEG. ....	36
Figure 4.9: Negative scan LC-MS of additive B1 for peak 1 (A) and alpha-D glucose (B). ....	37
Figure 4.10: Fragmentation pattern of glucose (A) and fructose (B) adapted from Taylor et al. ....	37
Figure 4.11: Negative scan LC-MS of additive B1 acquired for peak 3 (A) and peak 5 (B). ....	38
Figure 4.12: Negative scan LC-MS of additive B1 acquired for peak 8 (A) and peak 10 (B). ....	40
Figure 4.13: LC-ELSD (A) and positive TIC scan (B) of additive B1 acquired using a solvent gradient elution protocol.....	41
Figure 4.14: Positive scan LC-MS of additive B1 for peaks 12 (A) and 13 (B) acquired using a gradient elution protocol.....	42
Figure 4.15: Positive scan LC-MS of additive B1 for peak 14 acquired using a gradient elution protocol.....	42
Figure 4.16: Structures of PEG tridecyl ether phosphate (A), PEG tridecyl ether (B) and PEG monooleyl ether (C) detected in additive B1. ....	43
Figure 4.17: $^1\text{H}$ NMR spectrum of additive B1 in DMSO, 25°C, 600 MHz at 0 to 4 ppm. ....	44
Figure 4.18: $^1\text{H}$ NMR spectrum of additive B1 in DMSO, 25°C, 600 MHz at 4.5 to 8 ppm. ....	44
Figure 4.19: LC-ELSD (A), positive (B) and negative (C) TIC scans of additive B2. ....	46
Figure 4.20: Negative (A) and positive (B) LC-MS spectra of additive B2 for peak 1 and peak 2, respectively. ....	47
Figure 4.21: Fragmentation pattern of oligoglucoside, showing the molar mass of precursor ions. ....	47
Figure 4.22: $^1\text{H}$ NMR spectrum of additive B2 in DMSO, 25°C and 600 MHz at a chemical shift region of 0 to 4 ppm.....	48



## List of figures

Figure 4.23: $^1\text{H}$ NMR spectrum of additive B2 in DMSO, 25°C and 600 MHz at chemical shift region of 4.5 to 13 ppm.....	49
Figure 4.24: Structures of oligoglucoside (A) and PEG monomethyl ether (B) for additive B2. ....	49
Figure 4.25: LC-ELSD (A) and positive scan TIC (B) of additive B3. ....	51
Figure 4.26: Positive scan LC-MS of additive B3 using $2.5 \times 10^{-3}$ mol/L (A) and zero mol/L (B) ammonium formate.....	52
Figure 4.27: Structure of glycerol ethoxylate. ....	52
Figure 4.28: $^1\text{H}$ NMR of additive B3 in DMSO, 25°C and 600 MHz. ....	53
Figure 4.29: LC-UV at 230 nm (A) and positive scan TIC (B) of additive C1. ....	54
Figure 4.30: Positive scan LC-MS of additive C1 for peak 1.....	55
Figure 4.31: Positive scan LC-MS of additive C1 for peak 2 (A) and peak 3 (B).....	56
Figure 4.32: Positive scan LC-MS of additive C1 for peak 4 (A) and peak 6 (B).....	57
Figure 4.33: Structures of octylphenyl-, nonylphenyl- and decylphenyl-PEG.....	57
Figure 4.34: $^1\text{H}$ NMR spectrum of additive C1 in DMSO, 25°C and 600 MHz.....	58
Figure 4.35: LC-ELSD (A) and positive scan TIC (B) of additive C3 acquired at critical conditions. ....	59
Figure 4.36: Positive scan LC-MS of additive C3 for peak 1(A) and peak 2 (B).....	60
Figure 4.37: LC-ELSD (A) and positive scan TIC (B) of additive C3 acquired using a solvent gradient elution protocol.....	60
Figure 4.38: Positive scan TIC of additive C3 for peak 3(A) and peak 4 (B) acquired using a gradient elution protocol.....	61
Figure 4.39: Structures of glycerol ethoxylate (A) and PEG monooleyl ether (B). ....	61
Figure 4.40: $^1\text{H}$ NMR of additive C3 in DMSO, 25°C and 600 MHz at 0 to 3 ppm. ....	62
Figure 4.41: $^1\text{H}$ NMR of additive C3 in DMSO, 25°C and 600 MHz at 3 to 6.5 ppm. ....	63
Figure 4.42: Structure of butanoic acid, 4-amino, 4-oxosulfo disodium salt.....	64
Figure 4.43: LC-ELSD (A), positive (B) and negative (C) TIC scans of additive C4 at critical conditions of adsorption of PEG.....	65
Figure 4.44: Positive scan LC-MS for peaks 1 and 2 (A) and negative scan LC-MS for peak 2 (B) in additive C4.....	67
Figure 4.45: Positive (A) and negative (B) LC-MS of additive C4 for peak 3.....	68
Figure 4.46: Positive scan LC-MS of additive C4 for peak 4 (A) and peak 7 (B).....	69
Figure 4.47: Positive scan LC-MS of additive C4 for peak 8(A) and peak 10 (B).....	69
Figure 4.48: LC-ELSD (A) and positive scan TIC (B) of additive C4 acquired using a solvent gradient elution protocol.....	70

## List of figures

Figure 4.49: Structure of 9,12,15-octadecatrienoic acid detected by pyrolysis GC-MS. ....	70
Figure 4.50: $^1\text{H}$ NMR of additive C4 in DMSO, 25°C and 600 MHz. ....	71
Figure 4.51: $^{13}\text{C}$ NMR of additive C4 in DMSO, 25°C and 300 MHz. ....	71
Figure 4.52: FTIR-ATR spectrum of additive C4. ....	72
Figure 4.53: LC-UV at 230 nm (A) and negative scan TIC (B) of additive C5. ....	74
Figure 4.54: Negative scan TIC of additive C5 for peak 1(A) and peaks 2 to 10 (B). ....	74
Figure 4.55: FTIR-ATR spectrum of additive C5. ....	75
Figure 4.56: $^1\text{H}$ NMR of additive C5 in DMSO, 25°C and 600 MHz. ....	76
Figure 4.57: Positive (A) and negative (B) TIC scans of additive C6. ....	77
Figure 4.58: Positive scan LC-MS of additive C6 for peak 1 (A) and peak 2 (B). ....	77
Figure 4.59: Positive scan LC-MS of additive C6 for peak 3 (A) and peak 4 (B). ....	78
Figure 4.60: Positive scan LC-MS of additive C6 for peak 5. ....	79
Figure 4.61: Positive scan LC-MS of additive C6 for peak 6 (A) and peak 7 (B). ....	80
Figure 4.62: Negative scan LC-MS of additive C6. ....	80
Figure 4.63: FTIR-ATR of additive C6. ....	81
Figure 4.64: $^1\text{H}$ NMR of additive C6 in DMSO, 25°C and 600 MHz. ....	82
Figure 4.65: Positive (A) and negative (B) TIC scans of additive C7. ....	83
Figure 4.66: Positive LC-MS of additive C7 for peak 1 (A) and peak 2 (B). ....	84
Figure 4.67: Positive scan LC-MS of additive C7 for peaks 5(A) and 6 (B). ....	84
Figure 4.68: Examples of common zwitterionic surfactants. ....	85
Figure 4.69: Positive (A) and negative (B) LC-MS of additive C7 for peak 7. ....	85
Figure 4.70: $^1\text{H}$ NMR of additive C7 in DMSO, 25°C and 600 MHz at 0 to 3 ppm. ....	86
Figure 4.71: $^1\text{H}$ NMR of additive C7 in DMSO, 25°C and 600 MHz at 3 to 9 ppm. ....	87
Figure 4.72: $^{13}\text{C}$ NMR of additive C7 in DMSO, 25°C and 300 MHz. ....	87
Figure 4.73: FTIR-ATR spectrum of additive C7. ....	88
Figure 4.74: LC-UV chromatograms at 230 nm for additive C1 (A), extracted additives from the reddish-brown colourant (B) and additive C5 (C). ....	90
Figure 4.75: Negative scan LC-MS of peak 4 for the pure (A) and extracted (B) additive C5. ....	90
Figure 4.76: Positive scan LC-MS of peak 6 for the pure (A) and extracted (B) additive C1. ....	91
Figure 4.77: TIC scans of additive B3 (A), extracted additives of the bright yellow colourant (B) and additive C4 (C). ....	92
Figure 4.78: Positive scan LC-MS for the pure (A) and extracted (B) additive B3. ....	93
Figure 4.79: Positive scan LC-MS of peak 6 for the pure (A) and extracted (B) additive C4. ....	93

## List of tables

**List of tables**

Table 3.1: Molar masses of the PEG calibration standards. ....	21
Table 3.2 List of additives, showing the components as obtained from the suppliers.....	22
Table 4.1: $^1\text{H}$ NMR data and the calculated $M_n$ of additive A1.....	31
Table 4.2: $^1\text{H}$ NMR data and the calculated $M_n$ of additive A2.....	35
Table 4.3: Components of additive B1 for peaks 3 and 5.....	39
Table 4.4: Components of additive B1 for peaks 8 and 10.....	40
Table 4.5: Summary of the components of additive B1. ....	45
Table 4.6: Molar mass of additive B2 obtained from $^1\text{H}$ NMR and LC-MS.....	50
Table 4.7: LC-MS versus $^1\text{H}$ NMR molar masses of glycerol ethoxylate in additive B3. ....	53
Table 4.8: Experimental versus theoretical ammoniated molecular ions of additive C3. ....	62
Table 4.9: Components of additive C4, showing the molar mass of the most abundant ion.....	73
Table 4.10: Formulation of a reddish-brown colourant. ....	89
Table 4.11: Formulation of a bright yellow colourant. ....	91

## List of abbreviations

**List of abbreviations**

2D-LC	Two-dimensional liquid chromatography
APCI	Atmospheric pressure chemical ionization
API-ES	Atmospheric pressure ionization-electrospray
APPI	Atmospheric pressure photoionization
AES	Alcohol ether sulphate
AS	Alcohol sulphate
DAD	Diode array detector
DMSO	Dimethyl sulfoxide
ELSD	Evaporative light scattering detector
EO	Ethylene oxide
ESI	Electrospray ionization
ESI-MS	Electrospray ionization mass spectrometry
ESI-MS/MS	Electrospray ionization tandem mass spectrometry
FTIR-ATR	Fourier transform infrared spectroscopy in attenuated total reflectance mode
HPLC	High performance liquid chromatography
LAC	Liquid adsorption chromatography
LC	Liquid chromatography
LCCC	Liquid chromatography at critical conditions
LC-ELSD	Liquid chromatography coupled to evaporative light scattering detector
LC-MS	Liquid chromatography coupled to mass spectrometry
LEAC	Liquid exclusion-adsorption chromatography
MALDI-TOF	Matrix-assisted laser desorption/ionization time-of-flight
MMI	Multimode ionization
NMR	Nuclear magnetic resonance
PEG	Poly(ethylene glycol)
PEO	Poly(ethylene oxide)

List of abbreviations

PPG	Poly(propylene glycol)
Py-GC-MS	Pyrolysis gas chromatography coupled to mass spectrometry
SEC	Size exclusion chromatography
TIC	Total ion chromatogram
UV	Ultraviolet detector

## List of symbols

**List of symbols**

% v/v	Volume by volume percentage
$[M + z_i]^-$	Negatively charged adduct of parent ion M and anion $z_i$
$[M + z_i]^+$	Positively charged adduct of parent ion M and cation $z_i$
$[M-H]^-$	Negatively charged, deprotonated parent ion M
Å	Angstrom
$K_d$	Distribution coefficient
m/z	Mass-to-charge ratio
$M_e$	Combined molar mass of the end groups
$M_n$	Number-average molar mass
$M_o$	Molar mass of one repeat unit
$M_p$	Molar mass at peak maximum
$M_w$	Weight-average molar mass
D	Dispersity
R	Gas constant
T	Absolute temperature
$V_e$	Elution volume
$V_i$	Interstitial volume
$V_p$	Pore volume
$z_i$	Type of cation/anion
$\Delta G$	Change in Gibbs free energy
$\Delta H$	Change in enthalpy
$\Delta S$	Change in entropy

## Chapter 1

### Introduction and objectives

#### 1.1. Introduction

##### 1.1.1. Theoretical background of colourants

A colourant is defined as a highly concentrated pigment dispersion that is added to tint paint to a desired colour<sup>1</sup>. It is a multi-component polymeric system which consists of a solvent, organic or inorganic pigments, inorganic extenders, additives and other colourants. Water is typically used as primary solvent in a colourant, however, other solvents such as aliphatics, alcohols and aromatics may be used for solvent-based colourants. Pigments and extenders are added to provide properties such as opacity, colour and contrast ratio. The inorganic extenders are usually calcium carbonate, aluminium magnesium silicates and others. Typical organic and inorganic pigments are: phthalocyanine blue, ultra-marine blue, titanium dioxide, iron oxides, carbon black and many others.

Additives are components added in a colourant to enhance the end-use properties such as stability, viscosity, compatibility and anti-microbial abilities<sup>2</sup>. Examples of additives are glycols, humectants, wetting and dispersing agents, rheology modifiers, defoamers, biocides, emulsifiers and others. The types of glycols used in a colourant are mostly poly(ethylene glycol) (PEG) and poly(propylene glycol) (PPG). Humectants are added in colourants as moisturising agents to keep a colourant from drying out. The word *humectant* is derived from the latin term *humectare*, which means to moisten<sup>3</sup>. Hence, these additives are commonly polymers with hydrophilic end groups such as hydroxyls, amines or carboxyls<sup>4</sup>. The wetting and dispersing agents can be anionic, cationic, non-ionic or amphoteric surfactants. They are added as stabilisers for pigment dispersions. Rheology modifiers (thickeners) are added to adjust the viscosity of a colourant without significantly altering its properties. Defoamers are added to control the foam while biocides are added as anti-microbial agents for in-can preservation of a colourant. Other additives such as emulsifiers (e.g. soy lecithin) may be added to promote the dispersion of the pigments<sup>5</sup>.

Each of the aforementioned components of a colourant provides specific, important properties to the overall polymeric system. In order for colourant formulators to target that specific property and to enhance the optimum performance of the colourant, knowledge of the chemical composition of these components is crucial. However, in most cases commercial suppliers of the colourant raw materials do not provide the exact chemical composition of the components due to the company's confidentiality regulations. As a result of the lack of that knowledge, colourant formulators often evaluate the performance of a number of additives from various suppliers to determine the optimum

## Chapter 1: Introduction and objectives

combination in a formulation. This may be a disadvantage during the product development cycle as it is a lengthy and costly process. Methods are required to determine the chemical composition of each of the components of the colourant formulation. This can enable formulators to evaluate the additives' properties from a molecular level and optimise the colourant's performance.

Ideally, a complete characterization of all the components of a colourant is essential. However, due to the extensive work required to achieve this, the characterization of pigments, extenders, thickeners, biocides and defoamers were excluded from the project. The other additives such as glycols, humectants and wetting and dispersing agents were chosen as a focus of this research.

In most cases, the additives are a blend of two or more components which may be different in terms of complexity, molar mass and chemical nature. The characterization of each component in a multi-component polymeric system can be very challenging and complicated<sup>5,6</sup> and a suitable method is required. Successful analyses can depend on factors such as the number of components, the chemical composition, the concentration of each of the components, the method used for the separation as well the type, number, sensitivity, selectivity and detection limit of the analytical techniques<sup>7,8</sup>.

### 1.1.2. Identification and characterization of additives

The information acquired from the additive's suppliers showed that most of the glycols, humectants and wetting and dispersing agents utilised in the project were PEG-based. As a result, liquid chromatography (LC) and nuclear magnetic resonance (NMR) were chosen as powerful techniques for the separation, identification and characterization of these additives. Extensive research has been performed on the analyses of the complex PEG-based polymers. The separation modes such as size exclusion liquid chromatography (SEC)<sup>9,10</sup>, liquid adsorption chromatography (LAC)<sup>11,12</sup> and liquid chromatography at critical conditions (LCCC)<sup>13-15</sup> with ultraviolet (UV), mass spectrometer (MS) and evaporative light scattering detectors (ELSD) have been investigated. Other techniques such as matrix-assisted laser desorption/ionization time-of-flight (MALDI-TOF)<sup>8,16,17</sup> mass spectrometry have been used for the characterization of complex polymers. The coupling of liquid chromatography and NMR either online with one- or two-dimensional analysis<sup>18-20</sup> and pyrolysis gas chromatography coupled to mass spectrometry (py-GC-MS)<sup>21-23</sup> have also been reported.



## 1.2. Aims and objectives

### 1.2.1. Aim of the research

The aim of this research is to determine the molar mass distribution and chemical composition of the various PEG-based commercial additives that are used in water-based colourants. The project will also focus on the extraction of the additives from a colourant formulation followed by the identification and characterization, to determine the traceability of the additives to the original formulation.

### 1.2.2. Objectives

The objectives of this research are:

1. To find critical conditions of adsorption of PEG calibration standards using LC-ELSD and LC-UV.
2. To determine the number and type of end groups in various colourant additives using liquid chromatography with ELSD and UV detection.
3. To determine the chemical composition and molecular ion distribution of each additive by LC-MS.
4. To identify and characterize the polymer end groups using LC-MS, proton ( $^1\text{H}$ ) and carbon ( $^{13}\text{C}$ ) NMR.
5. To extract the additives from a known colourant sample for identification and comparison to the original formulation.

## 1.3. Layout of the thesis

### Chapter 1 – Introduction and objectives

This chapter outlines the theory of the composition of a colourant and the properties of each component. It also explains the challenges encountered in attempting to formulate colourants due to lack of knowledge on the chemical composition of the components. The types of analytical techniques used for the characterization of complex polymers are summarised and the objectives of the project are presented.

## **Chapter 2 – Theoretical and historical background**

The theoretical background on analytical techniques that will be utilised in the project is presented. A summary of the types of chemical structures encountered in commercial additives includes the different types of end groups that are common in surfactants in the coatings industry. The literature review section explores the research performed on the PEG-based polymers using various analytical techniques.

## **Chapter 3 – Experimental methodology**

In this chapter, the properties of the PEG calibration standards and the known chemical composition of the commercial additives are presented. The experimental conditions for the analyses of the additives by various techniques are also included.

## **Chapter 4 – Results and discussion**

PEG calibration standards with increasing molar masses are analysed by LC-ELSD using various mobile phase compositions to determine the critical conditions of adsorption of PEG. The identified critical point method as well as solvent gradient elution are applied to commercial additives using ELS and UV detectors to identify the type and number of end groups. The polymer repeat unit, average molar mass and the type of end groups are determined by LC-MS and NMR. The results obtained from other techniques such as Fourier transform infrared spectroscopy (FTIR) and pyrolysis-GC-MS are used for the confirmation of the end groups. The extraction of additives from two colourant formulations, followed by identification using LC-UV and LC-MS is also included.

## **Chapter 5 – Summary, conclusions and recommendations**

This chapter summarises the findings and conclusions from the preceding chapters. Recommendations for future work are presented.

### **1.4. References**

- (1) Encyclopedia of terms and definitions used in the surface coating industry <http://www.occa.org.za/paintopedia/> (accessed Jun 12, 2015).
- (2) Herrera, M.; Matuschek, G.; Kettrup, A. *J. Anal. Appl. Pyrolysis* **2003**, 70, 35–42.

## Chapter 1: Introduction and objectives

- (3) Lodén, M.; von Scheele, J.; Michelson, S. *Ski. Res. Technol.* **2013**, *19*, 438–445.
- (4) Elementis-Specialties. Decorative Paints and Coatings <http://www.elementis-specialties-asia.com> (accessed Jun 14, 2015).
- (5) Gooch, J. *Analysis and Deformulation of Polymeric Materials: Paints, Plastics, Adhesives, and Inks*, Kluwer Academic Publishers: Florida, 1997, pp 139-148.
- (6) Bruck, M. L.; Willard, G. F. *Met. Finish.* **2006**, *104*, 23–24.
- (7) Sidwell, J. *Wilson and Wilson's Comprehensive Analytical Chemistry*; Elsevier B.V., 2008; Vol. 53, pp 562–563.
- (8) Hoogland, F. G.; Boon, J. J. *Int. J. Mass Spectrom.* **2009**, *284*, 66–71.
- (9) Cho, D.; Hong, J.; Park, S.; Chang, T. *J. Chromatogr.* **2003**, *986*, 199–206.
- (10) Sun, C.; Baird, M.; Simpson, J. *J. Chromatogr. A* **1998**, *800*, 231–238.
- (11) Trathnigg, B.; Fraydl, S.; Veronik, M. *J. Chromatogr. A* **2004**, *1038*, 43–52.
- (12) Trathnigg, B.; Veronik, M. *J. Chromatogr. A* **2005**, *1091*, 110–117.
- (13) Trathnigg, B.; Rappel, C.; Fraydl, S.; Gorbunov, A. *J. Chromatogr. A* **2005**, *1085*, 253–261.
- (14) Petit, C.; Beaudoin, E.; Gigmes, D.; Bertin, D. *J. Chromatogr. A* **2007**, *1163*, 128–137.
- (15) Mekap, D.; Macko, T.; Brüll, R.; Cong, R.; W, A.; Parrott, A.; Cools, P. J. C. H.; Yau, W. *Polymer*. **2013**, *54*, 5518–5524.
- (16) Broberg, S. Studies of Oligo- and polysaccharides by MALDI-TOF and ESI-ITMS<sup>n</sup> Mass Spectrometry, PhD Thesis, Swedish University of Agricultural Sciences, 2004.
- (17) Zhang, B.; Zhang, H.; Myers, B. K.; Elupula, R.; Jayawickramarajah, J.; Grayson, S. M. *Anal. Chim. Acta* **2014**, *816*, 28–40.
- (18) Pasch, H.; Hiller, W. *Macromolecules* **1996**, *29*, 6556–6559.
- (19) Pasch, H.; Trathnigg, B. *Multidimensional HPLC of Polymers*; Springer: New York, 2013, pp 95-242.
- (20) Baumgaertel, A.; Altuntas, E.; Schubert, U. S. *J. Chromatogr. A* **2012**, *1240*, 1–20.
- (21) Kaal, E. R.; Alkema, G.; Kurano, M.; Geissler, M.; Janssen, H. *J. Chromatogr. A* **2007**, *1143*, 182–189.
- (22) Sobeih, K. L.; Baron, M.; Gonzalez-Rodriguez, J. *J. Chromatogr. A* **2008**, *1186*, 51–66.
- (23) Wang, F. C. *J. Chromatogr. A* **2000**, *883*, 199–210.

## Chapter 2

### Theoretical and historical background

#### 2.1. Theory

This section outlines the theory of the analytical techniques that will be utilised in the project. In each of the mentioned techniques, the detection mode for the polymers is discussed in detail.

##### 2.1.1. Liquid Chromatography

Liquid chromatography is a technique whereby the eluent (which contains the analyte) is transferred by a pressurized mobile phase through a column packed with a stationary solid material. The components of the analyte are partitioned and distributed between the mobile and stationary phase according to their degree of interaction<sup>1</sup>.

The distribution coefficient ( $K_d$ ) is a function of the concentration of species retained in the stationary phase and those present in the mobile phase as shown<sup>2</sup>:

$$K_d = \frac{[\text{Polymer}]_{\text{stationary phase}}}{[\text{Polymer}]_{\text{mobile phase}}} \quad (2.1)$$

The distribution coefficient can be represented by the interstitial volume  $V_i$  (volume outside the particles of the packing material on the stationary phase) and the pore volume  $V_p$  (volume inside the pores of the packing material). The relationship between  $K_d$ ,  $V_i$ ,  $V_p$  and the elution volume  $V_e$  is illustrated by Equation 2.2 as shown<sup>3</sup>:

$$K_d = \frac{V_e - V_i}{V_p} \quad (2.2)$$

Furthermore,  $K_d$  can be represented by the change in Gibbs free energy ( $\Delta G$ ) of the polymer chain as the molecules are transferred from the mobile phase to the stationary phase. This is illustrated by Equation 2.3, where  $\Delta H$  is a change in enthalpy,  $\Delta S$  is a change in entropy,  $R$  is the gas constant,  $K$  is the distribution coefficient and  $T$  is the absolute temperature<sup>4</sup>:

$$\Delta G = \Delta H - T\Delta S = -RT \ln K \quad (2.3)$$

The polymer retention behaviour gives rise to modes of separation which are governed by either the enthalpic or entropic interactions. The first mode of separation is size exclusion chromatography (SEC). *Ideal* SEC mode is directed by entropic interactions hence the interaction parameter is negative ( $\Delta G < 0$ ) and the distribution coefficient lies between zero and one ( $0 < K < 1$ )<sup>3</sup>. SEC

## Chapter 2: Theoretical and historical background

occurs when larger molecules are excluded from the pores of the stationary phase and are therefore eluted first from the column. Smaller molecules tend to penetrate the pores of the stationary phase and are retained longer in the column<sup>5,6</sup>.

The second mode of chromatographic separation is liquid adsorption chromatography (LAC). It occurs when polymers interact very strongly with the stationary phase, resulting in adsorption of the molecules which leads to longer retention times. The *ideal* LAC mode is directed by enthalpic interactions and the interaction parameter is positive ( $\Delta G > 0$ )<sup>5,6</sup>. The distribution coefficient is much greater than one ( $K \gg 1$ ) and it increases exponentially as the number of polymer repeat unit is increased<sup>3</sup>.

Liquid chromatography at the critical point of adsorption (LCCC) is regarded as a special case of separation techniques. This is a chromatographic phenomenon where the entropic ( $\Delta S$ ) and enthalpic ( $\Delta H$ ) interactions between the polymer molecules in the mobile and stationary phase are balanced<sup>2,3</sup>. This mode occurs under well-defined conditions that are determined by the type of mobile phase composition, stationary phase, temperature, and type of polymer. This means that at the critical point of adsorption, there is no contribution from the interaction parameter ( $\Delta G = 0$ ) and  $K_d$  is unity. As a result, polymers with similar chemical structures will elute at the same elution volume regardless of their molar mass<sup>2,3</sup>. The benefit of LCCC is that polymers can be separated with respect to the number and type of functionalised end groups, polymer blends, chemical composition and presence of co-monomers<sup>6</sup>.

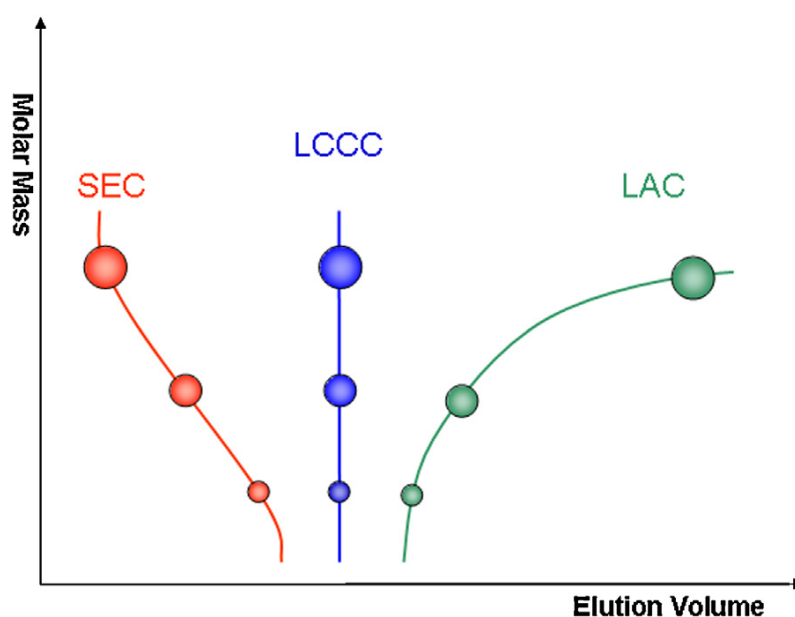


Figure 2.1: The modes of separation in liquid chromatography<sup>7</sup>

## Chapter 2: Theoretical and historical background

The aforementioned separation modes such as SEC, LAC and LCCC are often performed with isocratic elution. This is a separation mode whereby the mobile phase composition stays constant throughout an analysis. Some of the disadvantages of isocratic elution are peak broadening, poor sensitivity, irreversible adsorption of analytes onto the stationary phase and longer retention times. This phenomenon is particularly common when analysing the more hydrophobic analytes<sup>1,3,8</sup>.

An alternative separation mode that can be used to overcome problems associated with the isocratic mode is gradient elution. This is a process whereby the composition of two or more solvents is varied in a pre-programmed manner either continuously or in a series of steps<sup>1,3</sup>. Gradient elution mode is considered advantageous to isocratic elution due to its ability to enhance the strength of the mobile phase, thereby allowing shorter retention times, improved peak resolution, better detection and separation of complex analytes<sup>1,3</sup>. The use of gradient elution has been reported by various authors for the separation of homopolymers, copolymers and polymer blends<sup>9-12</sup>.

### 2.1.2. Evaporative light scattering detector

Liquid chromatographic analyses are often coupled to multiple detectors such as MS, UV and ELSD. The process of how analytes are detected by ELSD works in three stages shown in Figure 2.2. In the first stage, the eluent from the liquid chromatographic system is nebulized by a carrier gas such as nitrogen (N<sub>2</sub>), by converting it into a fine aerosol. In the second stage, the fine aerosol is passed through a tube whereby it is heated until the mobile phase evaporates<sup>13</sup>. The target analytes that have less volatility than the mobile phase are carried by the gas as ‘dry’ microparticles to the ELS detector<sup>14</sup>. The solvent that is used as a mobile phase must therefore be of a lower boiling point for an optimum evaporation. In the third stage, the microparticles are carried to the detector unit where they are irradiated by a light source and the intensity of the scattered light from the particles is measured by a photomultiplier<sup>13</sup>. The concentration of the analyte of interest is directly proportional to the intensity of the scattered light, as shown by Equation 2.4:

$$I = km^b \quad (2.4)$$

where  $I$  is the light intensity,  $k$  and  $b$  are constants which depend on experimental conditions and  $m$  is the mass of the scattering particles<sup>13</sup>.

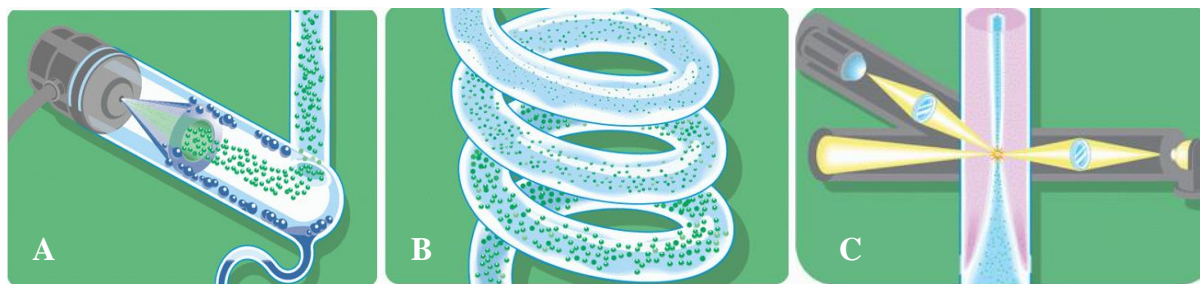


Figure 2.2: Principles of the ELS detection system showing nebulization (A), evaporation (B) and light scattering detection (C)<sup>13</sup>.

### 2.1.3. Liquid chromatography coupled to mass spectrometry

Liquid chromatography coupled to mass spectrometry (LC-MS) is a technique whereby molecules that are separated by LC are converted to ions when they are bombarded by high energy electrons. LC-MS operates with various ionization sources such as atmospheric pressure ionization-electrospray (API-ES), atmospheric pressure photoionization (APPI), multimode ionization (MMI) and atmospheric pressure chemical ionization (APCI).

API-ES occurs in three stages which are nebulization, desolvation and ion evaporation (Figure 2.3). The formation of ions occurs based on the chemistry of the analyte or the addition of ionizing agents such as formic acid, ammonium formate and ammonium acetate to the mobile phase. The eluent ions in solution are nebulized to form a spray of charged droplets due to the presence of strong electrostatic forces<sup>15</sup>. The solvent is then evaporated by a heated drying gas ( $N_2$ ) to form a bare ion<sup>16</sup>. The bare ion consists of a cluster of likely charged species, which can be further separated and evaporated due to the effects of Coulomb repulsion forces. The resultant ions are then passed through a capillary and are detected by a mass analyser<sup>10</sup>.

In APPI, sample molecules are ionized using a photon beam from a krypton lamp. Dopants are usually added to the mobile phase to enhance the photoionization process. MMI is a process whereby ionization can occur by a combination of APCI, electrospray ionization (ESI) or simultaneous APCI/ESI<sup>16</sup>.

In APCI, the solvent and target analyte are introduced into a nebulizer, where they are converted into a fine aerosol. A gas flow (typically  $N_2$ ) transports the droplets to the desolvation/evaporation chamber where the solvent and analyte are vapourised<sup>17</sup>. The vapour mixture is then passed along a corona discharge electrode<sup>17</sup>. This is where the reactant gas ions are formed from ionization of the solvent vapour. The reactant gas ions promote ionization of the sample molecules as well as their introduction into the capillary<sup>16</sup>.

## Chapter 2: Theoretical and historical background

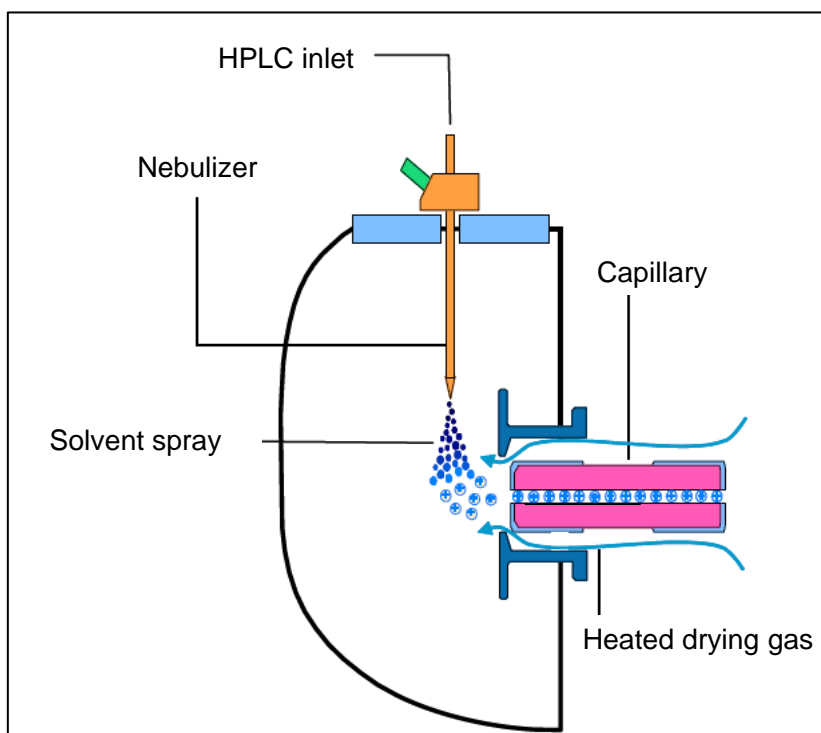


Figure 2.3: Schematics of the API-ES ion source<sup>16</sup>.

The resultant ions from the ion source are introduced into a vacuum in a mass spectrometer. The ions travel in vacuum from the capillary until they are separated by a mass analyzer according to the differences in mass-to-charge ratio. Each of the ions is then detected by a detector as a signal<sup>16</sup>.

In a mass spectrometer, ionization occurs in either the positive or negative mode. In the positive mode, the mechanism happens either by proton transfer or formation of adducts depending on the differences in the proton affinity. Proton transfer occurs when a solvent has a higher proton affinity than the analyte while adducts form when the solvent and analyte have similar proton affinities<sup>17,18</sup>. In the negative mode, formation of ions occurs due to proton abstraction, associative electron capture, presence of anions or dissociative electron capture<sup>18</sup>.

APCI has been found to be an advantageous ionization method because it is performed at atmospheric conditions, has a high collision frequency and it forms molecular species with little or no fragmentation. Furthermore, API-ES is often preferred as it does not thermally degrade the analytes. It also allows for the analysis of larger molecules ( $> 15\,000$  amu) due to the multiple charge effect. As a result, the APCI and API-ES are considered as soft ionization techniques compared to other methods<sup>19</sup>.



#### 2.1.4. Nuclear magnetic resonance spectroscopy

NMR is one of the most popular and powerful techniques used for characterization of complex polymers. The results acquired from techniques such as proton ( $^1\text{H}$ ), carbon ( $^{13}\text{C}$ ), phosphorus ( $^{31}\text{P}$ ) and nitrogen ( $^{15}\text{N}$ ) NMR analyses can be directly correlated to the molecular structures of the components of the sample and the information can be used to determine the chemical compositions and types of polymer end groups<sup>20</sup>. The application of NMR has been reported on the identification and characterization of various types of additives such as PEG<sup>21,22</sup>, alcohol ethoxylates<sup>23</sup>, amine-based PEG<sup>24</sup>, alkylphenol ethoxylates<sup>25,26</sup> and polysaccharides<sup>27,28</sup>.

#### 2.1.5. Pyrolysis gas chromatography

The use of py-GC-MS has been investigated by various authors to identify and characterize polymers<sup>29–33</sup>. In this technique, a sample is injected into a pyrolyser and heated to a specified temperature. The applied thermal energy causes the polymer molecules to be broken down into smaller volatile components. These components are fragments of the original molecular structure of the analyte<sup>30</sup>. Due to the complexity of spectra arising from py-GC-MS analyses, this technique is often used in combination with LC-MS or MALDI-TOF to determine the molecular structures of polymers<sup>33–35</sup>.

#### 2.1.6. Fourier transform infrared spectroscopy

Fourier transform infrared spectroscopy in attenuated total reflectance mode (FTIR-ATR) is one of the techniques that are sometimes used complimentary to liquid chromatography for the identification of unknowns<sup>36</sup>. When molecules in a sample absorb infrared radiation, it causes the stretching and bending vibrations of the covalent bonds<sup>20</sup>. The amount of energy required to stretch, bend or twist these covalent bonds can be directly correlated to the chemical groups arising from the analyte.

### 2.2. Literature review

This section presents the different types of chemical structures encountered in commercial additives under investigation. Literature studies on the identification and characterization of the additives by various techniques are also included.

### 2.2.1. The types of chemical structures in additives

The additives' industry is an extensive market, applicable to the coatings, cosmetics, detergents, agriculture, paper, textile and leather. These additives are often synthesized with various types of polymer backbones and end groups depending on whether they are defoamers, thickeners or wetting and dispersing agents. In the coatings industry, poly(ethylene oxide) (PEO), poly(propylene oxide) (PPO) and block-PEO/PPO are commonly used as repeat units in additives such as humectants and wetting and dispersing agents<sup>37–39</sup>. These polymers are functionalized with the different types of end groups to enhance the overall properties of the surfactants in paints and colourants.

The hydroxyl group (OH) is one of the most common end groups, found in PEG, PPG and star-PEG additives<sup>40–42</sup>. The linear alcohol end group ( $C_nH_nO-$ ), derived from oleochemical (natural) or petrochemical (synthetic) processes are extensively used in the surfactants industry to form the non-ionic fatty alcohol ethoxylates. Tridecanol, which comprises of a mixture of  $C_{12}$  to  $C_{16}$  alcohols is typically used<sup>39,43</sup>. The fatty acid and fatty ester ethoxylates are the non-ionic surfactants that are used as dispersants, emulsifiers and wetting agents<sup>44</sup>. The use of a blend of fatty acids such as caprylic ( $C_8$ ), perlagonic ( $C_9$ ) and capric ( $C_{10}$ ) acids for the industrial production of ethoxylated fatty acids has been reported<sup>45,46</sup>. The types of fatty ester-based additives are typically fatty acid methyl ester ethoxylate<sup>44</sup> or a mixture of mono- and diester-PEGs<sup>39,47</sup>.

The ethoxylated amine- and amide-based additives are classified as amphoteric or zwitterionic surfactants because of their ability to act as non-ionics in neutral and alkaline conditions as well as cationics at an acidic pH<sup>43,48</sup>. In the coatings' industry, these types of additives are excellent anchoring groups for organic and inorganic pigments<sup>49–52</sup>.

Naturally derived surfactants such as alkyl glucoside, oligo- and polyglucoside are also often used in paints and colourants because they are non-toxic, biodegradable and are compatible with most other surfactant types. Long chain alcohols such as n-octanol ( $C_8$ ), n-decanol ( $C_{10}$ ) and n-dodecanol ( $C_{12}$ ) are commonly used to form octyl, decyl and lauryl glucoside surfactants, respectively<sup>53</sup>.

Alkylphenyl-based end groups are one of the popular surfactants, which include alkylphenyl ethoxylates and alkylbenzene sulfonate. These surfactants can be a mixture of linear and branched isomers depending on their synthesis route. However, the branched isomers have been banned in some countries because they biodegrade too slowly, making them toxic to the environment<sup>54,55</sup>. Alkylbenzene sulfonate is sold commercially as a neutralized salt of bases such as sodium hydroxide, potassium hydroxide, isopropyl amine and many others<sup>39,56,57</sup>. Alkylphenyl ethoxylate is often a mixture of linear and/or branched octyl, nonyl and decylphenyl products<sup>43</sup>.

## Chapter 2: Theoretical and historical background

Each of the aforementioned end group types play an important role in the functionality and properties of the additives. This created an opportunity to explore the various techniques of identifying and characterizing the commercial additives used in colourants.

**2.2.2. Identification and characterization of complex polymers****2.2.2.1. Determination of polymer end groups and molar mass distributions**

Additives such as glycols, humectants, wetting and dispersing agents are extensively used in coatings and colourants. Each commercial supplier claims certain functionalities of these additives that will give optimum performance to a colourant. The chemical composition of these additives is always changing as new technologies emerge; hence continuous improvements to colourant formulations are necessary. Knowledge of the additive's chemical composition is thus imperative for colourants formulators for accurate quality control and characterization of the final formulation.

Several studies have been reported on the analysis of various types of additives used in the coatings industry. In most of the literature, a combination of several techniques for the analysis of complex polymers were investigated as one technique may have a better sensitivity and selectivity than the others. Techniques such as FTIR can provide information on the type of additive, however, some additives have similar chemical groups and a conclusive differentiation is not always possible. Py-GC-MS thermally degrades the polymer into simple components but this can complicate the spectra and make it challenging to determine the starting material<sup>31,32</sup>. MALDI-TOF-MS has gained significant popularity because of its improved sensitivity in determining the identity and the concentration of polymer end groups, compared to NMR and FTIR<sup>58</sup>.

NMR is one of the most important, complimentary techniques used for the characterization of complex polymers. Due to the lower concentration of the polymer end group, its NMR signal is often weaker compared to that of the repeat unit. As a result, this may be one of the disadvantages of NMR<sup>59</sup>. However, over the last decade several publications have been reported on hyphenation of NMR and chromatographic techniques either offline or online. Studies by Schlotterbeck *et al.* demonstrated that the separation of fatty alcohol ethoxylates by exclusion-adsorption chromatography followed by online coupling with <sup>1</sup>H NMR could provide useful information on the chemical structure of the end groups as well as the degree of polymerization<sup>60</sup>. This was in agreement with Hiller *et al.* where fatty alcohol ethoxylates could also be separated using LCCC and online characterization by <sup>1</sup>H NMR<sup>61</sup>.

## Chapter 2: Theoretical and historical background

The other modes of separation that have been studied are two-dimensional liquid chromatography (2D-LC) where polymers were separated based on chemical composition, molar mass and functional end groups<sup>62</sup>. Studies by Murphy *et al.* had demonstrated the power of 2D-LC over the conventional one-dimensional technique. In their research they have shown that 2D-LC has superior selectivity in the separation of alcohol ethoxylate from the ethylene oxide (EO) repeat unit and alkyl components<sup>63</sup>. This study was further supported by Elsner *et al.* in their publication on 2D-LC analysis of a mixture of fatty alcohol ethoxylates, fatty alcohol sulphates (AS), fatty alcohol ether sulphates (AES), alkyl polyglucosides and amphoteric surfactants. A simultaneous separation of EO and alkyl components could also be achieved. However, their method showed low sensitivity in the detection of AS and AES in the positive mode of ESI. This could be improved by performing the analysis of these two components in negative mode ESI<sup>64</sup>.

Derivatization is another method that has been reported for identification and characterization of polymers using UV, fluorescence or MS detection. This method involves the modification of a compound to produce a different compound that has chemical properties that are suitable for separation or quantification<sup>65</sup>. Polymers such as PEGs or fatty alcohol ethoxylates are not UV detectable due to the absence of chromophores<sup>12</sup>. Studies by Sun *et al.* and Micó-Tormos *et al.* have demonstrated that derivatization agents such as dinitrobenzol, and diphenic anhydride can be used to enhance the UV detectability of PEGs and fatty alcohol ethoxylates<sup>12,66</sup>. However, some authors argued that derivatization is time consuming and can cause ionization suppression, degradation of derivatives, formation of by-products as well as negative effects on the separation of polymers<sup>67,68</sup>.

Liquid chromatography has by far been the most common technique for the analysis of complex polymers. Separation modes such as SEC have been applied mostly to polymers with higher molecular size, however, obtaining an optimum resolution of individual oligomers and the ability to analyse heterogeneous polymers is a challenge<sup>69,70</sup>. Liquid exclusion-adsorption chromatography (LEAC) has been named by some authors as a superior separation method than SEC in the separation of homopolymers<sup>71</sup> and block copolymers<sup>10</sup>. In this technique, a mobile phase composition allows for the elution of the ethylene oxide chain in SEC mode while the hydrophobic alkyl groups are adsorbed to the reverse phase column. As a result, the individual oligomers elute in SEC mode and the resolution is improved<sup>68</sup>.

The other mode of separation that has gained much popularity is LCCC, with its theoretical discovery dating back to the 1970s. Since then, a vast number of papers have been published on the analysis of homopolymers<sup>2,4,62,72,73</sup>, copolymers<sup>74,75</sup>, block copolymers<sup>76,77</sup> as well as polymer blends<sup>78,79</sup>. In this project, we will further demonstrate the power of LCCC as well as the

combination of LCCC and solvent gradient elution in identifying the number of different components in each of the commercial PEG-based additives.

#### **2.2.2.2. Analysis of multi-component polymeric systems**

The analysis of a multi-component polymeric material such as a paint or colourant is often required by paint manufacturers for formulation benchmarking, cost reductions, product development and resolution of paint related failures. As a result, method developments for the identification of the components in a paint or colourant matrix are necessary. These methods will require important aspects such as highly resolved separation techniques and a good response sensitivity of the different analytical techniques. Successful extraction and identification of the different components of a paint or colourant can often be challenging as these components are present in various concentrations and each of them responds differently to various detectors. Currently, there are very few literature studies found where a complete characterization of a paint or colourant was performed. In the literature that was available, two or more analytical techniques were used to separate and characterize the paint components.

Studies were performed by Hoogland and Boon where they investigated the use of MALDI-TOF-MS and nano electrospray ionisation mass spectrometry (nano ESI-MS) to identify PEG additives in artists' paints as well as in microsamples from old acrylic paintings. In their study, they could determine the molar mass distribution and end groups of the PEG-based additives in the artists' paints. Furthermore, other additives such as PPG and PEG/PPG block copolymers could also be identified. The same analytical technique was applied to microsamples acquired from artists' old paintings and the composition of the paint used by the original artists could be matched to a specific brand<sup>80,81</sup>.

In another study by Chiantore *et al.*, two commercial artists' acrylic emulsion paints were characterized using techniques such as py-GC-MS, NMR, SEC, FTIR and thermogravimetric analyses<sup>82</sup>.

In both the aforementioned literature studies, the type of extraction technique chosen depended on the type of material being analysed, whether it was a liquid or solid. Hoogland and Boon used dried paint material and performed a two weeks' water extraction of the additives from the dried flake. Chiantore *et al.* used tetrahydrofuran to extract the polymeric components of the liquid paint. Gooch recommended the use of centrifugation to separate the solid pigments from the liquid components

## Chapter 2: Theoretical and historical background

followed by the distillation of the liquid materials for a qualitative and quantitative characterization of the additives<sup>83</sup>.

In this project, we present the use of liquid chromatography, NMR, FTIR and py-GC-MS to determine the molar mass distribution and the types of end groups of commercial additives that are used in colourants. We will also report on the extraction of the additives from known colourant formulations, followed by analyses with LC-MS.

### 2.3. Conclusions

Liquid chromatography coupled to various detection systems is beneficial in separating and analysing complex polymers. These types of polymers could be commercial additives based on alcohol, acid, ester, amine and amide ethoxylates as well as alkyl polyglucoside. Extensive research has been performed on characterising complex polymers by various techniques. This provided a good platform for developing a method of determining the chemical composition and molar mass distribution of commercial additives.

### 2.4. References

- (1) Skoog, D. A.; Holler, F. J.; Crouch, S. R. *Principles of Instrumental Analysis*; Thompson Brooks/Cole: Canada, 2007; pp 819–820.
- (2) Petit, C.; Beaudoin, E.; Gigmes, D.; Bertin, D. *J. Chromatogr. A* **2007**, *1163*, 128–137.
- (3) Pasch, H.; Trathnigg, B. *Multidimensional HPLC of Polymers*; Springer: New York, 2013; pp 27–30.
- (4) Trathnigg, B.; Rappel, C.; Fraydl, S.; Gorbunov, A. *J. Chromatogr. A* **2005**, *1085*, 253–261.
- (5) Weismantel, G. E. *Paint Handbook*; McGraw Hill: New York, 1981, pp 1-50.
- (6) Pasch, H.; Trathnigg, B. *HPLC of Polymers*; Springer: Berlin, 1999, pp 128-137.
- (7) Hiller, W.; Sinha, P.; Hehn, M.; Pasch, H. *Prog. Polym. Sci.* **2014**, *39*, 979–1016.
- (8) Nikitas, P.; Pappa-Louisi, A. *J. Chromatogr. A* **2009**, *1216*, 1737–1755.
- (9) Brun, Y.; Alden, P. *J. Chromatogr. A* **2002**, *966*, 25–40.
- (10) Jandera, P.; Holčápek, M.; Kolářová, L. *J. Chromatogr. A* **2000**, *869*, 65–84.
- (11) Radke, W. *J. Chromatogr. A* **2013**, *49*, 2–18.

## Chapter 2: Theoretical and historical background

- (12) Sun, C.; Baird, M.; Simpson, J. *J. Chromatogr. A* **1998**, *800*, 231–238.
- (13) Agilent Technologies. Agilent 1200 series evaporative light scattering detector user manual <http://www.chem.agilent.com/Library/usermanuals/> (accessed Jun 11, 2015).
- (14) Waters Corporation. *2424 evaporative light scattering detector: operator's guide*; Milford, USA, 2009, pp 2-3.
- (15) Block, C.; Wynants, L.; Kelchtermans, M.; De Boer, R.; Compennolle, F. *Polym. Degrad. Stab.* **2006**, *91*, 3163–3173.
- (16) Agilent 6100 Series Quadrupole LC / MS Systems <http://www.agilent.com/cs/library/usermanuals/public/> (accessed Aug 21, 2015).
- (17) De Hoffmann, E.; Stroobant, V. *Mass Spectrometry: Principles and Applications*; Wiley: England, 2007; pp 10–50.
- (18) CHROMacademy. Mass Spectrometry Fundamental LC-MS Atmospheric Pressure Chemical Ionisation (APCI) <http://www.chromacademy.com/lms/> (accessed Jun 13, 2015).
- (19) Zaikin, V.; Halket, J. *Eur. J. Mass Spectrom.* **2006**, *12*, 79–115.
- (20) Pavia, D. L.; Lampman, G. M.; Kriz, G. S. *Introduction to Spectroscopy*; Vondeling, J., Kiselica, S., Eds.; Brooks/Cole Thompson Learning, 2001; pp 13–17.
- (21) Dust, J. M.; Fang, Z.; Harris, J. M. *Macromolecules* **1990**, *23*, 3742–3746.
- (22) Postma, A.; Davis, T. P.; Donovan, a. R.; Li, G.; Moad, G.; Mulder, R.; O'Shea, M. S. *Polymer*. **2006**, *47*, 1899–1911.
- (23) Vermeersch, G.; Aubry, J.; Azaroual, N. *Colloids Surfaces A: Physicochem. Eng. Asp.* **2008**, *331*, 16–24.
- (24) Izunobi, J. U.; Higginbotham, C. L. *J. Chem. Educ.* **2011**, *88*, 1098–1104.
- (25) Charuk, J. H. M.; Grey, A. A.; Reithmeier, R. A. F. *Am. Physiol. Soc.* **1998**, *274*, 1127–1139.
- (26) Ding, J.; Song, B.; Wang, C.; Xu, J.; Wu, Y. *J. Surfactants Deterg.* **2011**, *14*, 43–49.
- (27) Prozil, S. O.; Costa, E. V; Evtuguin, D. V; Popez, L. P.; Domingues, M. R. M. *Carbohydr. Res.* **2012**, *356*, 252–259.
- (28) Sanghi, R.; Dhar, D. N. *J. Sci. Ind. Res.* **2001**, *60*, 463–492.
- (29) Bart, J. C. J. *J. Anal. Appl. Pyrolysis* **2001**, *58-59*, 3–28.
- (30) Sobeih, K. L.; Baron, M.; Gonzalez-Rodriguez, J. *J. Chromatogr. A* **2008**, *1186*, 51–66.
- (31) Wang, F. C. *J. Chromatogr. A* **2000**, *883*, 199–210.



Chapter 2: Theoretical and historical background

- (32) Herrera, M.; Matuschek, G.; Kettrup, a. *J. Anal. Appl. Pyrolysis* **2003**, 70, 35–42.
- (33) Kaal, E. R.; Kurano, M.; Gei, M.; Janssen, H. *J. Chromatogr. A* **2008**, 1186, 222–227.
- (34) Kaal, E. R.; Alkema, G.; Kurano, M.; Geissler, M.; Janssen, H. *J. Chromatogr. A* **2007**, 1143, 182–189.
- (35) Trimpin, S.; Wijerathne, K.; Mcewen, C. N. *Anal. Chim. Acta* **2009**, 654, 20–25.
- (36) Chiantore, O.; Learner, T. J. S.; Scalarone, D. *Int. J. Polm. Anal. Charact.* **2003**, 8, 67–82.
- (37) Koleske, J. V. In *Paint and coating testing manual: Fifteenth edition of the Gardner-Sward handbook*; ASTM International: New Jersey, 2012; pp 320–331.
- (38) Schmitt, T. M. *Analysis of surfactants*, Second Edn.; Marcel Dekker, Inc.: New York, 2001, pp 1-483.
- (39) Texter, J. *Reactions and synthesis in surfactant systems: Surfactant Science*; CRC Press: New York, 2001; pp 1–44.
- (40) Holmberg, K.; Bo, J.; Kronberg, B.; Lindman, B. *Surfactants and polymers in aqueous solutions*; J. Wiley & Sons, LTD: England, 2003; pp 7–23.
- (41) Lapienis, G. *Prog. Polym. Sci.* **2009**, 34, 852–892.
- (42) Wesley, R. D.; Cosgrove, T.; Thompson, L. *Langmuir* **1999**, 15, 8376–8382.
- (43) Salager, J.-L. *Surfactants types and uses*, Second Edn.; Universidad de Los Andes: Merida-Venezuela, 2002, pp 3-47.
- (44) Hama, I.; Okamoto, T.; Nakamura, H. *J. Am. oil Chem. Soc.* **1995**, 72, 781–784.
- (45) Liu, X.; Han, R.; Wang, Y.; Li, X.; Zhang, M.; Yan, Y. *Plant Pathol. J.* **2014**, 13, 65–70.
- (46) Wang, Y. Antimicrobial compositions containing mixtures of fatty and hydroxyl carboxylic acids. US Patent 2014/0170237 A1, 2014.
- (47) Falbe, J. *Synthesis of surfactants*; Springer Science and Business Media: Berlin, 2012, pp 1-100.
- (48) Lim, J.; Han, D. *Colloids Surfaces A Physicochem. Eng. Asp.* **2011**, 389, 166–174.
- (49) Ma, S.-H. Polymeric pigment dispersants having multiple pigment anchoring groups. US Patent 6451950 B1, 2002.
- (50) The Role of Fatty Acid Modified Emulsifiers (FAME) <https://www.dispersions-pigments.basf.com/portal/basf/> (accessed Jul 11, 2015).
- (51) Mößmer, S.; Roch, M.; Göbelt, B.; Johann, S. *Eur. Coatings J.* **2010**, 2, 28–31.



Chapter 2: Theoretical and historical background

- (52) Specialty Additives product selection guide <http://www.pcimag.com/ext/resources/> (accessed Jul 11, 2015).
- (53) Balzer, D.; Luders, H. *Nonionic Surfactants: Alkyl Polyglucosides*, Volume 91.; Balzer, D., Luders, H., Eds.; CRC Press: Germany, 2000, pp 36-76.
- (54) Jensen, J. *Sci. Total Environ.* **1999**, 226, 93–111.
- (55) Soares, A.; Guieysse, B.; Jefferson, B.; Cartmell, E.; Lester, J. N. *Environ. Int.* **2008**, 34, 1033–1049.
- (56) Molever, K. *J. Surfactants Deterg.* **2005**, 8, 199–202.
- (57) Zoller, U.; Sosis, P. *Handbook of Detergents, Part F: Production (Surfactant Science)*; CRC Press: Boca Raton, FL, USA, 2008; pp 83–115.
- (58) Myers, B. K.; Zhang, B.; Lapucha, J. E.; Grayson, S. M. *Anal. Chim. Acta* **2014**, 808, 175–189.
- (59) Ji, H.; Nonidez, W. K.; Advincula, R. C.; Smith, G. D.; Kilbey, S. M.; Dadmun, M. D.; Mays, J. W. *Macromolecules* **2005**, 38, 9950–9956.
- (60) Schlotterbeck, G.; Albert, K.; Pasch, H. *Polym. Bull.* **1997**, 679, 673–679.
- (61) Hiller, W.; Brull, A.; Argyropoulos, D.; Hoffmann, E.; Pasch, H. *Magn. Reson. Chem.* **2005**, 43, 729–735.
- (62) Maiko, K. G. Multidimensional separation of complex polymers according to microstructure, PhD Thesis, Stellenbosch University, 2014.
- (63) Murphy, R. E.; Schure, M. R.; Foley, J. P. *Anal. Chem.* **1998**, 70, 4353–4360.
- (64) Elsner, V.; Laun, S.; Melchior, D.; Köhler, M.; Schmitz, O. J. *J. Chromatogr. A* **2012**, 1268, 22–28.
- (65) Knapp, D. R. In *Handbook of Analytical Derivatization Reactions*; John Wiley & Sons: New York, 1979; pp 13–20.
- (66) Bianchi, F. *J. Chromatogr. A* **2009**, 1216, 3023–3030.
- (67) Qi, B.-L.; Liu, P.; Wang, Q.-Y.; Cai, W.-J.; Yuan, B.-F.; Feng, Y.-Q. *Trends Anal. Chem.* **2014**, 59, 121–132.
- (68) Trathnigg, B.; Fraydl, S.; Veronik, M. *J. Chromatogr. A* **2004**, 1038, 43–52.
- (69) Trathnigg, B.; Veronik, M. *J. Chromatogr. A* **2005**, 1091, 110–117.
- (70) Radke, W. *J. Chromatogr. A* **2014**, 1335, 62–79.
- (71) Trathnigg, B. *J. Chromatogr. A* **2001**, 915, 155–166.

Chapter 2: Theoretical and historical background

- (72) Bashir, M.; Brüll, A.; Radke, W. *Polymer*. **2005**, *46*, 3223–3229.
- (73) Jiang, X.; Schoenmakers, P. J.; Lou, X.; Lima, V.; Dongen, J. L. J. Van. *J. Chromatogr. A* **2004**, *1055*, 123–133.
- (74) Elhrari, W. K. S. Synthesis and characterization of multiphase copolymers, PhD Thesis, Stellenbosch University, 2011.
- (75) Mekap, D.; Macko, T.; Brüll, R.; Cong, R.; W, A.; Parrott, A.; Cools, P. J. C. H.; Yau, W. *Polymer*. **2013**, *54*, 5518–5524.
- (76) Abrar, S.; Trathnigg, B. *J. Chromatogr. A* **2010**, *1217*, 8222–8229.
- (77) Trathnigg, B.; Abrar, S. *Procedia Chem.* **2010**, *2*, 130–139.
- (78) Hiller, W.; Hehn, M.; Sinha, P.; Raust, J.; Pasch, H. *Macromolecules* **2012**, *45*, 7740–7748.
- (79) Pasch, H. *Polymer*. **1993**, *34*, 4095–4099.
- (80) Hoogland, F. G.; Boon, J. J. *Int. J. Mass Spectrom.* **2009**, *284*, 66–71.
- (81) Hoogland, F. G.; Boon, J. J. *Int. J. Mass Spectrom.* **2009**, *284*, 72–80.
- (82) Chiantore, O.; Scalarone, D.; Learner, T. *Int. J. Polym. Anal. Charact.* **2003**, *8*, 67–82.
- (83) Gooch, J. *Analysis and Deformation of Polymeric Materials: Paints, Plastics, Adhesives, and Inks*; Katritzky, A., Sabongi, G., Eds.; Kluwer Academic Publishers: Florida, 1997; pp 139–148..

## Chapter 3

### Experimental methodology

#### 3.1. Introduction

The materials and samples utilised in this project are presented. The research samples are the additives bought from the various commercial suppliers in the coatings industry. The exact trade names of the additives are not identified due to confidentiality considerations. This section also includes the experimental parameters of the analytical equipment used during the research.

#### 3.2. Experimental design

##### 3.2.1. Materials

The reagents used in all the analyses were of analytical grade. Methanol (HPLC Chromasolv®, ≥99%), water (HPLC Chromasolv®, ≥99%) and alpha-D glucose (Analytical grade, 96%) were bought from Sigma Aldrich. The PEG standards of molar masses of 194 to 7830 g/mol were bought from Agilent Technologies. Ammonium formate (ReagentPlus, ≥99%) from Sigma Aldrich was used as an ionising agent in the LC-MS analyses. Deuterated dimethyl sulfoxide (DMSO-d<sub>6</sub>) (99.6%, Sigma Aldrich) was used for all the <sup>1</sup>H and <sup>13</sup>C NMR experiments.

##### 3.2.1. List of samples

Table 3.1 presents the PEG calibration standards that were used to find the critical conditions of absorption. The properties listed include the molar mass at peak maximum ( $M_p$ ), number-average molar mass ( $M_n$ ), weight-average molar mass ( $M_w$ ) and dispersity ( $\mathcal{D}$ ).

## Chapter 3: Experimental methodology

*Table 3.1: Molar masses of the PEG calibration standards.*

Standard	M <sub>p</sub> (g/mol)	M <sub>n</sub> (g/mol)	M <sub>w</sub> (g/mol)	D
PEG 194	194	-	-	-
PEG 420	420	385	420	1.09
PEG 610	610	580	620	1.07
PEG 1010	1010	980	1020	1.04
PEG 1480	1480	1410	1470	1.04
PEG 4040	4040	3990	4110	1.03
PEG 7830	7830	7130	7460	1.05

The additives used in this project were bought from various paint industry suppliers and they were all analysed without any prior purification. The general chemical composition of the additives in Table 3.2 was as specified from the manufacturer's safety data sheets. The additives were divided into three types; **Type A** were the PEG and PPG types. **Type B** additives were moisturizing agents (commonly known as humectants). They usually consist of hydrophilic end groups that enhance the dry-out resistance in colourant formulations. **The Type C** additives were the wetting and dispersing agents that are used to stabilize the organic and inorganic pigments in aqueous dispersions. They are commonly blends of anionic, non-ionic surfactants and/or amphoteric surfactants.

*Table 3.2 List of additives, showing the components as obtained from the suppliers.*

Additive names	Supplier's component description
<b>Type A</b>	
Additive A1	Poly(ethylene glycol)
Additive A2	Poly(propylene glycol)
Additive A3	Ethylene glycol
<b>Type B</b>	
Additive B1	Alkyl glucosides
	Poly(ethylene glycol) monooleyl ether
	Alkyl alcohol ethoxylate, phosphated salt
Additive B2	Polysaccharide
Additive B3	Glycerol ethoxylate
<b>Type C</b>	
Additive C1	Poly(ethylene glycol)
	Nonylphenol ethoxylate, branched
Additive C2	Poly(ethylene glycol)
	Nonylphenol ethoxylate, branched
Additive C3	Fatty alcohol ethoxylate
	Butanoic acid, 4-amino-4-oxosulfo-disodium salts
Additive C4	Fatty acid based polymer
	Polymer with a tertiary amine polar head
	Unsaturated hydrophobic chains
Additive C5	Amine salt based on dodecyl phenol ethoxylate
Additive C6	Unknown
Additive C7	Mixture of anionic and non-ionic surfactants

### 3.2.2. Analytical techniques

#### 3.2.2.1. Liquid chromatography with ELS detection

The experimental conditions for the analysis of additives were chosen based on the known molecular structures from Table 3.2, which are comprised mostly of ethylene oxide derivatives with various end groups. Due to the similarities of the repeat unit, liquid chromatography at critical conditions of PEG was chosen as a feasible separation technique. In this separation mode, the molar mass effect of the different polymers is excluded and identification is performed based solely on the differences in functional end groups or polymer blends. Additionally, a combination of LCCC and solvent gradient elution was performed in some additives to enhance the detection of hydrophobic components that may not be observed when only LCCC is employed.

## Chapter 3: Experimental methodology

The PEG calibration standards and additives were analysed using an Agilent Technologies 6100 LC system. The instrument was equipped with a quaternary pump, auto-sampler, fraction collector and a thermostatted column compartment. The detection was performed with a 1260 Infinity ELSD and UV detector (Agilent Technologies, USA). Data processing was performed with Agilent LC/MSD Chemstation Software (Revision B.04.03 (16)).

The PEG standards with molar masses of 194 to 7300 g/mol were each dissolved in various compositions in a mobile phase of methanol/water at a concentration of 1 mg/mL. Each standard was analysed in triplicate. The separation of the polymers was achieved using a Symmetry C<sub>18</sub> stationary phase (Waters, USA). The parameters of the stationary phase were as follows: pore size of 100 Å, particle size of 5 µm, column length of 250 mm and an internal diameter of 4.6 mm. The flow rate was set to 1 mL/min, using an injection volume of 20 µL and the column temperature was maintained at 30°C. The detectors used were ELSD and UV. The ELSD was set at the following conditions: gain 5, nebulization temperature 85°C, filter 5 seconds and N<sub>2</sub> gas pressure of 3.5 bars. The UV signal was acquired at a wavelength range of 210 to 280 nm.

The critical point of adsorption of PEG was determined by analysing the PEG standards at various mobile phase compositions, from 100% methanol to 70%/30% methanol/water (v/v). At each mobile phase composition, a plot of the retention time of each PEG versus the logarithm of the molar mass at peak maximum (M<sub>p</sub>) was drawn. The critical point was chosen as the point at which all PEG standards eluted at the same retention time regardless of the molar mass.

The additives were dissolved in the methanol/water mobile phase at a concentration of 1 mg/mL and analysed at 100% methanol, 90%/10% methanol/water (v/v) as well as at the critical conditions of adsorption of PEG. In some additives, solvent gradient elution was performed by first separating the polymeric components using critical conditions of adsorption of PEG for the first specified minutes, and the methanol concentration was increased up to 100% methanol for the duration of the run.

### 3.2.2.2. Liquid chromatography coupled to mass spectrometry

LC-MS experiments for the analysis of additives were performed with the same sample preparation and LC conditions as specified in Section 3.2.2.1. Ammonium formate (HCOONH<sub>4</sub>) was used as an ionizing agent in all LC-MS analyses. The ionizing agent was added equally in each of the water/methanol mobile phases, at various concentrations of 0 to 5x10<sup>-3</sup> mol/L. The detectors used were the UV and the 6120 quadrupole mass spectrometer (Agilent Technologies, USA). The MS

data was acquired using the atmospheric pressure electrospray ionization (AP-ESI). Samples were analysed in the positive and negative scan modes at a mass range 10 to 2000 Da. The fragmentor voltage was set to 100 V with a threshold of 150 using a gain of 1.0. The chromatographic peaks were acquired at a step size of 0.10 and peak width of 0.1 mm.

#### **3.2.2.3. Analyses by nuclear magnetic resonance spectroscopy**

The additives were each dissolved at a mass of 45-50 mg in 1 mL of DMSO- $d_6$ . All samples were analysed without any prior purification or drying. NMR spectra were obtained using the 300 MHz and 600 MHz Varian Unity Inova Spectrometers (Varian Inc., USA). The  $^1H$  NMR spectra were acquired at a resonance frequency of 600 MHz, temperature of 25°C using an acquisition time of 1.7068 seconds and 32 number of scans. The  $^{13}C$  NMR spectra were acquired at a resonance frequency of 300 MHz at 25°C, using an acquisition time of 1.30 seconds. Data processing was performed using MestReC software version 4.5.6.0 (Mestrelab, USA). The chemical shift referencing was performed using the DMSO residual peaks at 2.50 ppm for  $^1H$  and 39.43 ppm for  $^{13}C$  NMR.

#### **3.2.2.4. Analyses by Fourier transform infrared spectroscopy**

Fourier transform infrared spectroscopy in attenuated total reflectance mode (FTIR-ATR) was used as a complimentary technique to LC-MS and NMR to confirm the additives' end groups. Each of the additives were analysed with no prior modification, using a VERTEX 70 FTIR spectrometer equipped with the PLATINUM Diamond ATR accessory (Bruker, USA). Spectra were acquired at 4000 to 350  $cm^{-1}$ , collecting 64 scans at a resolution of 4  $cm^{-1}$ . Each sample was analysed in duplicate and a background spectrum was collected prior to each duplicate run. Data collection was performed with the OPUS software version 7.5. The OMNIC software version 8.2.0.387 (Thermo Fisher Scientific Inc., USA) was used for data processing.

#### **3.2.2.5. Analyses by pyrolysis GC-MS**

Some of the more complex additives were analysed with pyrolysis GC-MS to confirm the polymer end groups. The GC-MS system consisted of a FOCUS gas chromatograph and a DSQ quadrupole mass detector (Thermo Fisher Scientific Inc., USA), equipped with SGE Pyrojector II™ and the SI-1 solids syringe (SGE Analytical Science, Australia). The additives were dried at 50°C for two hours prior to analyses in order to evaporate any residual water. A sample of about 1 mg was placed

onto the syringe and injected into the pyrolysis chamber. The temperature of the chamber was maintained at 650°C. The sample was held in the chamber for 15s. The pyrolysed products were transferred from the chamber to the GC by a constant helium flow of 20 mL/min, at a split ratio of 1:100. The BPX5 stationary phase (SGE Analytical Science, Australia) used for the separation of the pyrolysed products had the following parameters: length 30 m, internal diameter 0.25 mm and particle size of 0.25 µm. The GC oven temperature was initially kept at 40°C prior to the start of the analysis. The temperature was then increased linearly at 20°C/min to 300°C and maintained at 300°C for the duration of the run. The pyrolysed products were separated according to the mass-to-charge ratio using a single quadrupole mass detector. Data analysis was performed using Xcalibur software version 3.0.63 (Thermo Fisher Scientific Inc., USA). The National Institute of Standards and Technology (NIST) version 2.0. was used for all the mass spectral searches.

#### **3.2.2.6. Extraction of the additives from known colourants**

Two colourant formulations consisting of a solvent (water), pigments, extenders, additives and other colourants were prepared. An amount of 2 g of each colourant was weighed into a centrifuge tube and diluted with 55 mL of distilled water. The contents were mixed for 1 minute using Vortex-2-Genie mixer (Scientific Industries Inc., USA). Each colourant was weighed in triplicate. The contents of the centrifuge tubes were subjected to a mechanical gravitational force using the Sorvall RC-5B superspeed refrigerated centrifuge (DuPont, USA). The centrifuge was set to 12 000 rpm for 30 minutes to separate the colourant components according to the difference in density. After 30 minutes had elapsed, each of the colourants was separated into two layers of pigment+extenders and water+additives. The supernatant water layer (with the separated additives) was decanted into a clean beaker and dried at 50°C to constant weight. After drying, 2 mg of the extracted additives was dissolved into 2 mL of the methanol/water mobile phase from the liquid chromatography pump system. The solution was filtered with a 0.45 µm filter and dispensed into a vial for LC-MS analyses.



## Chapter 4

### Results and discussion

#### 4.1. Introduction

This chapter presents the results obtained from the analyses of the additives by LC-ELSD, LC-UV, LC-MS, NMR, FTIR-ATR and pyrolysis-GC-MS. The PEG standards were analysed by LC-ELSD at various methanol/water mobile phase compositions to search for the critical conditions of adsorption of PEG. The characterization of the three types of colourant additives was achieved by using a combination of the aforementioned techniques. Selected additives were then incorporated in a colourant formulation, extracted and identified by LC-MS analyses.

#### 4.2. The search for critical conditions of adsorption for PEG

The critical point of adsorption of PEG was achieved according to a discussion outlined in section 3.2.2.1. The plot in Figure 4.1 shows the logarithm of the molar mass of PEG versus the retention time. The SEC mode was operating at 100% to 81% methanol mobile phase composition. At these compositions, the separation is governed by entropic interactions. The larger molecules are excluded from the pores of the stationary phase and are thus eluted first, while the smaller molecules penetrate the pores and are retained longer in the column<sup>1,2</sup>.

The LAC mode was observed at 70%/30% methanol/water (v/v) and it is influenced by enthalpic interactions. The shorter polymer chains (e.g. 420 g/mol) have less interaction with the non-polar C<sub>18</sub> stationary phase while the larger polymer molecules (7830 g/mol) showed strong adsorption to the stationary phase; causing an exponential increase in the retention time. The LCCC mode was achieved at 79.9%/20.1% methanol/water (v/v). At the critical point of adsorption, the enthalpic and entropic interactions compensate each other and all the PEG standards eluted at the same retention time regardless of the molar mass. The benefit of this phenomenon is the ability to separate the different components of complex polymer blends by their functional end groups, irrespective of the molar mass of the polymer<sup>1,2</sup>. This approach is thus instrumental for the characterization of commercial additives as reported in the next section.

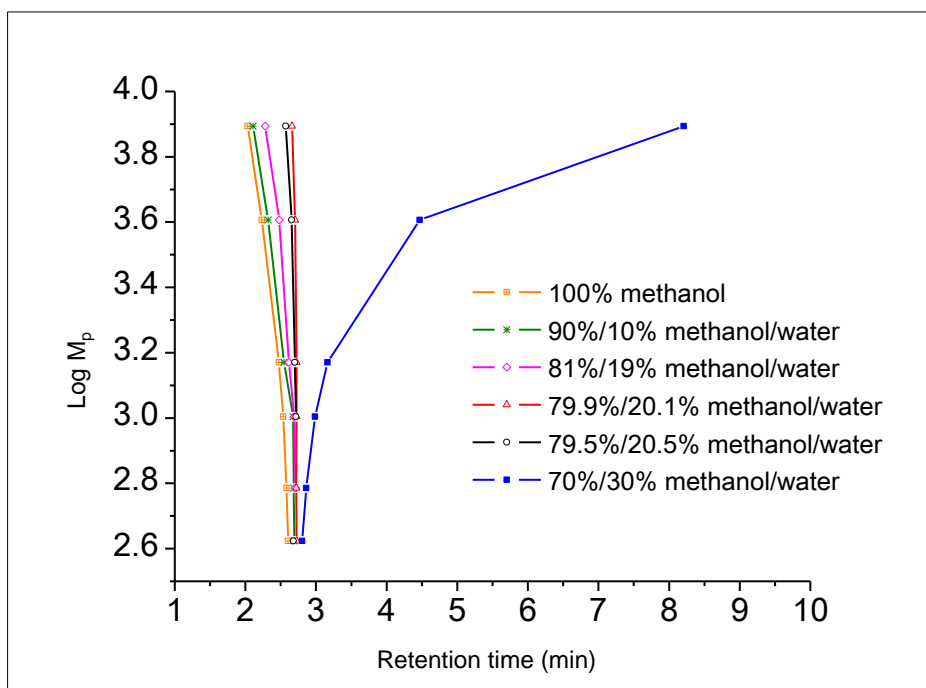


Figure 4.1 Plot of  $\log M_p$  versus retention time of PEG standards at various methanol/water (v/v) mobile phase compositions.

### 4.3. Characterization of the colourant additives

This section presents the analysis of commercial additives by various techniques. The LC-MS mass spectra were acquired using various concentrations of  $\text{HCOONH}_4$  at 0 to  $5 \times 10^{-3}$  mol/L to enhance ion formation. The variation of the concentration was based on factors such as ionizability, spectral complexity and the presence of other cations in the sample solution.

Commercial additives are typically manufactured with the use of acids and bases as catalysts or neutralizing agents. As a result, cations such as  $\text{H}^+$ ,  $\text{Na}^+$ ,  $\text{K}^+$  etc. can be present as part of the additive blend. When ammonium formate is used, the  $[\text{M} + \text{NH}_4]^+$  adduct is typically formed. However, due to the presence of other cations in the additive blend; additional molecular ion distributions such as  $[\text{M} + z_1]^+$ ,  $[\text{M} + z_2]^+$  or  $[\text{M} + z_1 + z_2]^{2+}$  are expected where M is the parent ion and  $z_i$  represents other cations. Very often, these additional distributions overlap with the  $[\text{M} + \text{NH}_4]^+$  adducts, complicating the mass spectra. Mass spectral interpretations that follow show the  $[\text{M} + \text{NH}_4]^+$  molecular ions highlighted in black (unless otherwise specified), and this molecular ion series was used for the characterization of most of the additives. The distributions from other cations are highlighted in other colours. In cases where the additive contains anionic components, the negative mode LC-MS was used to highlight the differences in chemical composition between the positive and negative scan modes.

All the reported total ion chromatograms (TIC) of the additives were acquired at either critical conditions of adsorption of PEG or by solvent gradient elution.

The average molar mass of the additive components from LC-MS was estimated using the most abundant ion in the mass spectrum ( $M_p$ ). The  $^1\text{H}$  NMR spectra were used to determine the number-average molar mass ( $M_n$ ) of the additives that consisted of a single PEG-based component.

### 4.3.1. Characterization of type A additives

#### 4.3.1.1. Analyses of additive A1

Figures 4.2 to 4.7 show the LC-ELSD, LC-MS and NMR results of Type A additives. In the colourant formulations, these additives are typically the pure ethylene glycol, PEG, propylene glycol and PPG.

Figure 4.2 presents the LC-ELSD and positive scan TIC of additive A1 acquired at critical conditions of adsorption of PEG. A single peak was detected at a retention time of 2.6 minutes.

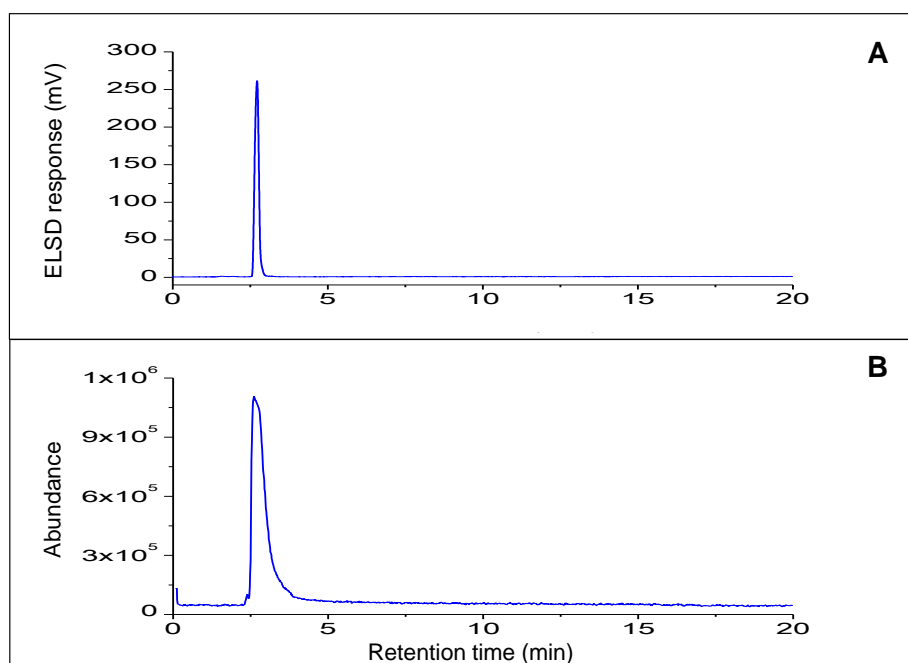


Figure 4.2: LC-ELSD (A) and positive scan TIC (B) of additive A1.

The mass spectrum in Figure 4.3 showed three molecular ion series which were highlighted in red, blue and black. The red series has peaks at the mass-to-charge ratio ( $m/z$ ) 45, 89, 133, 177, the blue has  $m/z$  151, 195, 239, 283 etc. while the black has peaks at  $m/z$  256, 300, 344, 388 etc. A peak-to-

## Chapter 4: Results and discussion

peak mass difference of 44 Da was observed in each series, which suggested the presence of an ethylene oxide (EO) repeat unit ( $\text{OCH}_2\text{CH}_2$ ) in the polymer chain.

The assignment of each of the series was performed according to Equation 4.1.

$$\frac{m}{z} = \frac{z \cdot m_{\text{cation}} + n \cdot m_{\text{monomer}} + m_{\text{residual}}}{z} \quad (4.1)$$

Where  $z$  is the number of cations,  $m_{\text{cation}}$  is the mass of the cation,  $m_{\text{monomer}}$  is the mass of the monomer unit,  $n$  is the number of monomers and  $m_{\text{residual}}$  is the combined masses of the end groups<sup>3</sup>.

The assignments of the most abundant peaks in each of the series according to Equation 4.1 were illustrated with comparison between the experimental and theoretical  $m/z$  ratios. The peak at  $m/z$  89 matched  $[\text{M} + \text{H}]^+$ , where  $\text{M}$  is a cyclic dimer of ethylene oxide as shown:

$$(m/z)_{\text{experimental}} = 89.15$$

$$(m/z)_{\text{theoretical}} = 1.0079 + 2 \cdot 44.0526 = 89.11$$

The peak at  $m/z$  283 was attributed to  $[\text{M} + \text{H}]^+$ , where  $\text{M}$  is a PEG with six EO repeat units as shown:

$$(m/z)_{\text{experimental}} = 283.15$$

$$(m/z)_{\text{theoretical}} = 1.0079 + 6 \cdot 44.0526 + (17.0073 + 1.0079) = 283.34$$

The most abundant peak of additive A1 at  $m/z$  388 corresponded to  $[\text{M} + \text{NH}_4]^+$ , which is a PEG with eight repeat EO units.

$$(m/z)_{\text{experimental}} = 388.30$$

$$(m/z)_{\text{theoretical}} = 18.0385 + 8 \cdot 44.0526 + (17.0073 + 1.0079) = 388.47$$

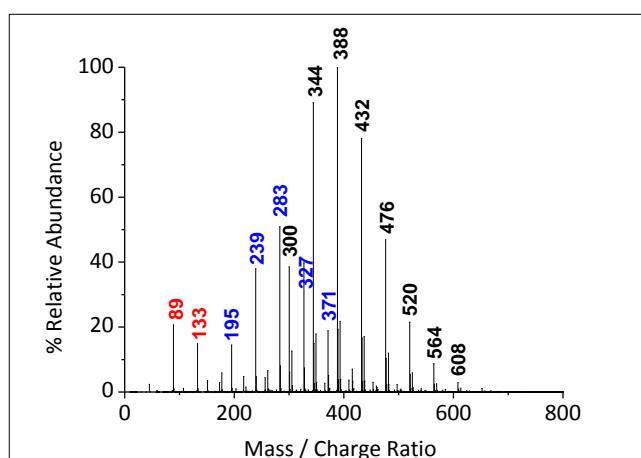


Figure 4.3: Positive scan mass spectrum of additive A1.

## Chapter 4: Results and discussion

Figure 4.4 shows the  $^1\text{H}$  NMR spectrum of additive A1 for confirmation of the end groups. A triplet at 4.57 ppm was characteristic of the two hydroxyl (OH) protons of the PEG. The peaks centered at 3.41 ppm and 3.48 ppm were assigned to the methylene protons at positions 3 and 4, respectively. The methylene protons of the EO repeat unit were assigned to a larger peak centered at 3.51 ppm, shown by position 2. A singlet peak at 3.34 ppm was due to intramolecular exchanges between the deuterium atoms in DMSO and the hydrogen of the water molecule to form HOD.

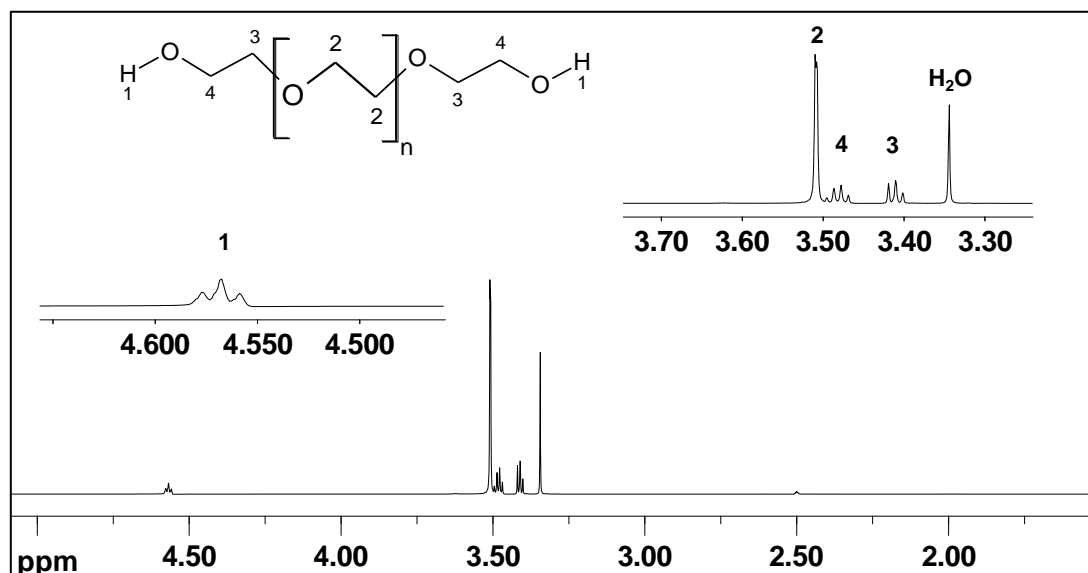
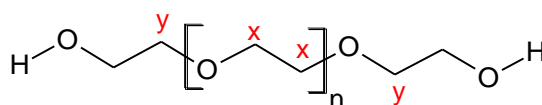


Figure 4.4:  $^1\text{H}$  NMR spectrum of additive A1 in DMSO, 25°C and 600 MHz.

The number of EO repeat units was calculated from the  $^1\text{H}$  NMR spectrum, using the peak areas of the repeat unit and end groups. The formula in Equation 4.2. was derived for moieties x and y in the PEG structure shown<sup>4</sup>.



$$n_x = \frac{a_x}{a_y} \quad (4.2)$$

Where  $n_x$  is the number of repeat units for moiety x,  $a_x$  and  $a_y$  are the peak areas of moieties x and y from the  $^1\text{H}$  NMR spectrum. The number-average molar mass ( $M_n$ ) was calculated using Equation 4.3:

$$M_n = nM_o + M_e \quad (4.3)$$

## Chapter 4: Results and discussion

Where  $n$  is the number of repeat units,  $M_o$  represents the molar mass of one repeat unit and  $M_e$  is the combined molar mass of the end groups<sup>4</sup>.

The number of repeat units in the additive A1 polymer chain was calculated using the  $^1\text{H}$  NMR peak areas of  $-(\text{OCH}_2\text{CH}_2)_n-$  at 3.51 ppm and  $-(\text{OCH}_2\text{CH}_2)-$  centered at 3.41 ppm as moieties  $x$  and  $y$ , respectively (see Table 4.1). Substituting into Equation 4.2, approximately five repeat units were obtained:

$$n_x = \frac{207060.17}{44991.60} = 4.60$$

Since the protons at positions 3 and 4 in Figure 4.4 also formed part of the ethylene oxide repeat unit, the total number of EO repeat units from NMR was seven. Consequently,  $M_n$  was obtained from Equation 4.3 as shown:

$$M_n = 7 \times 44.05 + (1.01 + 17.01) = 326.37 \text{ g/mol}$$

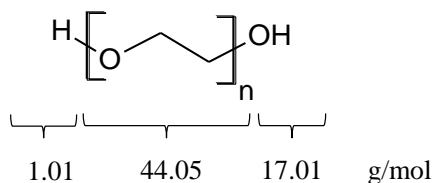


Table 4.1 shows the calculated  $M_n$  obtained from  $^1\text{H}$  NMR and  $M_p$  as the most abundant ion of the mass spectrum. The average  $M_p$  value from LC-MS was 44 units higher than  $M_n$  from NMR, which was equivalent to the difference of one EO repeat unit. Since  $M_n$  measured the number-average molar mass over the entire oligomer series and  $M_p$  was acquired at a peak maximum, a good correlation between the two molar masses was expected only if a perfect Gaussian molar mass distribution was obtained from LC-MS.

Table 4.1:  $^1\text{H}$  NMR data and the calculated  $M_n$  of additive A1.

Moiety	No. of protons	Chemical shift (ppm)	Peak area	$M_n$ ( $^1\text{H}$ NMR) g/mol	$M_p$ (LC-MS) g/mol
$-(\text{OCH}_2\text{CH}_2)-$	4	3.41	44991.60	326 g/mol with 7 repeat units	370 g/mol with 8 repeat units
$-(\text{OCH}_2\text{CH}_2)_n-$	4	3.51	207060.17		

The LC-MS and  $^1\text{H}$  NMR data showed that additive A1 is a PEG with an average of eight EO repeat units and an approximate molar mass of 370 g/mol. The LC-MS analyses of additive A3 showed a single peak at  $m/z$  63, which was characteristic of the protonated ethylene glycol.

#### 4.3.1.2. Analyses of additive A2

The results of additive A2 are presented in Figures 4.5 to 4.7. The LC-ELSD and the positive scan TIC chromatogram in Figure 4.5 were acquired at critical conditions of adsorption of PEG. A total of 12 oligomer peaks of propylene glycol were observed, with the MS detector showing all 12 peaks while the ELSD showed peaks 4 to 11. The absence of the other oligomers in the LC-ELSD chromatogram was attributed to either the low concentration of the species or possible evaporation of the lower molar mass components. Furthermore, in both the LC-ELSD chromatogram and the mass spectrum (Figure 4.6); peak 7 was identified as the oligomer with the largest peak area intensity (33%) and highest abundance at  $m/z$  616.

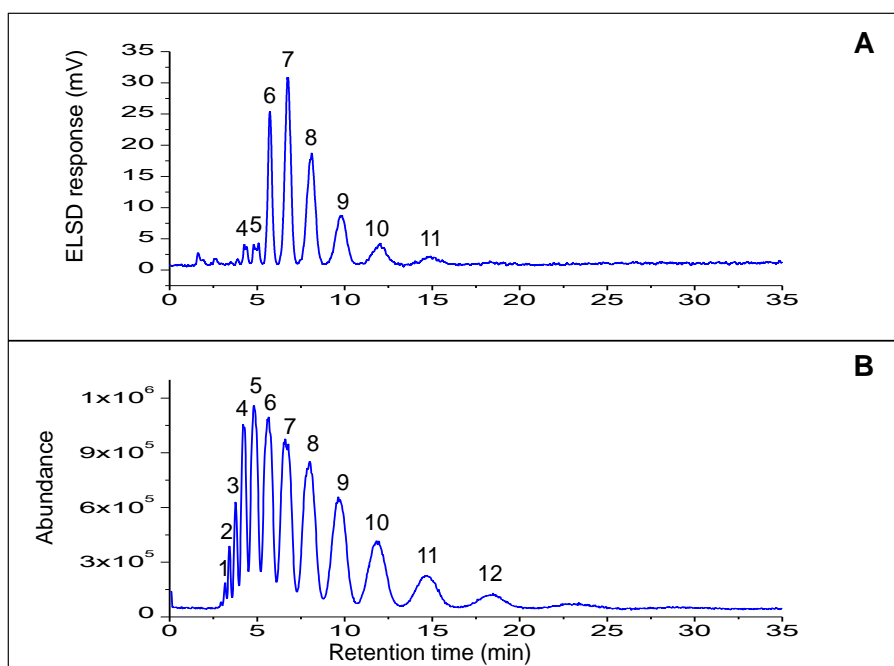


Figure 4.5: LC-ELSD (A) and positive TIC scan (B) of additive A2.

The molecular ion distribution of additive A2 in Figure 4.6 showed ions at  $m/z$  442, 500, 558, 616 etc. A peak-to-peak difference of 58 Da was observed; indicating the presence of propylene oxide (PO) repeat units ( $\text{OCH}(\text{CH}_3)\text{CH}_2$ ). The assignment of the most abundant peak ( $m/z$  616) according to Equation 4.1 is as shown:

## Chapter 4: Results and discussion

$$(m/z)_{\text{experimental}} = 616.65$$

$$(m/z)_{\text{theoretical}} = 18.0385 + 10 \times 58.0791 + (17.0073 + 1.0079) = 616.85$$

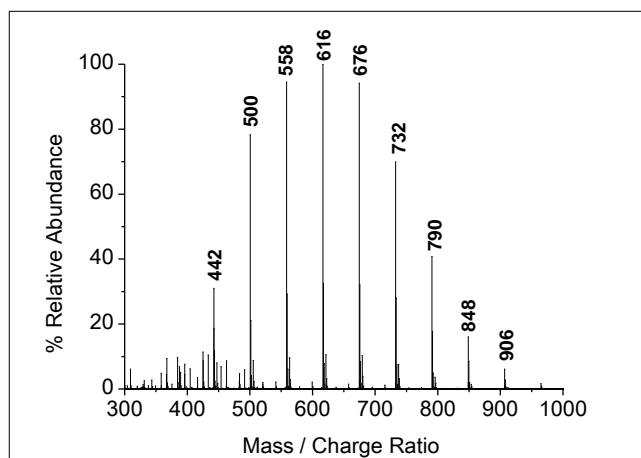


Figure 4.6: Positive scan mass spectrum of additive A2.

The  $^1\text{H}$  NMR spectrum in Figure 4.7 consisted of the residual DMSO solvent peak at 2.50 ppm and the OH group at 4.41 ppm. The two equivalent methyl groups shown by position 7 in the structure, were assigned to a doublet at 1.01 ppm. The complex peak centered at 1.04 ppm (position 6) was attributed to the methyl protons of the PO repeat unit. The peak at 3.31 ppm was assigned to the methylene protons of the PO repeat unit as illustrated by position 5. The multiplet centred at 3.21 ppm was due to the methylene protons at position 3.

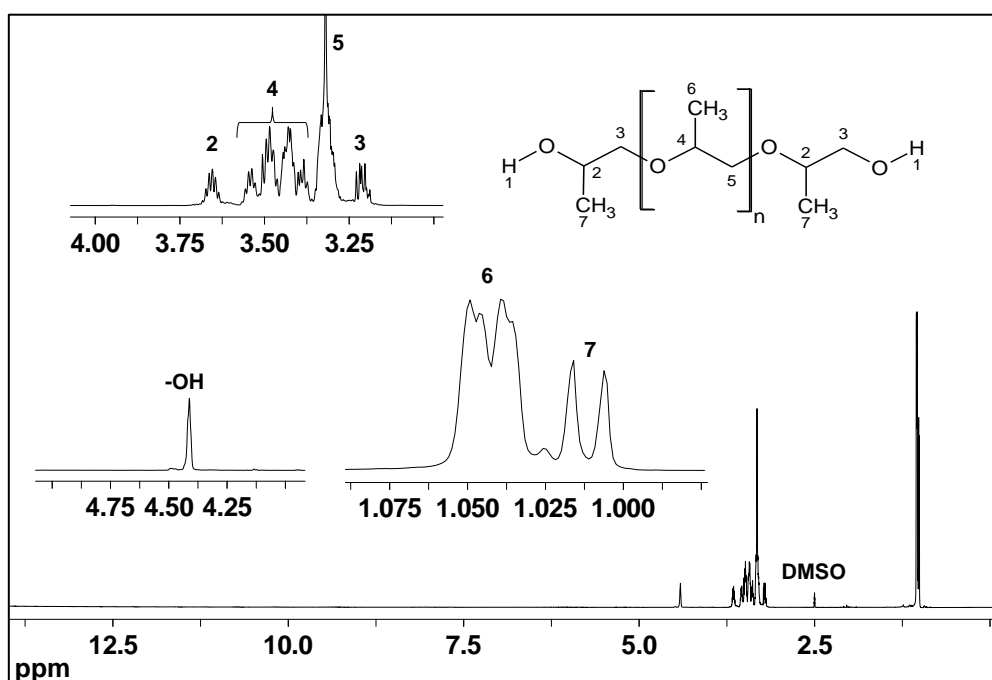


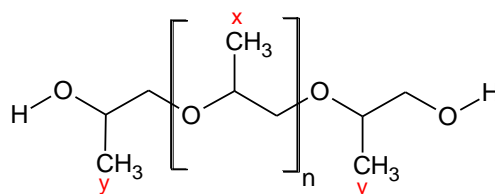
Figure 4.7:  $^1\text{H}$  NMR spectrum of additive A2 in DMSO, 25°C and 600 MHz.



## Chapter 4: Results and discussion

A methine proton at 3.66 ppm (position 2) was at a higher chemical shift due to the strong hydrogen bonding of the -OH group and the higher electronegativity of the oxygen atom. A complex multiplet centered at 3.47 ppm was attributed to the methine protons of the PO repeat unit shown by position 4 in the structure. The assignments of the PPG structure were in agreement with the study performed by Dauner and Pringle<sup>5</sup>.

Moieties labelled by positions x and y in the PPG structure below were used for the calculations of  $n_x$  and  $M_n$ .



The peak areas and number of protons for moieties x and y were substituted in the equation as shown:

$$n_x = \frac{54786.07/3}{15913.52/6} = 6.89$$

Approximately seven PO repeat units were calculated. However, since the protons at positions 2, 3 and 7 (Figure 4.7) formed part of the propylene oxide repeat unit; the total number of PO repeat units from  $^1\text{H}$  NMR was nine. Consequently,  $M_n$  was calculated as shown:

$$M_n = 9 \times 58.08 + (1.01 + 17.01) = 540.73 \text{ g/mol}$$

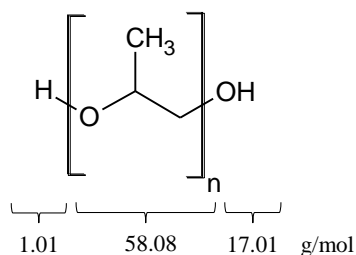


Table 4.2 shows the molar mass obtained from NMR and LC-MS. The calculated  $M_n$  value from  $^1\text{H}$  NMR was one PO repeat unit lower than the most abundant peak from the mass spectrum in Figure 4.6.

*Table 4.2:  $^1\text{H}$  NMR data and the calculated  $M_n$  of additive A2.*

Moiety	No. of protons	Chemical shift (ppm)	Peak area	$M_n$ ( $^1\text{H}$ NMR) g/mol	$M_p$ (LC-MS) g/mol
6	3	1.04	54786.07	540 with 9 repeat units	598 with 10 repeat units
7	6	1.01	15913.52		

LC-MS analyses showed that the most abundant peak of additive A2 is a PPG with 10 PO repeat units and an approximate average molar mass of 600 g/mol.

#### 4.3.2. Characterization of type B additives

The results presented in Figures 4.8 to 4.28 were acquired from the analyses of the type B additives. They are typically polymers with hydrophilic end groups which help to prevent the rapid drying-out of the packaged colourants. As discussed in Section 4.1., cations such as  $\text{Na}^+$ ,  $\text{H}^+$  and  $\text{K}^+$  may be associated with these types of additives, causing MS spectral overlaps. The molecular ion distribution and chemical composition of these additives were determined using MS in both the negative and positive scan modes.

##### 4.3.2.1. Analyses of additive B1

The chromatograms in Figure 4.8 showed peaks identified in additive B1 when analysed in positive and negative mode LC-MS at critical conditions of PEG. The positive scan (A) indicated three prominent peaks labelled 1, 5 and 10. The corresponding peaks 5 and 10 were also identified with the highest peak height by the negative scan (B). A total of eleven peaks were detected in the negative mode with a better signal-to-noise ratio compared to the positive mode, suggesting the presence of more anionic components in additive B1. The negative ion scan was therefore used for the characterization of additive B1 to investigate the chemical composition of the additive.

## Chapter 4: Results and discussion

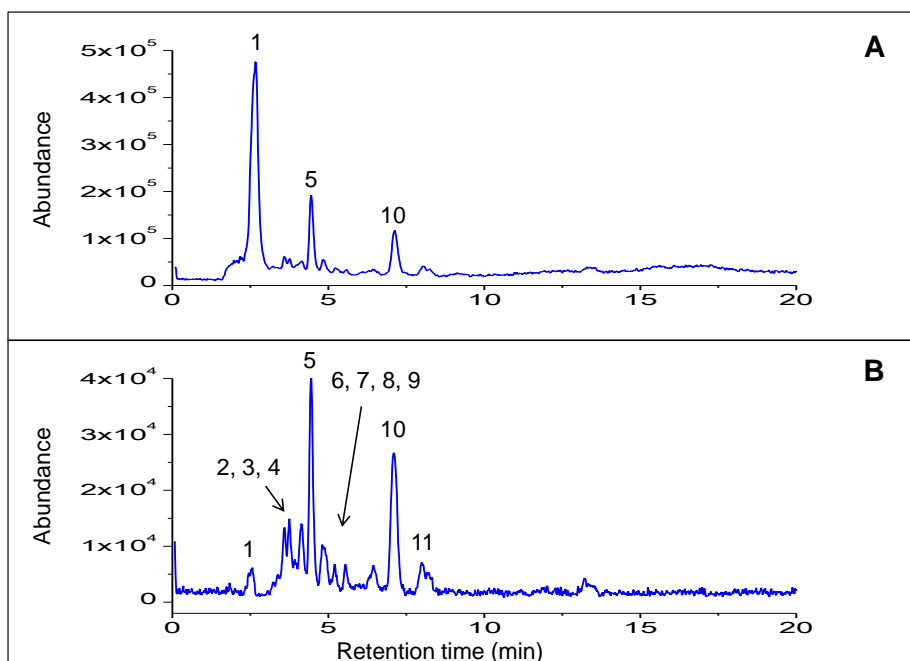


Figure 4.8: Positive (A) and negative (B) TIC scans of additive B1 acquired at critical conditions of PEG.

The negative scan mass spectrum in Figure 4.9A was acquired from peak 1 of additive B1. It showed characteristic peaks at  $m/z$  89, 131, 161, which corresponded to studies performed by Taylor *et al.* regarding the fragmentation patterns of glucose, fructose and sucrose by electrospray ionization tandem mass spectrometry (ESI-MS/MS)<sup>6</sup>. Their proposed fragmentation pathways for glucose and fructose are illustrated in Figure 4.10. The negative scan mass spectrum of glucose in Figure 4.9B further confirmed similar peaks to additive B1 at  $m/z$  89, 113, 161, and 179. The other peaks at  $m/z$  71, 101, 119 and 131 observed in Figure 4.9A and B were in agreement with the fragmentation pathway suggested by Taylor *et al.* in Figure 4.10.

In Figures 4.9A and B, the peak at  $m/z$  179 was attributed to the glucose anion,  $[C_6H_{12}O_6 - H]^-$ , while  $m/z$  207 (Figure 4.9A) was assigned to the ethyl glucoside anion  $[C_8H_{16}O_6 - H]^-$ . This was due to the difference of 28 Da between the two ions, indicating the presence of an additional  $CH_3CH_2-$  group. The theoretical versus experimental data are reported in Table 4.3.

## Chapter 4: Results and discussion

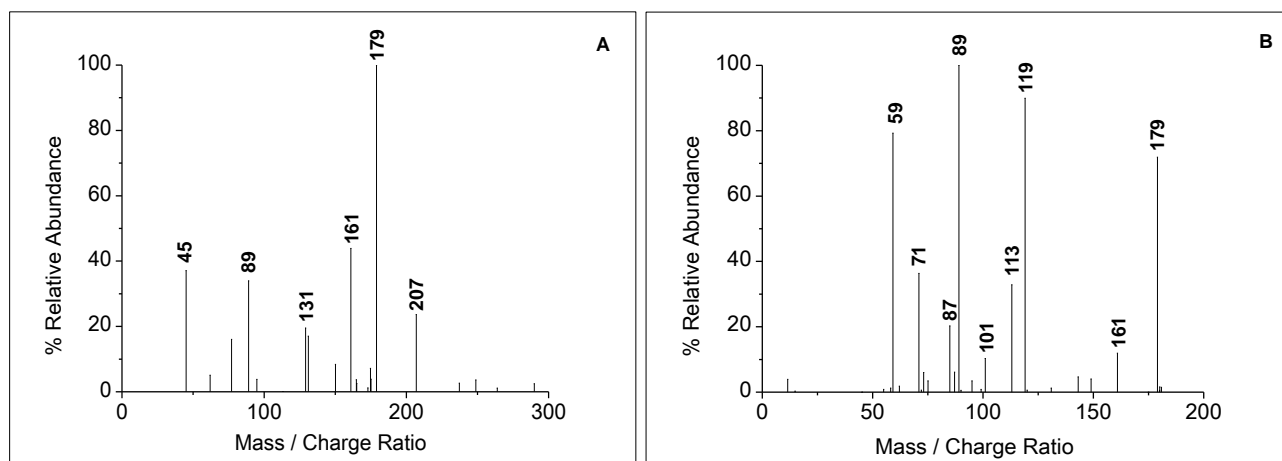


Figure 4.9: Negative scan LC-MS of additive B1 for peak 1 (A) and alpha-D glucose (B).

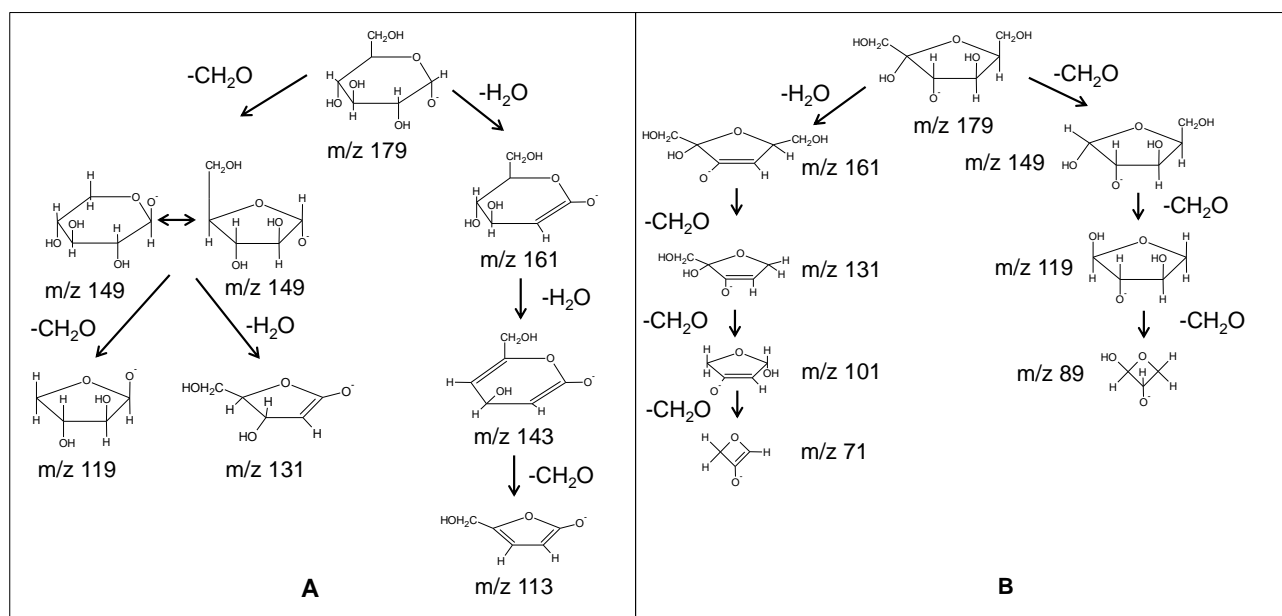


Figure 4.10: Fragmentation pattern of glucose (A) and fructose (B) adapted from Taylor et al.<sup>6</sup>

Figures 4.11A and B acquired from peaks 3 and 5, respectively, showed characteristic mass peaks at  $m/z$  453, 499, 291 and 337. The ion at  $m/z$  453 in Figure 4.11A was attributed to the octyl oligoglucoside anion with two glucose repeat units,  $[C_{20}H_{38}O_{11} - H]^-$ . The adduct of the same molecule with the formate anion was observed by the  $[C_{20}H_{38}O_{11} + HCOO]^-$  anion at  $m/z$  499 (Table 4.3). The precursor ions at peaks 2 and 4 were similar to that of peak 3, however, additional peaks arising from doubly charged species and fragmentation of the glucose unit were observed on their mass spectra.

## Chapter 4: Results and discussion

In Figure 4.11B, the ion at  $m/z$  291 was assigned to the anion of octyl glucoside  $[C_{14}H_{27}O_6 - H]^-$  while  $m/z$  337 was due to the adduct formation in  $[C_{14}H_{27}O_6 + HCOO]^-$ . The smaller peak (7% abundance) at  $m/z$  583 corresponded to a dimer with the two linked octyl glucoside molecules. A dimer formation was due to the strong hydrogen bonds between the hydrogen and oxygen atoms of the two molecules. The assignments of the peaks in Figure 4.11A and B were as illustrated in Table 4.3, with comparisons to the theoretical values. A precursor ion of peak 6 was observed to be similar to that of peak 5 as shown in Figure 4.3. Furthermore, a mass spectrum of peak 6 (not shown) consisted of the parent ion ( $m/z$  291), formate adduct ( $m/z$  337) as well as fragments of the glucose unit at  $m/z$  113 and 161.

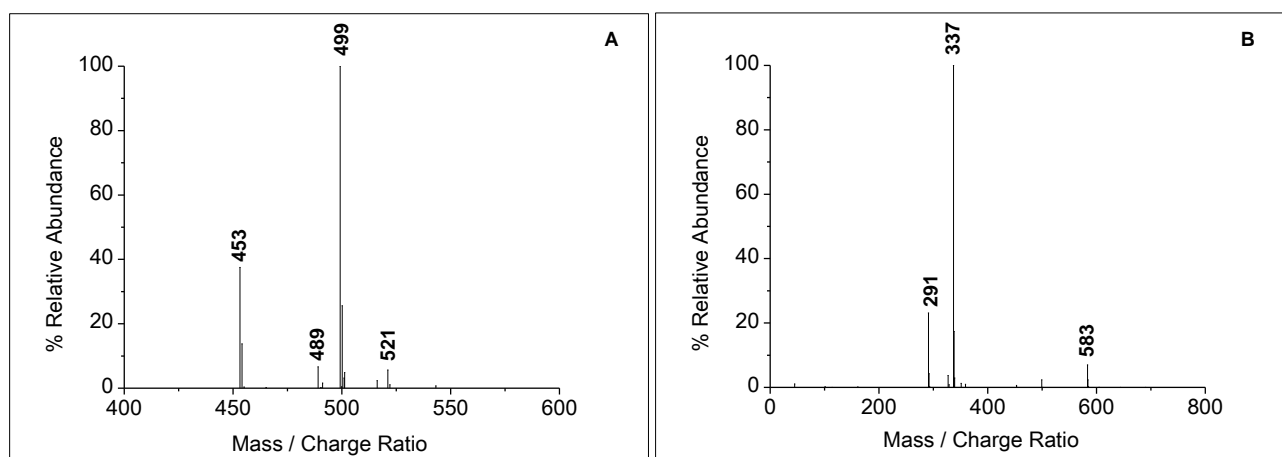
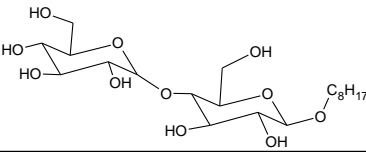
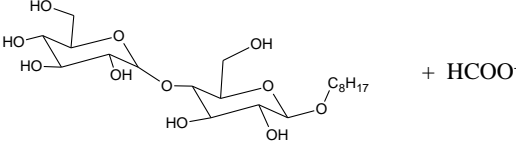
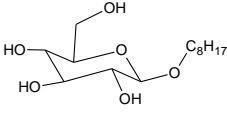
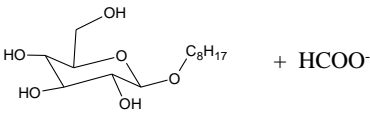


Figure 4.11: Negative scan LC-MS of additive B1 acquired for peak 3 (A) and peak 5 (B).

## Chapter 4: Results and discussion

Table 4.3: Components of additive B1 for peaks 3 and 5.

Experimental m/z	Theoretical m/z	Component structure
453.15	453.50	
499.25	499.53	 + HCOO <sup>-</sup>
291.15	291.36	
337.15	337.39	 + HCOO <sup>-</sup>

The mass spectra in Figure 4.12A and B were acquired from peaks 8 and 10, respectively. In Figure 4.12B, the three peaks at m/z 319, 365 and 639 were related to the anion of decyl glucoside ( $C_{16}H_{32}O_6$ ,  $M_w = 320.22$  g/mol), which was one of the constituents of additive B1 as illustrated in Table 3.2. The ion at m/z 319 matched  $[C_{16}H_{32}O_6 - H]^-$ , while m/z 365 was  $[C_{16}H_{32}O_6 + HCOO]^-$ . The decyl glucoside molecule also showed the dimer formation as indicated by a peak at m/z 639. Precursor ions of peaks 7 and 9 were similar to that of peak 8 in Figure 4.12A, however, their mass spectra (not shown) consisted of other fragments of the glucose unit at m/z 113

In Figure 4.12A, the two abundant peaks at m/z 481 and 527 were attributed to the presence of decyl oligoglucoside,  $C_{22}H_{42}O_{11}$ . The ion at 481 m/z matched the anion  $[C_{22}H_{42}O_{11} - H]^-$  while m/z 527 was due to the adduct formation in the form of  $[C_{22}H_{42}O_{11} + HCOO]^-$ . The mass spectrum of peak 11 was similar to that of peak 10. All the discussed molecular ions of peaks 8 and 10 are as presented in Table 4.4.

## Chapter 4: Results and discussion

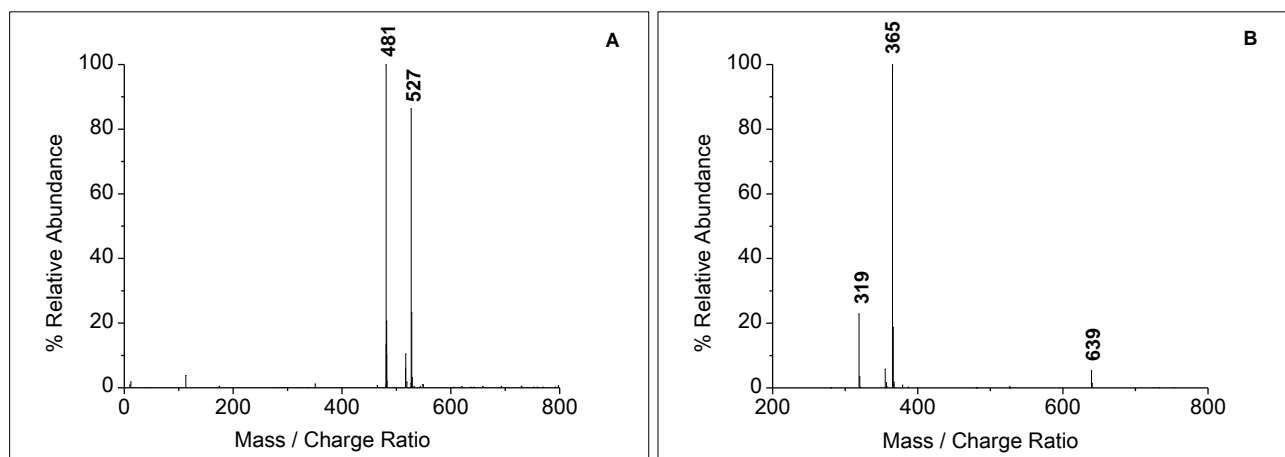
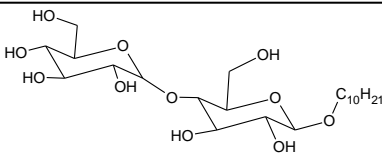
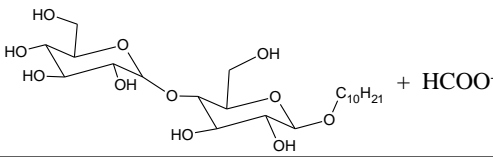
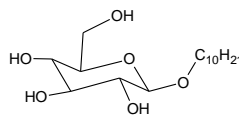
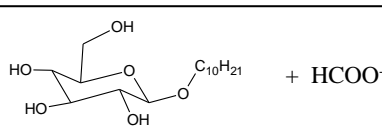


Figure 4.12: Negative scan LC-MS of additive B1 acquired for peak 8 (A) and peak 10 (B).

Table 4.4: Components of additive B1 for peaks 8 and 10.

Experimental m/z	Theoretical m/z	Component structure
481.20	481.55	
527.20	527.58	
319.15	319.41	
365.15	365.44	

Liquid chromatography with a combination of critical conditions and solvent gradient elution was performed on additive B1. Figure 4.13 presents LC-ELSD and positive scan TIC of additive B1 acquired by gradient analysis. The elution was carried out at critical conditions (79.9%/20.1% methanol/water) for the first 10 minutes and the concentration of methanol in the mobile phase was increased up to 100% methanol for the duration of the run. Positive scan TIC showed three peaks (12, 13 and 14) at the retention time of 10 to 30 minutes when gradient elution was employed while only peak 14 was observed on LC-ELSD chromatogram. These peaks were not observed when the analysis was performed at critical conditions at a 50 minutes run time. This phenomenon suggested

the presence of the more non-polar components, which adsorbed strongly to the C<sub>18</sub> stationary phase, causing either a later elution time (> 50 minutes) or no elution at all when analysed at critical conditions.

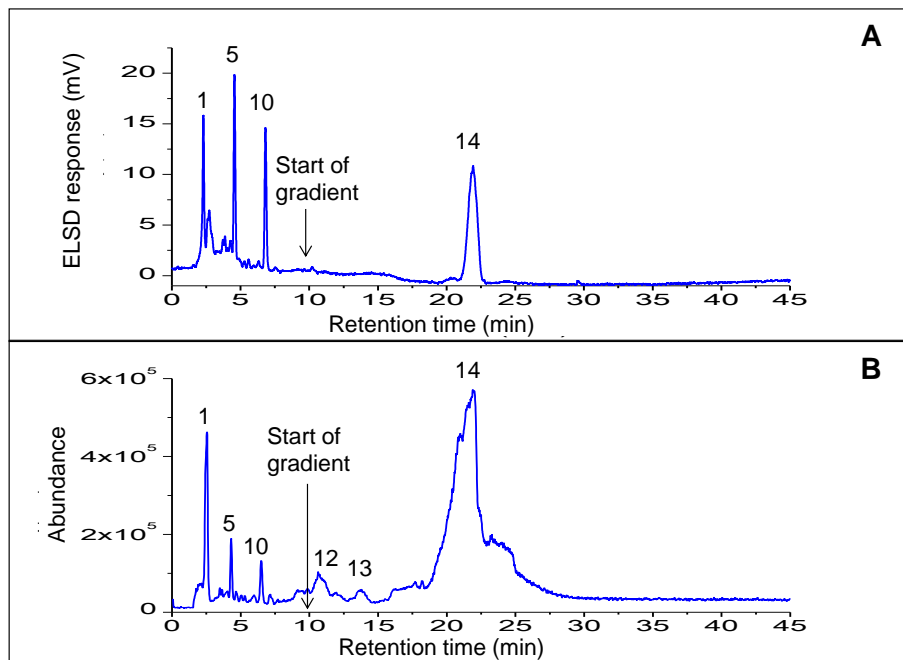


Figure 4.13: LC-ELSD (A) and positive TIC scan (B) of additive B1 acquired using a solvent gradient elution protocol.

Figure 4.14A and B presents the mass spectra acquired for peaks 12 and 13 in gradient analysis mode. In Figure 4.14A, the molecular ion series with  $m/z$  501, 545, 589, 633 etc. corresponded to the protonated ions of poly(ethylene glycol) tridecyl ether phosphate (Figure 4.16A), which was one of the constituents of additive B1 (Table 3.2). The most abundant peak at  $m/z$  633 was matched to  $[M + H]^+$  with eight repeat units, where M is  $C_{13}H_{27}-(OCH_2CH_2)_n-OP(O)(OH)_2=O$ . The molecular ion series with  $m/z$  391, 413, 435 etc. corresponded to the doubly charged species of the PEG tridecyl ether phosphate. The PEG alkyl ether phosphate surfactants are commonly synthesised by reacting the long hydrocarbon chain fatty alcohol ethoxylate with phosphoric acid. These types of surfactants are useful for the stabilization of foams in paints and colourants<sup>7</sup>.

The mass spectrum in Figure 4.14B showed the series  $m/z$  306, 350, 394, 438, 482 etc. The most abundant peak at  $m/z$  482 was attributed to the ammoniated PEG tridecyl ether (Figure 4.16B) with six repeat units, i.e.  $[M + NH_4]^+$ , where M is  $C_{13}H_{27}-(OCH_2CH_2)_n-OH$ .



## Chapter 4: Results and discussion

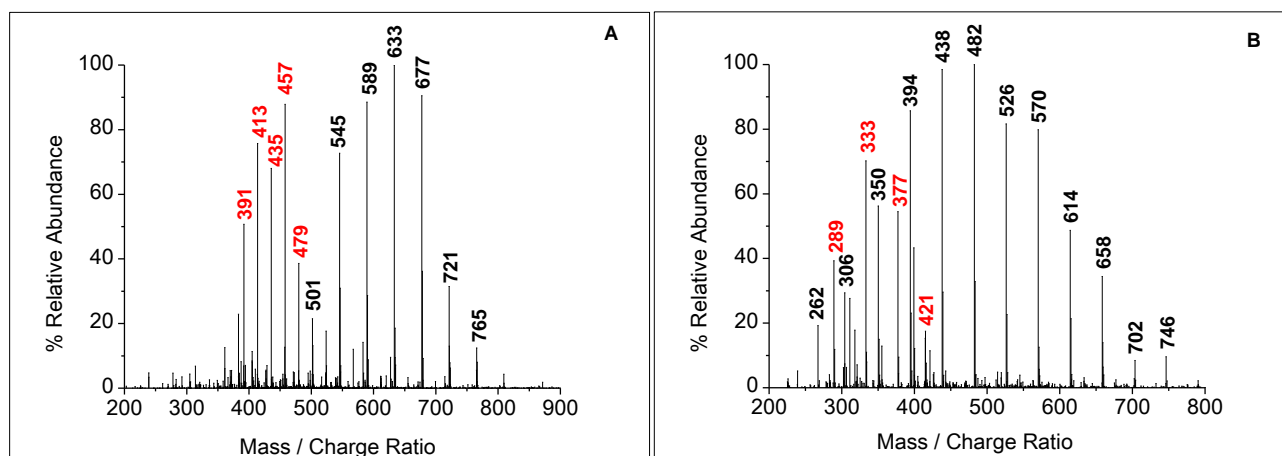


Figure 4.14: Positive scan LC-MS of additive B1 for peaks 12 (A) and 13 (B) acquired using a gradient elution protocol.

The mass spectrum in Figure 4.15 was acquired from peak 14 and it showed the molecular ion series with peaks at  $m/z$  418, 462, 506, 550, 594, etc. This spectrum was attributed to poly(ethylene glycol) monooleyl ether,  $C_{18}H_{35}-(OCH_2CH_2)_n-OH$  (Figure 4.16C) which was also one of the components of additive B1 according to Table 3.2. The abundant peak at  $m/z$  682 was attributed to  $[M + NH_4]^+$  with seven repeat units, where M is  $C_{18}H_{35}-(OCH_2CH_2)_n-OH$ .

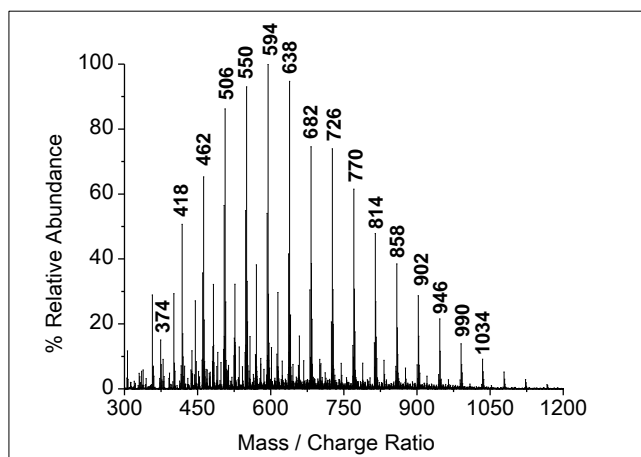


Figure 4.15: Positive scan LC-MS of additive B1 for peak 14 acquired using a gradient elution protocol.

The three components at peaks 12, 13 and 14 have  $C_{13}$  and  $C_{18}$  hydrocarbon chains and when separated on a  $C_{18}$  stationary phase at critical conditions, they were expected to show strong interactions. The analyses for these components by solvent gradient enhanced their elution from the column, as their non-polar interactions were minimized.

## Chapter 4: Results and discussion

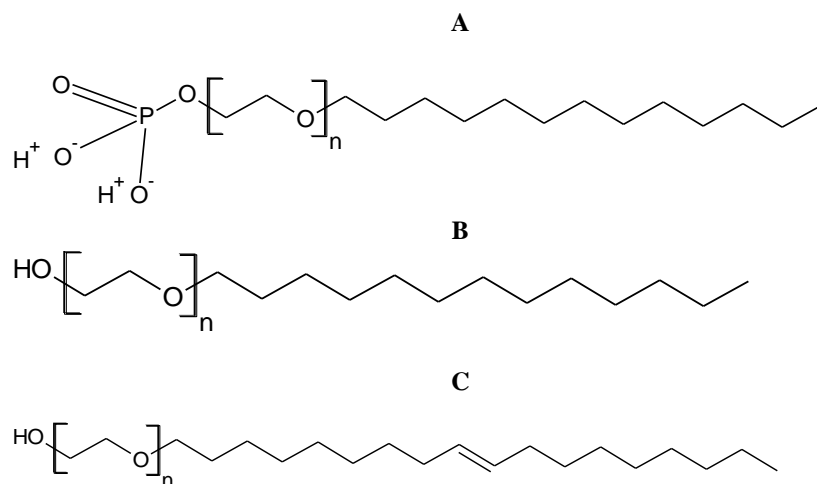


Figure 4.16: Structures of PEG tridecyl ether phosphate (A), PEG tridecyl ether (B) and PEG monooleyl ether (C) detected in additive B1.

The  $^1\text{H}$  NMR in Figures 4.17 (0 to 4 ppm) and 4.18 (4.5 to 8 ppm) were used to confirm the components of additive B1. The methyl and methylene protons of the alkyl chains were observed at 0.83 to 1.50 ppm. The resolution of these peaks was poor due to the presence of more than two components in the additive blend.

A quartet peak at 1.97 ppm was attributed to the allylic proton ( $-\text{C}=\text{C}-\text{CH}$ ) from PEG monooleyl ether (Figure 4.16C) while the vinyl proton ( $-\text{C}=\text{CH}-$ ) was found at 5.31 ppm. The methylene protons from the EO repeat unit were assigned to a peak at 3.51 ppm, while the hydroxyl protons were observed at 4.6 ppm. The peak area integration of a signal at 6.2 ppm showed the presence of two protons which were attributed to a non-polymeric amide ( $\text{H}_2\text{N}-\text{C}=\text{O}$ ) component of additive B1. The amide was further confirmed by a carbonyl ( $-\text{C}=\text{O}$ ) carbon at 162.42 ppm in the  $^{13}\text{C}$  NMR spectrum as well as the  $\text{C}=\text{O}$  ( $1660\text{ cm}^{-1}$ ) and  $\text{C}-\text{N}$  ( $1027\text{ cm}^{-1}$ ) stretching vibrations from FTIR-ATR (both spectra not shown).

A doublet at 4.58 ppm was attributed to the proton from the  $-\text{O}-\text{CH}-\text{O}$  group, as shown by position 6 in the decyl glucoside structure. The other protons arising from the glucose unit were observed at positions 1 to 5.

## Chapter 4: Results and discussion

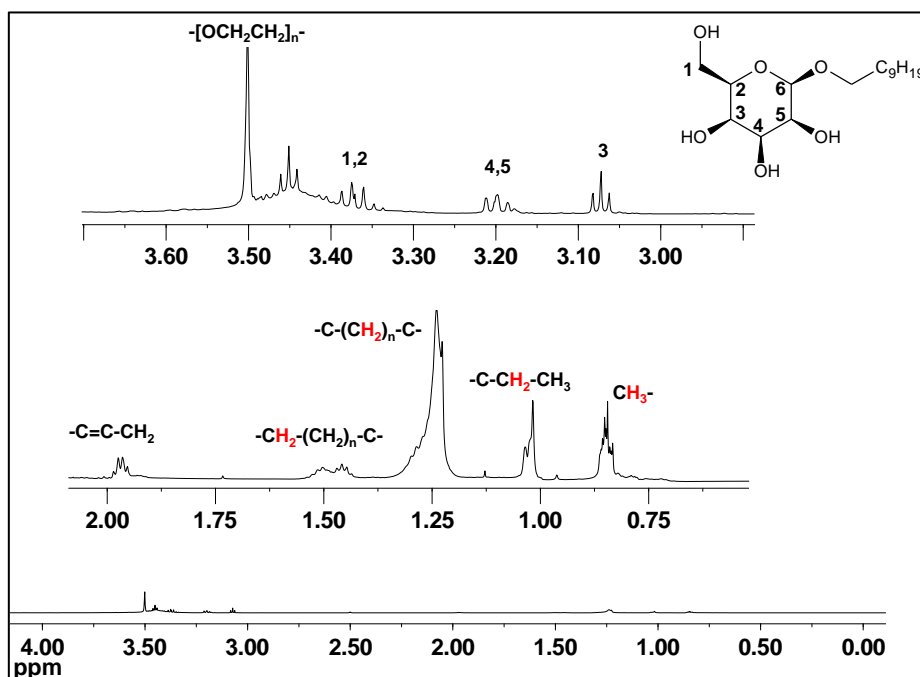


Figure 4.17:  $^1\text{H}$  NMR spectrum of additive B1 in DMSO,  $25^\circ\text{C}$ , 600 MHz at 0 to 4 ppm.

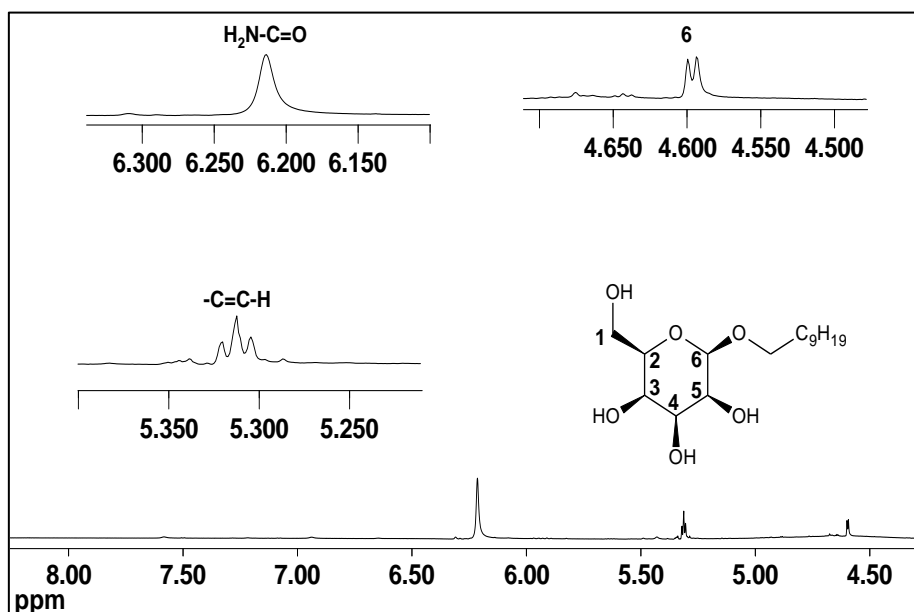
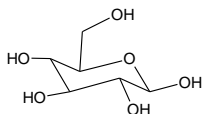
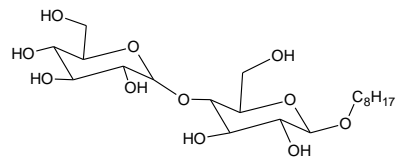
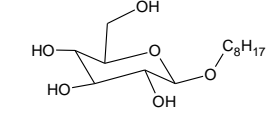
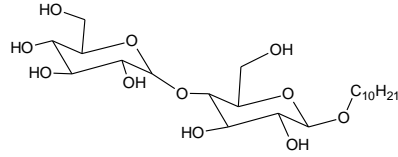
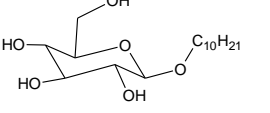
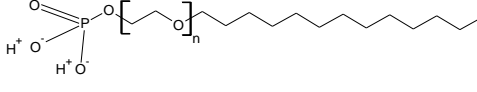
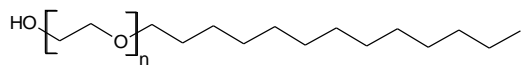
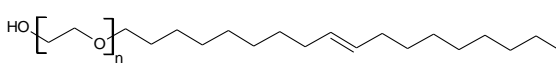


Figure 4.18:  $^1\text{H}$  NMR spectrum of additive B1 in DMSO,  $25^\circ\text{C}$ , 600 MHz at 4.5 to 8 ppm.

Table 4.5 shows a summary of the components detected in additive B1 by LC-MS and NMR. The molar mass was calculated from the most abundant peak of the mass spectra.

*Table 4.5: Summary of the components of additive B1.*

Peak No.	Molecular Structures	Average no. of repeat units	M <sub>p</sub> (g/mol)
1		N/A	180
2		2	454
5		N/A	292
7		2	482
10		N/A	320
12		8	633
13		6	464
14		7	576

**4.3.2.2. Analyses of additive B2**

Figure 4.19 shows LC-ELSD, positive and negative TIC scans of additive B2 acquired at critical conditions of adsorption of PEG. The ELS detector (A) indicated a larger peak area for peak 2 compared to peak 1, suggesting the higher concentration of the peak 2 component. Both components were further detected by the positive (B) and the negative (C) TIC scans. The presence of the two peaks in the negative scan suggested some anionic character for the components of the additive.

## Chapter 4: Results and discussion

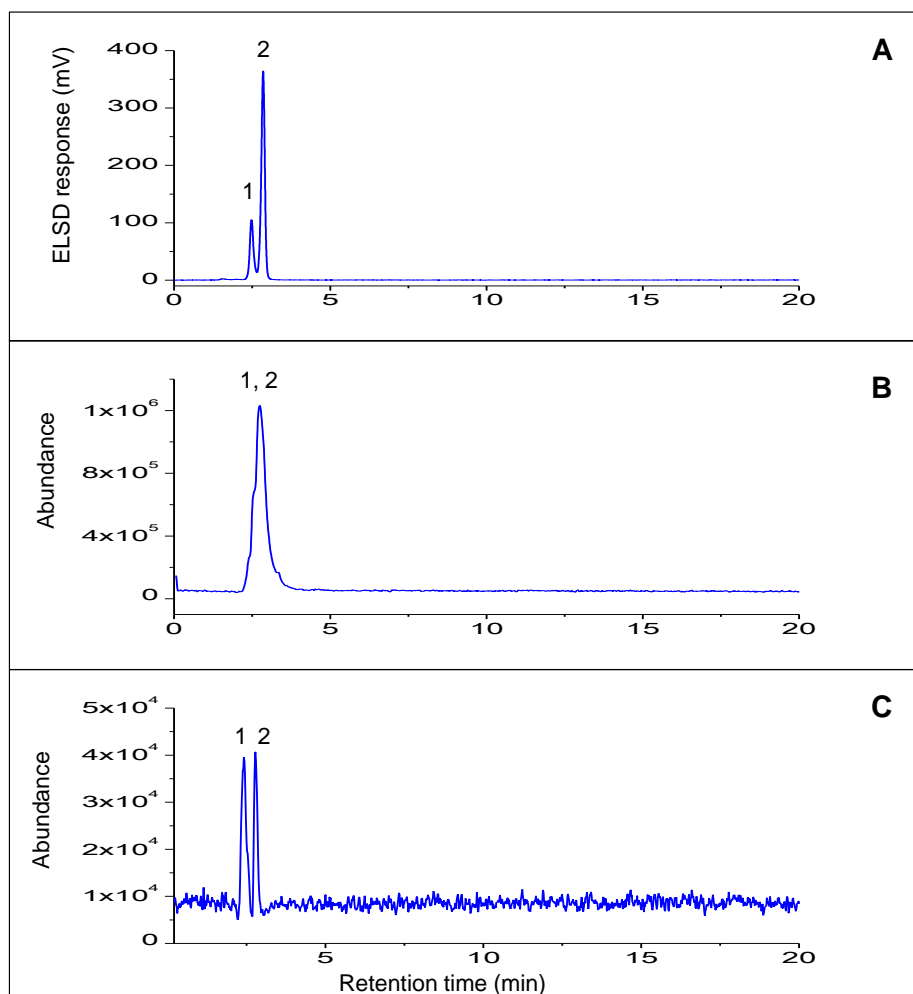


Figure 4.19: LC-ELSD (A), positive (B) and negative (C) TIC scans of additive B2.

The mass spectra in Figure 4.20 were acquired in the negative and positive mode for peaks 1 and 2, respectively. The characteristic peaks at  $m/z$  73, 101, 113, 143, 161 and 179 from peak 1 were attributed to the presence of glucose anions as illustrated in Figure 4.10. The characterization of additive B1 in Section 4.3.2.1 had verified that peaks at  $m/z$  73, 101, 113, 143 and 161 were from the fragmentation of the glucose molecule while  $m/z$  179 was the parent glucose anion.

It was noted in Figure 4.20A that peaks at  $m/z$  179, 221, 341, 503 and 664 matched the product ions arising from the cross-ring ( $m/z$  221) and glycosidic ( $m/z$  341, 503 and 664) bond cleavages of an oligoglucoside. This finding was first introduced by Domon and Costello in 1988 and was further supported by other authors<sup>8,9</sup>. They proposed that when low-energy collision was employed during mass spectral analyses; polyglucoside became subjected to glycosidic bond cleavages, which formed various product ions shown by B, C, Y and Z (Figure 4.21). Alternatively, at high collision conditions cross-ring cleavages were formed, as shown by A and X in Figure 4.21<sup>9</sup>. The formation of either a glycosidic or cross-ring cleavage depended on whether the precursor ion was cationic,

anionic, protonated or metallated. The cross-ring cleavages were mostly favoured when the precursor ion was a sodium adduct<sup>9-12</sup>.

The mass spectrum in 4.20B showed the  $[M + NH_4]^+$  molecular ion series with peaks at  $m/z$  314, 358, 402, 446, 490 etc. A peak-to-peak mass difference of 44 Da confirmed the EO repeat unit. The parent ion of this series was identified as poly(ethylene glycol) monomethyl ether, with the molecular formula:  $CH_3-(OCH_2CH_2)_n-OH$ . This component was also detected in the negative mode. A comparison between the experimental and theoretical values of the most abundant ion are as shown:

$$(m/z)_{\text{experimental}} = 490.40$$

$$(m/z)_{\text{theoretical}} = 18.0385 + 10 \cdot 44.0526 + (15.0345 + 17.0073) = 490.61$$

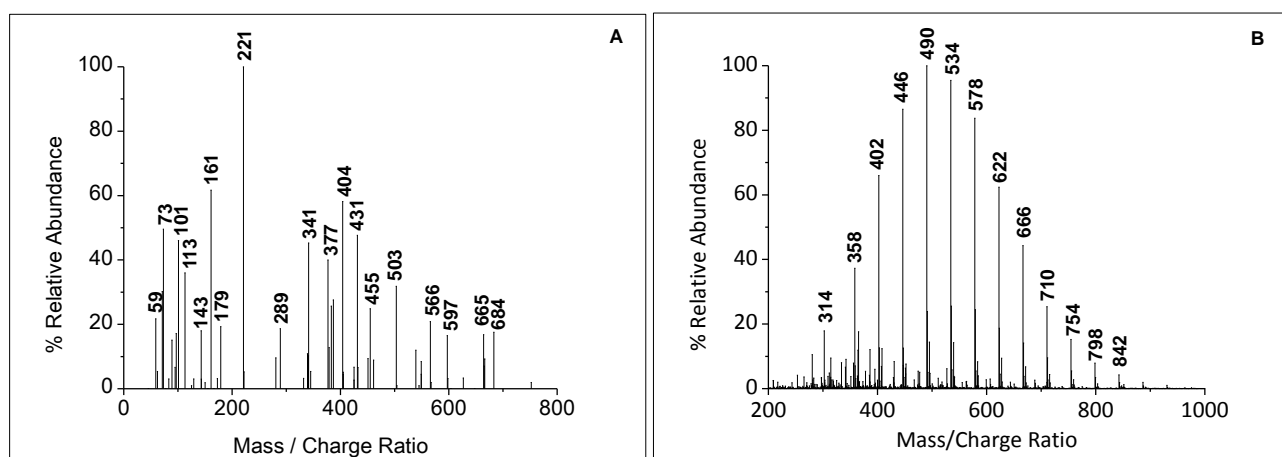


Figure 4.20: Negative (A) and positive (B) LC-MS spectra of additive B2 for peak 1 and peak 2, respectively.

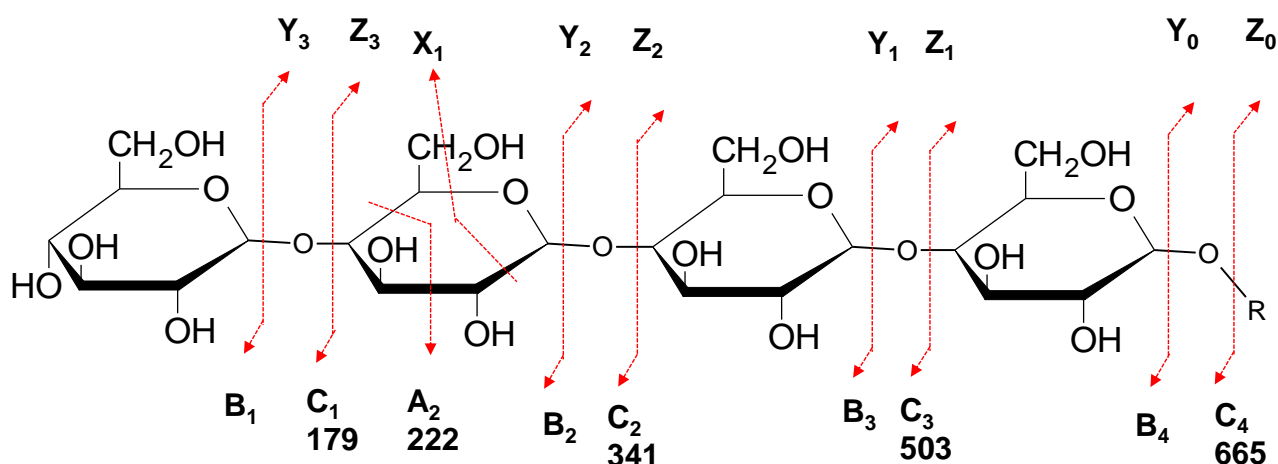


Figure 4.21: Fragmentation pattern of oligoglucoside, showing the molar mass of precursor ions.

## Chapter 4: Results and discussion

The  $^1\text{H}$  NMR spectra of additive B1 in Figures 4.22 and 4.23 are plotted at the chemical shift regions of 0 to 4 ppm and 4.5 to 13 ppm, respectively. In Figure 4.22, the methine protons at positions 3, 4 and 5 in the glucose unit were assigned at 3.06 to 3.21 ppm. The peak observed at 3.24 ppm (position 1) was assigned to the  $\text{CH}_3\text{O}-$  protons from the  $\text{CH}_3-(\text{OCH}_2\text{CH}_2)_n\text{-OH}$  polymer. The water peak at 3.37 ppm was due to hydrogen-deuterium exchange. The methylene protons from the EO repeat unit (position 4) were assigned at 3.51 ppm while the protons at positions 2, 3, 5 and 6 of the PEG monomethyl ether were expected in the region of 3.39 to 3.48 ppm.

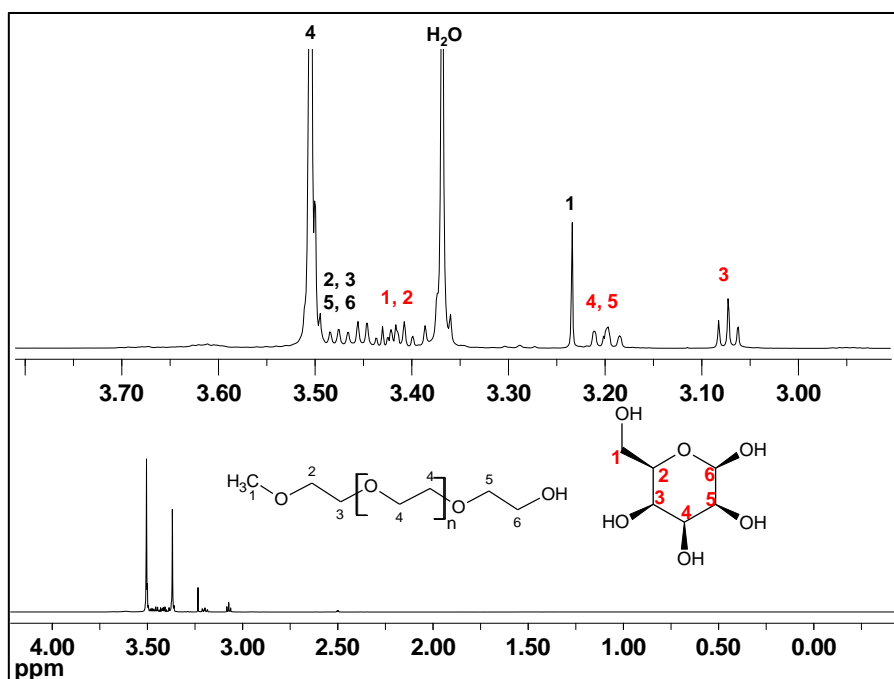


Figure 4.22:  $^1\text{H}$  NMR spectrum of additive B2 in DMSO,  $25^\circ\text{C}$  and 600 MHz at a chemical shift region of 0 to 4 ppm.

In Figure 4.23, the presence of oligoglucoside was confirmed by a multiplet at 4.32 to 5.00 ppm. An oligoglucoside structure consists of multiple repeat units of the glucose molecule (Figure 4.24A). A glucose molecule has five hydroxyl groups per unit, while subsequently linked molecules have four hydroxyl groups. The multiplet at 3.39 to 3.48 ppm was attributed to the hydroxyl protons on the inter-linked glucose molecules. The methine group (position 6) was assigned at the chemical shift of 5.25 to 5.50 ppm. The presence of this peak at a higher chemical shift was due to the influence of the higher electronegativity of the oxygen atom. The peak area integration of peak 6 indicated that there are four -CH- groups, suggesting oligoglucoside with four glucose repeat units. Further evidence of the presence of the four inter-linked glucose units was confirmed by the anions at  $m/z$  665 (16% abundance) and  $m/z$  666 (9% abundance) in the negative scan LC-MS in Figure 4.20A.

## Chapter 4: Results and discussion

LC-MS and NMR assignments of oligoglucoside in additive B2 were in agreement with publications from various authors<sup>13–16</sup>.

The other peaks at 6.22, 6.33 and 6.67 ppm in Figure 4.23 were attributed to the non-polymeric components that were possibly added during the polymerization of additive B2. The peak at 6.22 ppm was identified by the  $^1\text{H}$  NMR,  $^{13}\text{C}$  NMR and FTIR-ATR techniques as an amide-type component ( $\text{H}_2\text{NCOR}$ ). The two separate peaks at 6.33 and 6.67 ppm could not be accurately assigned, however they are also present in the chemical shift region of an amide-type component.

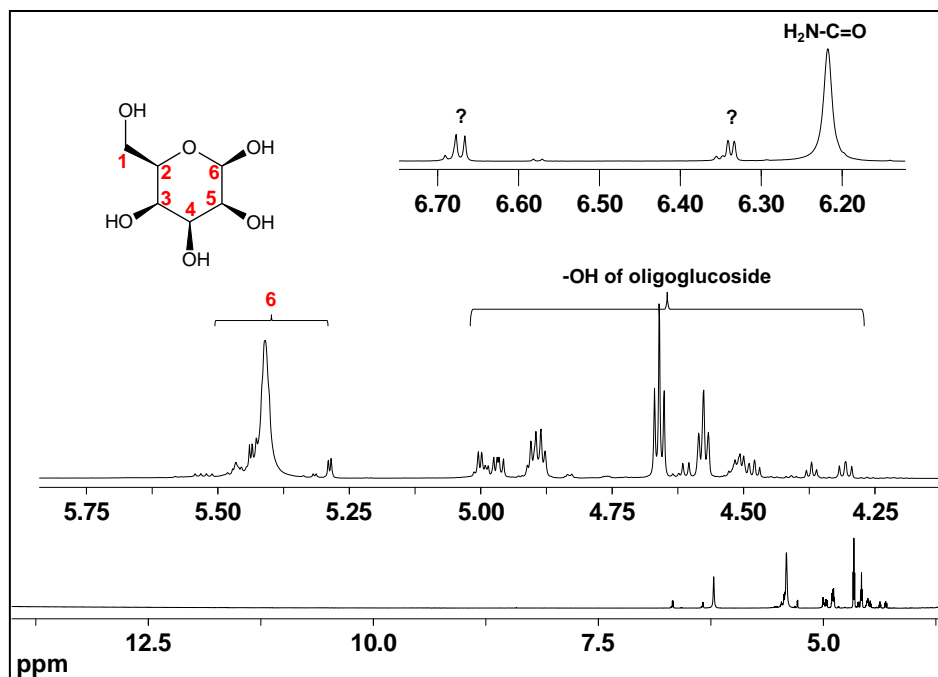


Figure 4.23:  $^1\text{H}$  NMR spectrum of additive B2 in DMSO, 25°C and 600 MHz at chemical shift region of 4.5 to 13 ppm.

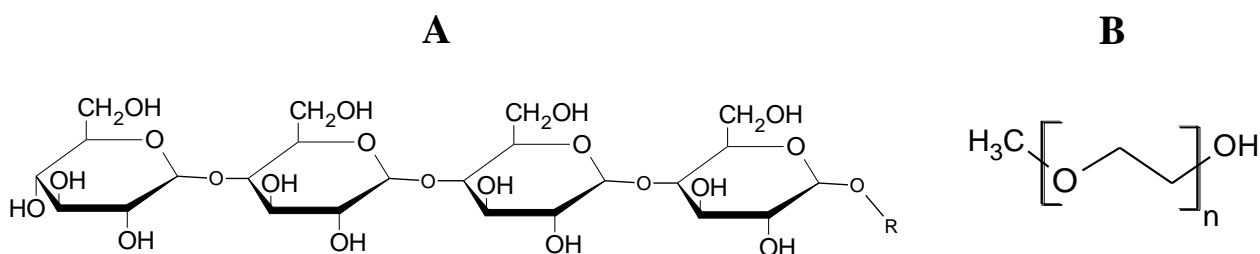


Figure 4.24: Structures of oligoglucoside (A) and PEG monomethyl ether (B) for additive B2.



## Chapter 4: Results and discussion

The molar mass obtained from LC-MS ( $M_p$ ) and  $^1\text{H}$  NMR ( $M_n$ ) was evaluated by using the peak areas of the ethylene oxide repeat unit (3.51 ppm) and the methyl group (3.24 ppm) from peaks 4 and 1, respectively as shown in Figure 4.22. The  $^1\text{H}$  NMR showed  $M_n$  of 502 g/mol with 11 repeat units while the  $M_p$  value obtained from LC-MS in Figure 4.20 was 472 g/mol at 10 repeat units.

*Table 4.6: Molar mass of additive B2 obtained from  $^1\text{H}$  NMR and LC-MS.*

Moiety	No. of protons	Chemical shift (ppm)	Peak area	$M_n$ ( $^1\text{H}$ NMR) g/mol	$M_p$ (LC-MS) g/mol
$-(\text{CH}_2\text{CH}_2\text{O})_n-$	4	3.51	131131.2	502 with 11 repeat units	472 with 10 repeat units
$\text{CH}_3\text{O}-$	3	3.24	9208.11		

The results showed that additive B2 consists of oligoglucoside with four glucose repeat units and a molar mass of 666 g/mol. The  $^1\text{H}$  NMR confirmed that the additive also contains poly(ethylene glycol) monomethyl ether with an average of 11 EO repeat units and an average molar mass of 502 g/mol.

#### 4.3.2.3. Analyses of additive B3

The results in Figures 4.25 to 4.28 for additive B3 were analysed at critical conditions of adsorption of PEG. The LC-ELSD and LC-TIC chromatograms in Figure 4.25 both indicated a single peak at the elution time of 2.6 minutes.

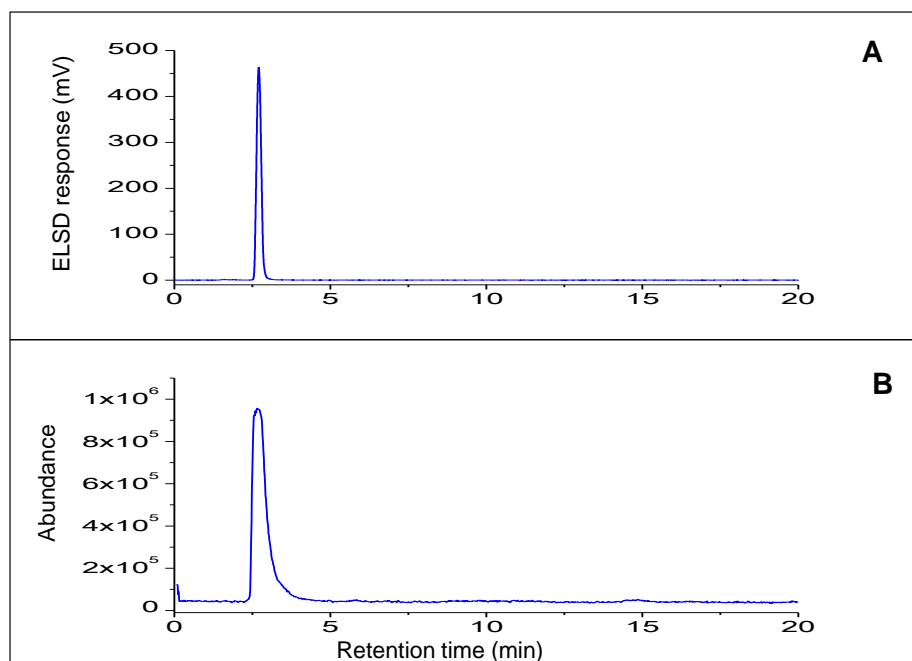


Figure 4.25: LC-ELSD (A) and positive scan TIC (B) of additive B3.

The mass spectra of additive B3 were acquired with a mobile phase that contained various concentrations of the ionizing agent ( $\text{HCOONH}_4$ ). In Figure 4.26A, a concentration of  $2.5 \times 10^{-3}$  mol/L of  $\text{HCOONH}_4$  was used and three molecular ion distributions were observed, suggesting the presence of three different cations. The first series, highlighted in red consisted of peaks at  $m/z$  203, 247, 291, 335 etc. The blue series had peaks at  $m/z$  225, 269, 313 etc., while the black molecular ion series showed  $m/z$  300, 374, 418 etc. A repeat unit of 44 Da in each of the molecular ion series confirmed the presence of EO.

In Figure 4.26B, there was no  $\text{HCOONH}_4$  added to the mobile phase. This was performed to identify which of the molecular ion series was ammoniated:  $[\text{M} + \text{NH}_4]^+$ , protonated:  $[\text{M} + \text{H}]^+$  or sodiated:  $[\text{M} + \text{Na}]^+$ . When the ionising agent was eliminated from the mobile phase, the black series (i.e.  $m/z$  300, 374, 418 etc.) was not observed in the mass spectrum; which confirmed it as the  $[\text{M} + \text{NH}_4]^+$  ion series. Both the red ( $m/z$  203, 247, 291, 335 etc.) and the blue ( $m/z$  225, 269, 313 etc.) series were present in both the mass spectra obtained with and without  $\text{HCOONH}_4$ .

The two peaks at  $m/z$  89 and 133 in Figure 4.26A confirmed the hydroxyl group as one of the polymer end groups. According to the known chemical structures in Table 3.2, additive B3 was made up of glycerol ethoxylate (Figure 4.27), which is a three-arm, star-shaped PEG. These types of polymers are known to have better water solubility and chemical stability compared to the linear PEGs<sup>17,18</sup>.

## Chapter 4: Results and discussion

The most abundant peaks at  $m/z$  313, 335 and 418 in Figure 4.26 A were assigned to the following ion adducts:  $[M + H]^+$ ,  $[M + Na]^+$  and  $[M + NH_4]^+$ , respectively; where M is glycerol ethoxylate. The  $[M + NH_4]^+$  peak at  $m/z$  418 consisted of a total of seven EO repeat units, which corresponded to the sum of a, b and c EO units in Figure 4.27.

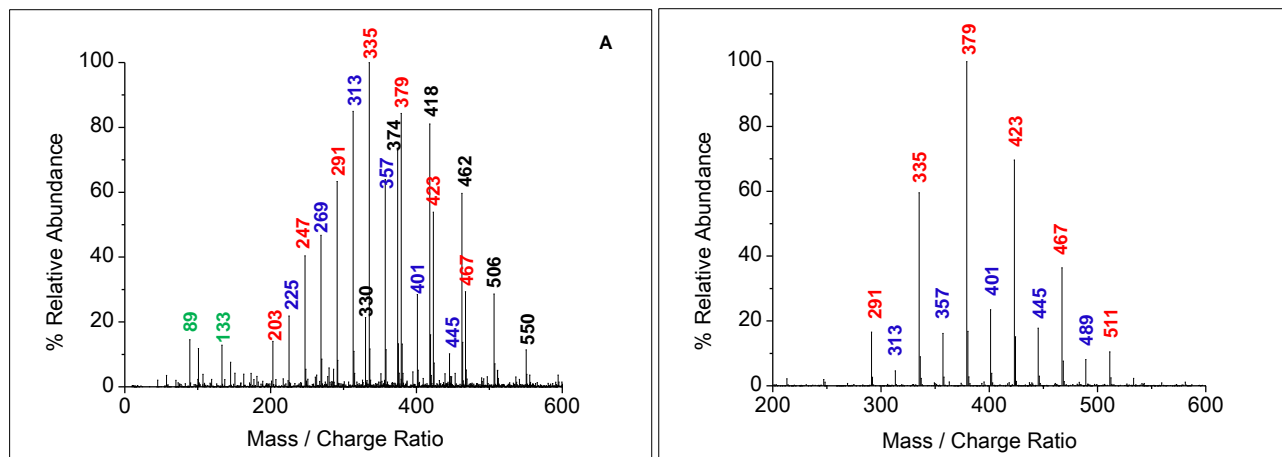


Figure 4.26: Positive scan LC-MS of additive B3 using  $2.5 \times 10^{-3}$  mol/L (A) and zero mol/L (B) ammonium formate.

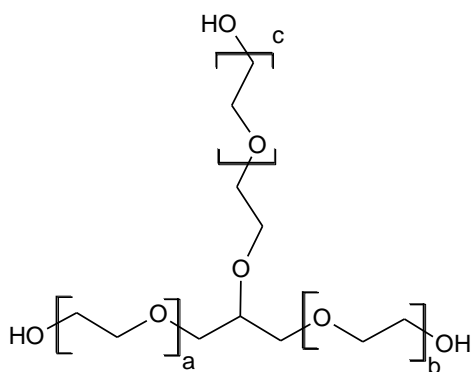


Figure 4.27: Structure of glycerol ethoxylate.

The  $^1\text{H}$  NMR spectrum in Figure 4.28 showed a multiplet at a chemical shift region of 4.56 to 4.77 ppm which was attributed to the three hydroxyl groups in the glycerol ethoxylate structure. A high intensity singlet at 3.35 ppm was assigned to the exchange of the water protons with the deuterium from DMSO. The methine proton ( $-\text{CH}-$ ) was observed by a quintet at 3.69 ppm, shown by position 4. The methylene protons of the EO repeat unit were assigned at 3.51 ppm (position 2) while the methylene protons at positions 3, 5, 6 and 7 were observed at 3.4 to 3.49 ppm.

## Chapter 4: Results and discussion

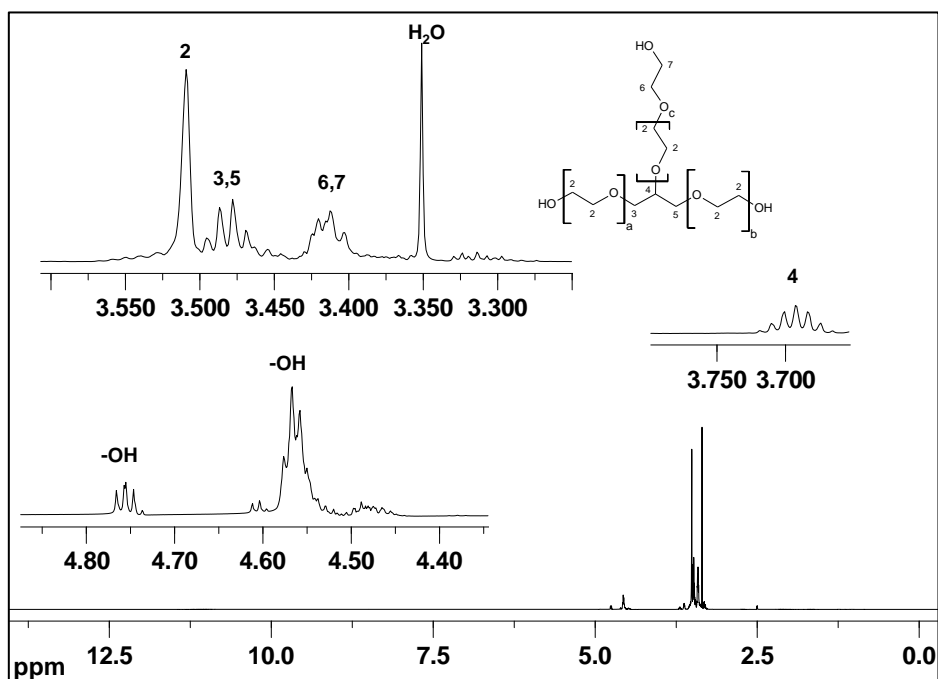


Figure 4.28:  $^1\text{H}$  NMR of additive B3 in DMSO,  $25^\circ\text{C}$  and 600 MHz.

The number of repeat units ( $n_x$ ) and number-average molar mass ( $M_n$ ) were calculated similar to additive A2 using peak areas and number of protons of  $-(\text{OCH}_2\text{CH}_2)_n-$  (peak 2) and  $-\text{CH}-$  (peak 4) as moieties x and y, respectively.

The results in Table 4.7 showed seven EO repeat units, with  $M_n$  and  $M_p$  of 400 g/mol.

Table 4.7: LC-MS versus  $^1\text{H}$  NMR molar masses of glycerol ethoxylate in additive B3.

Moiety	No. of protons	Chemical shift (ppm)	Peak area	$M_n$ ( $^1\text{H}$ NMR) g/mol	$M_p$ (LC-MS) g/mol
$-(\text{CH}_2\text{CH}_2\text{O})_n$	4	3.51	91508.68	402 with 7 repeat units	400 with 7 repeat units
$-\text{CH}-$	1	3.69	3255.15		

In summary, LC-MS and  $^1\text{H}$  NMR confirmed that additive B3 is a glycerol ethoxylate, which is a star-shaped PEG having three poly(ethylene oxide) (PEO) arms. The polymer consists of a total average of seven EO repeat units and an average molar mass of 400 g/mol.

### 4.3.3. Characterization of type C additives

The results that follow are the LC-ELSD, LC-UV, LC-MS, NMR and FTIR-ATR of type C additives. These are mostly the non-ionic, anionic, cationic or amphoteric surfactants that are used as wetting and dispersing agents in colourant formulations.

#### 4.3.3.1. Analyses of additives C1 and C2

Figures 4.29 to 4.34 present the components identified in additive C1 when analysed at critical conditions of adsorption of PEG. The LC-UV chromatogram acquired at 230 nm (A) showed a weak PEG signal (peak 1) at the retention time of 2.6 minutes as well as peak 4 with a larger peak area. The positive scan TIC indicated a total of six peaks compared to only two peaks in the LC-UV chromatogram. This was attributed to the sensitivity of the MS to detect other oligomers of additive C1 compared to the UV detector. Furthermore, PEG at peak 1 was not UV-detectable as it contained no chromophores.

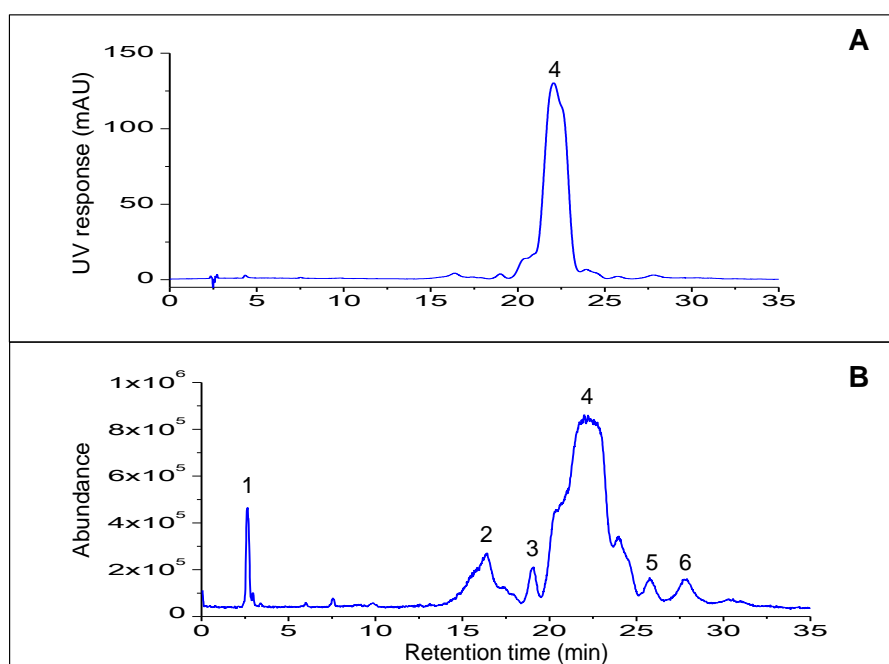


Figure 4.29: LC-UV at 230 nm (A) and positive scan TIC (B) of additive C1.

The mass spectrum in Figure 4.30 was acquired at peak 1. There were two molecular ion series observed with peaks at  $m/z$  344, 388, 432 etc (black) as well as  $m/z$  401, 423, 445, 467, 51 etc (red). The peak-to-peak mass difference of 44 Da in the black series confirmed EO repeat units while the red series showed a difference of 22 Da between the subsequent peaks. The black series was attributed to PEG:  $[M + NH_4]^+$ , where M is  $H-(OCH_2CH_2)_n-OH$ . The red series was attributed to the

## Chapter 4: Results and discussion

doubly charged species such as  $[M + z_1 + z_2]^{2+}$ , involving two cations; where  $z_1$  and  $z_2$  are possibly  $H^+$  and  $Na^+$ . The presence of the cations  $z_1$  and  $z_2$  was evaluated by varying the concentration of  $HCOONH_4$  from  $5 \times 10^{-3}$  mol/L to  $1 \times 10^{-3}$  mol/L and there was a little effect observed on the peak intensity of the doubly charged series, indicating the dominance of the  $z_1$  and  $z_2$  cations as the alternative ionizing agents in the solution.

Using the most abundant peak of the series:  $[M + NH_4]^+$ , the experimental versus theoretical calculations are as follows:

$$(m/z)_{\text{experimental}} = 564.35$$

$$(m/z)_{\text{theoretical}} = 18.0385 + 12 \times 44.0526 + (1.0079 + 17.0073) = 564.68$$

The peak at  $m/z$  564 was therefore attributed to the ammoniated  $H-(OCH_2CH_2)_n-OH$  with 12 repeat units.

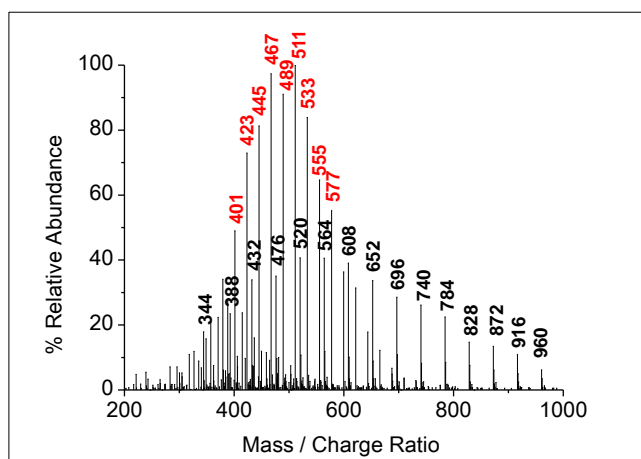


Figure 4.30: Positive scan LC-MS of additive C1 for peak 1.

The mass spectra in Figure 4.31A and B were acquired from peaks 2 and 3, respectively. Both spectra showed the EO repeat unit. The peak at  $m/z$  576 in Figure 4.31A showed a difference of 14 Da compared to  $m/z$  590 in Figure 4.31B, for the same number of repeat units. This suggested the presence of an additional  $-CH_2-$  in the polymer chain.

According to Table 3.2, one of the components of additive C1 is nonylphenol ethoxylate with a structure shown in Figure 4.33B. Using this information and the fact that the separation of polymers at critical conditions of adsorption occurs according to the differences in polarity and hydrophobicity, the polymers with a shorter carbon chain were expected to elute at an earlier retention time. As a result, the molecular ion at  $m/z$  576 in Figure 4.31A was assigned to the ammoniated octylphenyl-PEG with eight EO repeat units:  $(C_8H_{17}-C_6H_4-(OCH_2CH_2)_n-OH)$ . The

## Chapter 4: Results and discussion

theoretical calculations are as shown, using the molar masses of the octylphenyl and hydroxyl end groups.

$$(m/z)_{\text{experimental}} = 576.50$$

$$(m/z)_{\text{theoretical}} = 18.0385 + 8 \cdot 44.0526 + (189.3165 + 17.0073) = 576.78$$

The molecular ion at  $m/z$  590 in Figure 4.31B corresponded to the ammoniated nonylphenyl-PEG with eight EO repeat units ( $\text{C}_9\text{H}_{19}\text{-C}_6\text{H}_4\text{-(OCH}_2\text{CH}_2)_n\text{-OH}$ ).

$$(m/z)_{\text{experimental}} = 590.40$$

$$(m/z)_{\text{theoretical}} = 18.0385 + 8 \cdot 44.0526 + (203.3431 + 17.0073) = 590.81$$

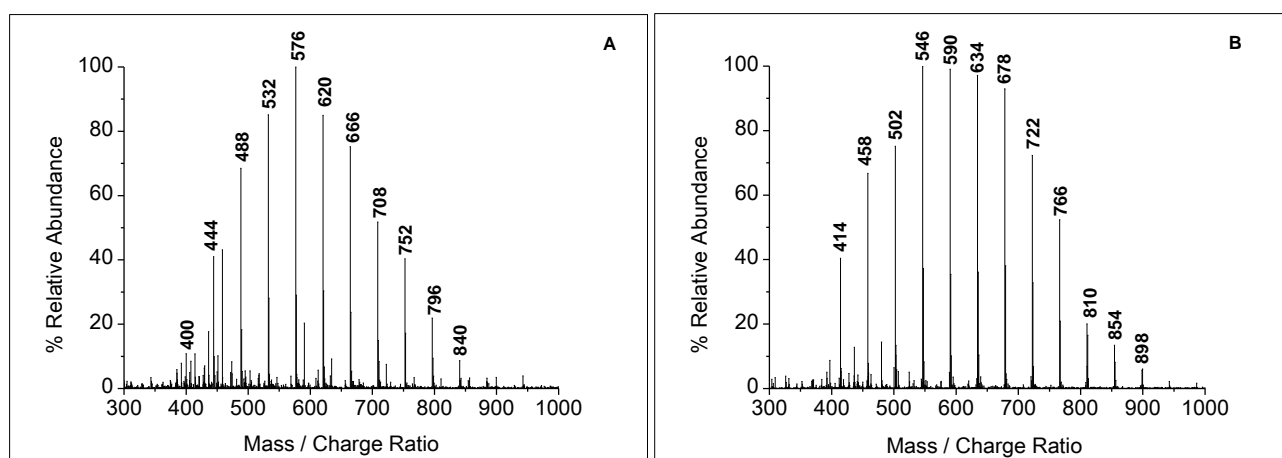


Figure 4.31: Positive scan LC-MS of additive C1 for peak 2 (A) and peak 3 (B).

The mass spectrum in Figure 4.32A was acquired from peak 4, which had the largest peak area on the TIC scan. The molecular ion at  $m/z$  590 was assigned to nonylphenyl-PEG with eight repeat units: ( $\text{C}_9\text{H}_{19}\text{-C}_6\text{H}_4\text{-(OCH}_2\text{CH}_2)_n\text{-OH}$ ) as shown:

$$(m/z)_{\text{experimental}} = 590.40$$

$$(m/z)_{\text{theoretical}} = 18.0385 + 8 \cdot 44.0526 + (203.3431 + 17.0073) = 590.81$$

Similarly, the peak at 604  $m/z$  in Figure 4.32B was matched to decylphenyl-PEG with eight repeat units: ( $\text{C}_{10}\text{H}_{21}\text{-C}_6\text{H}_4\text{-(OCH}_2\text{CH}_2)_n\text{-OH}$ ).

$$(m/z)_{\text{experimental}} = 604.40$$

$$(m/z)_{\text{theoretical}} = 18.0385 + 8 \cdot 44.0526 + (217.3697 + 17.0073) = 604.84$$

## Chapter 4: Results and discussion

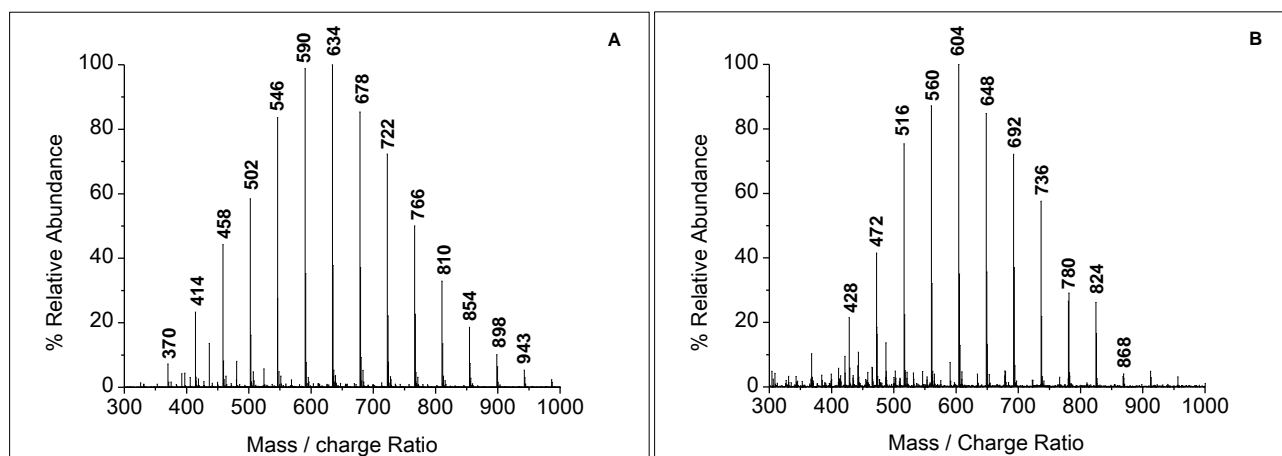


Figure 4.32: Positive scan LC-MS of additive C1 for peak 4 (A) and peak 6 (B).

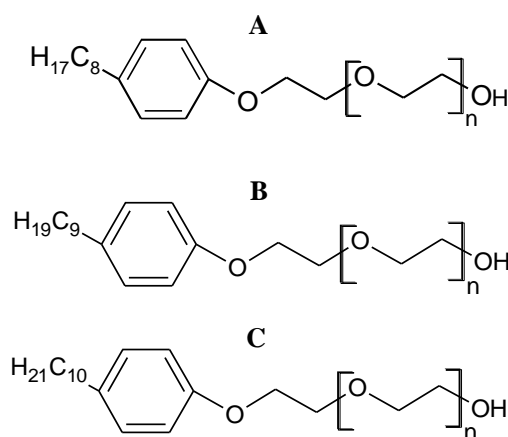


Figure 4.33: Structures of octylphenyl-, nonylphenyl- and decylphenyl-PEG.

The  $^1H$  NMR of additive C1 in Figure 4.34 showed two separate multiplets in the aromatic region at 7.18 and 6.85 ppm, confirming the phenyl protons. The peak at 3.51 ppm (position 2) was assigned to the methylene protons of the EO repeat unit. The two peaks at 3.72 and 4.04 ppm were attributed to the  $-CH_2CH_2-$  attached to the phenolic oxygen atom as shown by positions 5 and 6, respectively. A broad peak at 4.57 ppm was assigned to the hydroxyl ( $-OH$ ) group. The two methylene protons at positions 2 and 3 were assigned to the signals at 3.41 and 3.58 ppm, respectively. The proton exchange peak at 3.33 ppm was due to the formation of HDO.

The complex peaks arising from the alkyl protons were observed at the chemical shift range of 0.42 to 1.75 ppm. These multiplets were attributed to the methyl and methylene protons from the octyl, nonyl and decyl hydrocarbon chains. The complexity of these peaks at this region suggested the presence of branched methyl components as shown by the structure in Figure 4.34. The branching



## Chapter 4: Results and discussion

in alkylphenyl structure arises from the synthesis route during the production process. When alkylphenols are synthesized from the reaction of alpha-olefins and an aromatic ring, the formed products are a mixture of linear and branched isomers<sup>19</sup>.

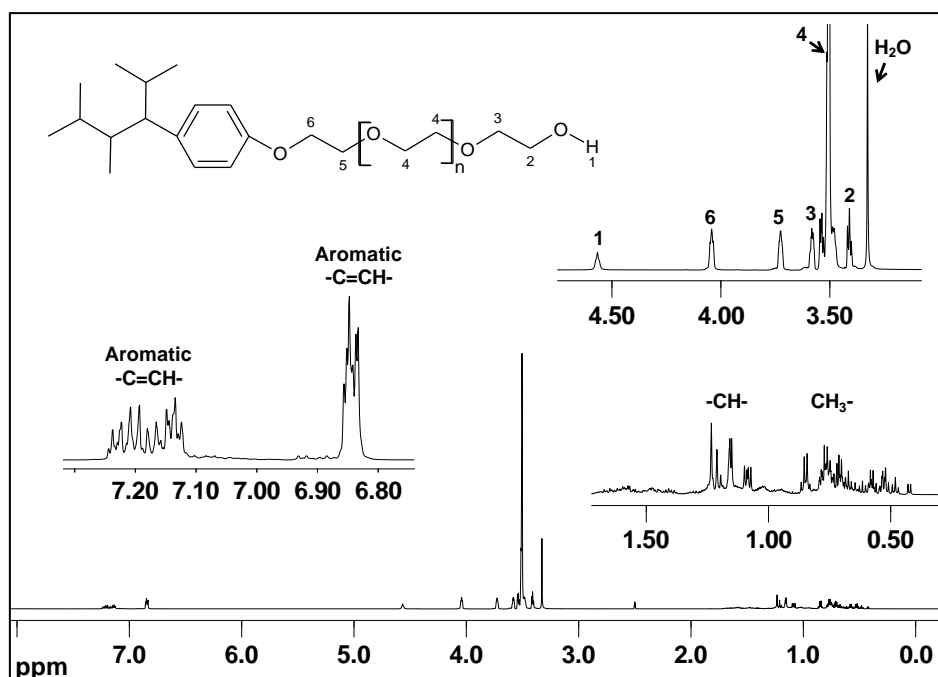


Figure 4.34: <sup>1</sup>H NMR spectrum of additive C1 in DMSO, 25°C and 600 MHz.

The results of additive C1 showed that it consists of a PEG with an average of 12 EO repeat units and an average molar mass of 546 g/mol. The major component is nonylphenyl ethoxylate with an average molar mass of 572 g/mol and eight EO repeat units. The additive also consists of octyl and decyl phenyl ethoxylate components, both with an average of eight EO repeat units. NMR studies showed the presence of branching in the octyl, nonyl and/or decylphenyl hydrocarbon chains. The characterization of additive C2 was performed similarly to additive C1. The results showed that both additives contain components with the same chemical structures.

#### 4.3.3.2. Analyses of additive C3

In Figure 4.35 of additive C3, both the ELSD and TIC showed component 1 with a larger peak area while component 2 was only detected by the mass spectrometer, when analysed at critical conditions of PEG.

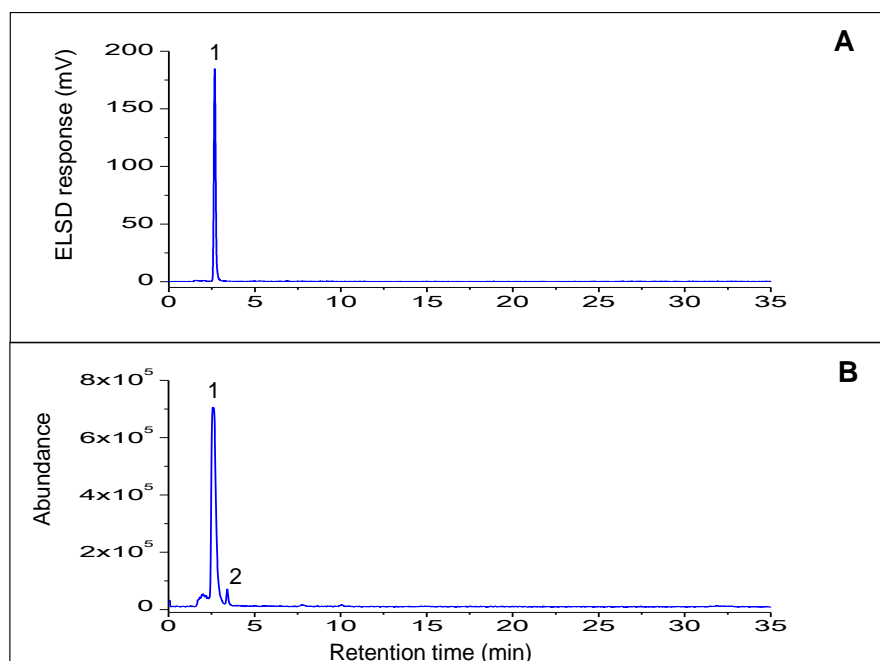


Figure 4.35: LC-ELSD (A) and positive scan TIC (B) of additive C3 acquired at critical conditions.

The mass spectra of additive C3 for peaks 1 and 2 are shown in Figure 4.36A and B, respectively. In spectrum A, three molecular ion series highlighted in blue ( $m/z$  225, 269, 313 etc), red ( $m/z$  247, 291, 335 etc.) and black ( $m/z$  330, 374, 418 etc.) were observed. Each series showed the presence of EO repeat units and these were attributed to  $[M + H]^+$ ,  $[M + Na]^+$  and  $[M + NH_4]^+$ , respectively; where M is glycerol ethoxylate (Figure 4.39A). The mass spectrum is the same as additive B3 in section 4.3.2.3.

Figure 4.36B showed the most abundant peak at  $m/z$  91, the  $[M + H]^+$  molecular ion series ( $m/z$  197, 241, 285 etc.) and the  $[M + NH_4]^+$  series ( $m/z$  258, 302, 346 etc.). The LC-MS analyses could not conclusively confirm the structure of peak 2; however, FTIR analyses showed that this component is possibly a nitrogenated polymer due to the presence of the N-H stretch at  $1643\text{ cm}^{-1}$ .

## Chapter 4: Results and discussion

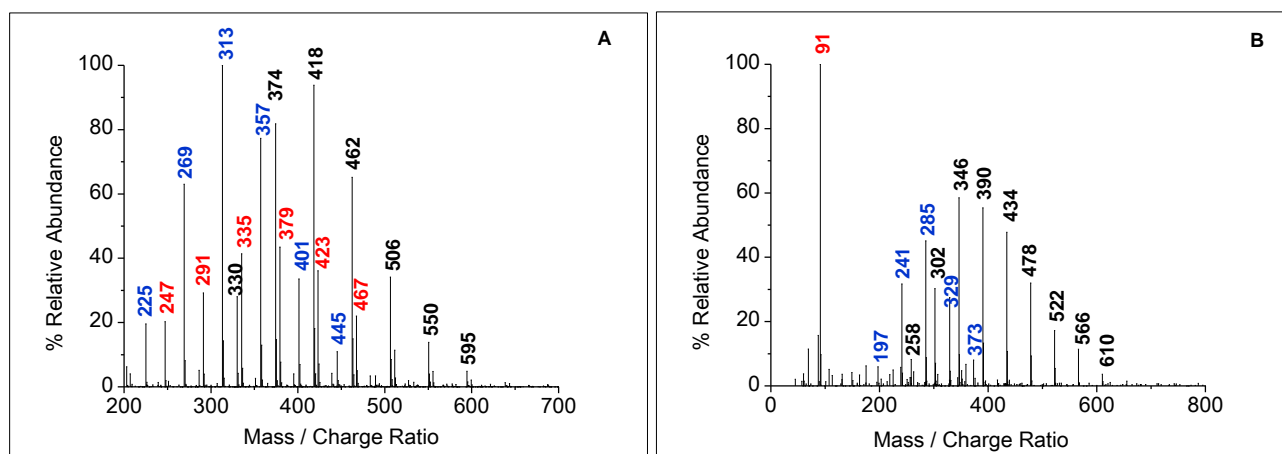


Figure 4.36: Positive scan LC-MS of additive C3 for peak 1(A) and peak 2 (B).

Further tests were performed by first eluting additive C3 at critical conditions of PEG for the first 10 minutes, followed by 100% methanol for the duration of the run. The positive scan TIC in Figure 4.37 showed two additional, hydrophobic components labelled 3 and 4. Gradient elution enhanced the detection of these components by minimising adsorptive interactions with the stationary phase.

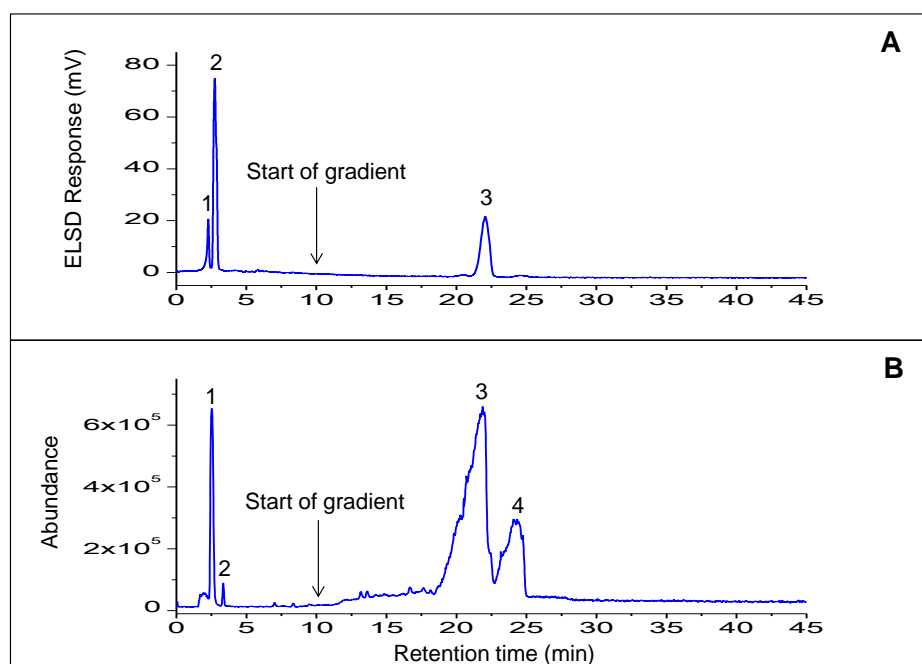


Figure 4.37: LC-ELSD (A) and positive scan TIC (B) of additive C3 acquired using a solvent gradient elution protocol.

The molecular ion series in Figure 4.38A for peak 3 was similar to that observed in peak 14 of additive B1, which was identified as PEG monooleyl ether (Figure 4.39B). The mass spectrum in

## Chapter 4: Results and discussion

Figure 4.38B showed a difference of 2 Da, for the same number of repeat units. Since it had been established that component 3 is an unsaturated alkyl-PEG, the difference of 2 Da between the two mass spectra suggested the following: either component 4 was a saturated alkyl-PEG with the same alkyl chain length as component 3 or the two peaks were oligomers of the same component. However, the difference of 2 Da was within the experimental error of the MS detection conditions. Furthermore, the  $^1\text{H}$  NMR spectrum in Figure 4.40 showed the presence of one  $\text{CH}_3$ - group at 0.85 ppm, confirming a single hydrocarbon chain component. It followed that the molecular structure of both components 3 and 4 is PEG monooleyl ether:  $\text{C}_{18}\text{H}_{35}-(\text{OCH}_2\text{CH}_2)_n-\text{OH}$ . The experimental versus theoretical calculations for the most abundant  $[\text{M} + \text{NH}_4]^+$  ions are as presented in Table 4.8.

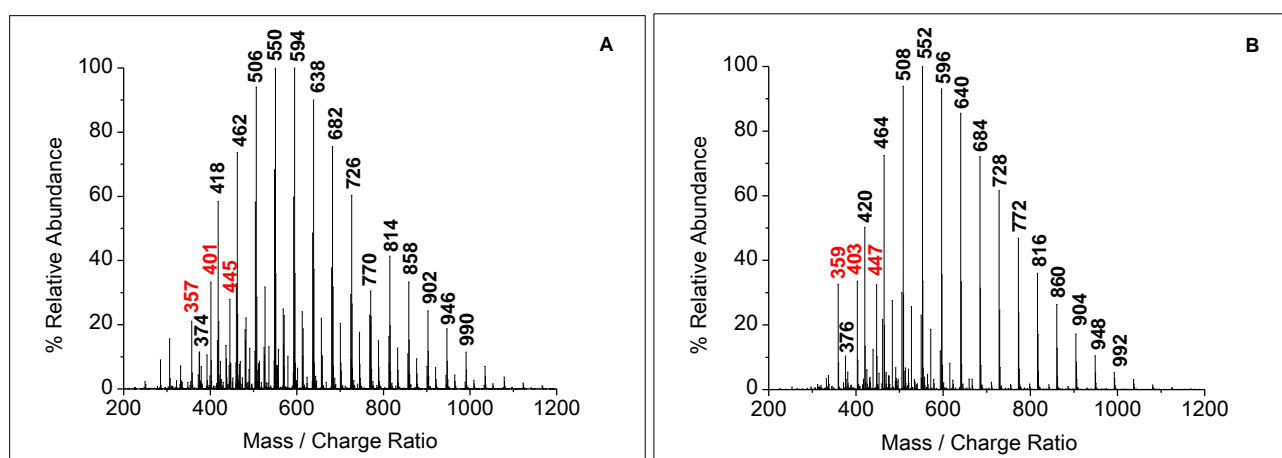


Figure 4.38: Positive scan TIC of additive C3 for peak 3(A) and peak 4 (B) acquired using a gradient elution protocol.

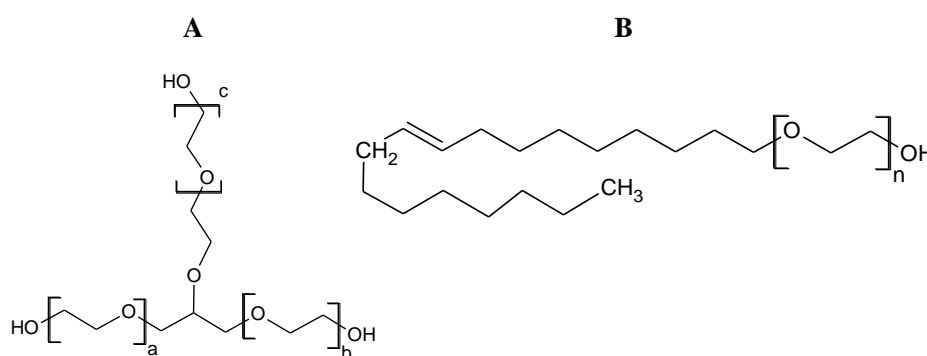
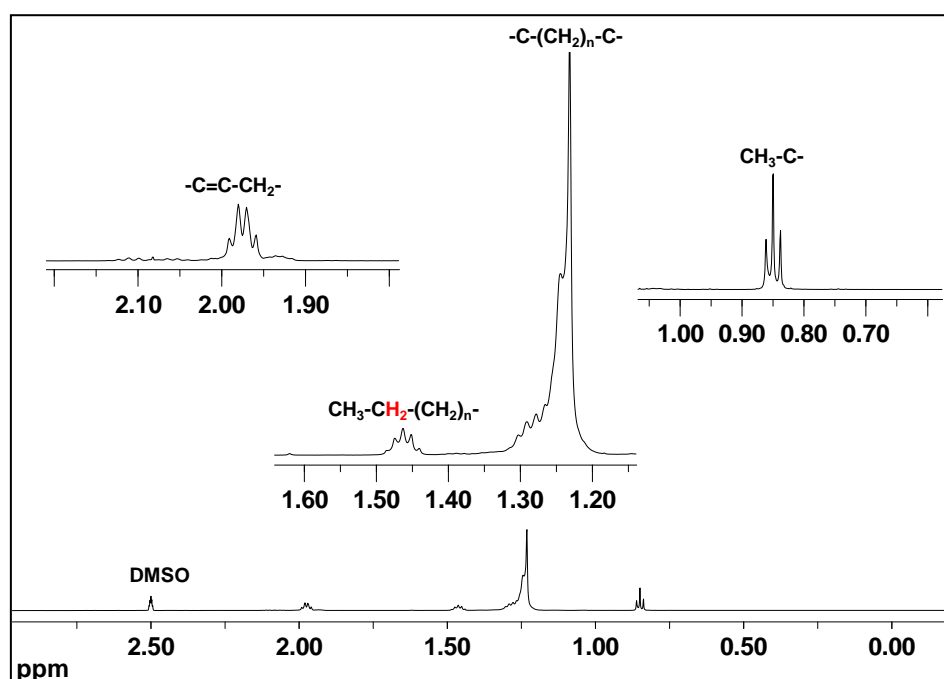


Figure 4.39: Structures of glycerol ethoxylate (A) and PEG monooleyl ether (B).

Table 4.8: Experimental versus theoretical ammoniated molecular ions of additive C3.

Peak No.	Experimental m/z	Average No. of EO repeat units (n)	Theoretical m/z
1	418.35	7	418.50
2	346.30	5	346.39
3	594.55	7	594.88

The end groups of the components of additive C3 were confirmed by the  $^1\text{H}$  NMR spectra in Figures 4.40 (0 to 3 ppm) and Figure 4.41 (3 to 6.5 ppm). In Figure 4.40, a triplet at 0.85 ppm was assigned to the  $\text{CH}_3$ - protons while a quartet at 1.98 ppm was attributed to the allylic protons from PEG-monooleyl ether ( $-\text{C}=\text{C}-\text{CH}_2-$ ). The multiplet at 1.46 ppm was assigned to the  $-\text{CH}_2-$  group that is bonded to a  $\text{CH}_3$ - group on one side and a  $-(\text{CH}_2)_n-$  repeat unit on the other side. The  $-(\text{CH}_2)_n-$  repeat unit was observed by the highly intense peak at 1.23 to 1.30 ppm.

Figure 4.40:  $^1\text{H}$  NMR of additive C3 in DMSO, 25°C and 600 MHz at 0 to 3 ppm.

## Chapter 4: Results and discussion

In Figure 4.41, the protons of the  $-(\text{CH}_2\text{CH}_2\text{O})_n-$  repeat unit were observed at 3.51 ppm, shown at position 2. The multiplet at 3.41 to 3.48 ppm was assigned to the  $-\text{CH}_2-$  protons at positions 3, 5, 6 and 7 while a quintet at 3.69 ppm was due to the  $-\text{CH}-$  proton at position 4.

A weak triplet at 4.77 ppm and a larger peak at 4.58 ppm are characteristic of the hydroxyl protons. The vinyl proton ( $-\text{C}=\text{CH}$ ) arising from PEG monooleyl ether was assigned to a triplet at 5.32 ppm.

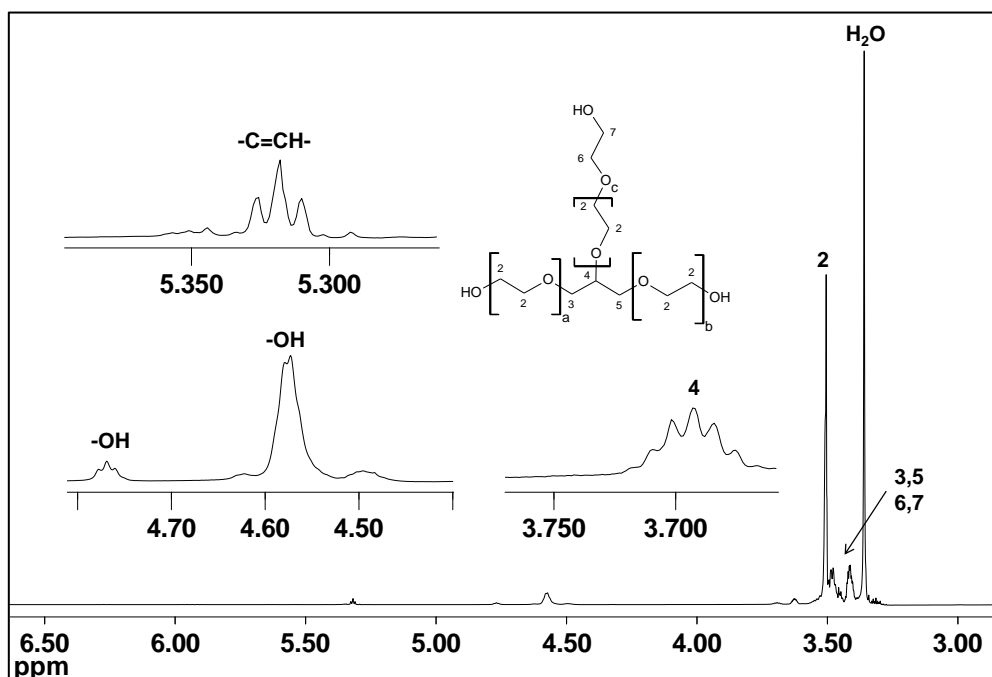


Figure 4.41:  $^1\text{H}$  NMR of additive C3 in DMSO, 25°C and 600 MHz at 3 to 6.5 ppm.

There was another constituent of additive C3 as listed in Table 3.2, with the structure shown in Figure 4.42. The peaks expected in the NMR spectra of this molecule were from the amide group, ( $\text{R}(\text{CO})-\text{NH}_2$ ), the alpha hydrogens from the carbonyl group ( $-\text{CH}_2-\text{CONH}_2$ ) as well as the methine hydrogen adjacent to the sulfo group ( $-\text{CH}-\text{SO}_3-$ ). The protons attached to the nitrogen atom can vary in the chemical shift region of 5.5 to 8.5 ppm, depending on the temperature, type of solvent and concentration of the analyte. There was no evidence in the  $^1\text{H}$  NMR to suggest the presence of the amide group. A doublet arising from alpha protons shown by position 2 were expected in the region of 2.1 to 2.5 ppm, however, this was not observed in Figure 4.40. The methine group at position 3 did not show a triplet as expected at a chemical shift region of 2 to 4 ppm. These findings suggested that either this component was absent in the additive blend or was present at very low concentrations.

## Chapter 4: Results and discussion

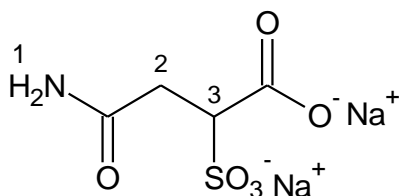


Figure 4.42: Structure of butanoic acid, 4-amino, 4-oxosulfo disodium salt.

The results showed that additive C3 consists of glycerol ethoxylate ( $M_p$  400 g/mol,  $n = 7$ ), PEG monooleyl ether ( $M_p$  576 g/mol,  $n = 7$ ) as well as an unidentified component of  $M_p$  328 g/mol and five EO repeat units.

#### 4.3.3.3. Analyses of additive C4

Figure 4.43 presents the chromatograms of additive C4, analysed at critical conditions of adsorption of PEG. There were five components detected by ELSD (A), while the positive scan TIC (B) showed a total of ten peaks, some of which were not baseline separated. Peaks 1, 2 and 3 were further detected in the negative scan TIC (C), suggesting the presence of anionic components.

## Chapter 4: Results and discussion

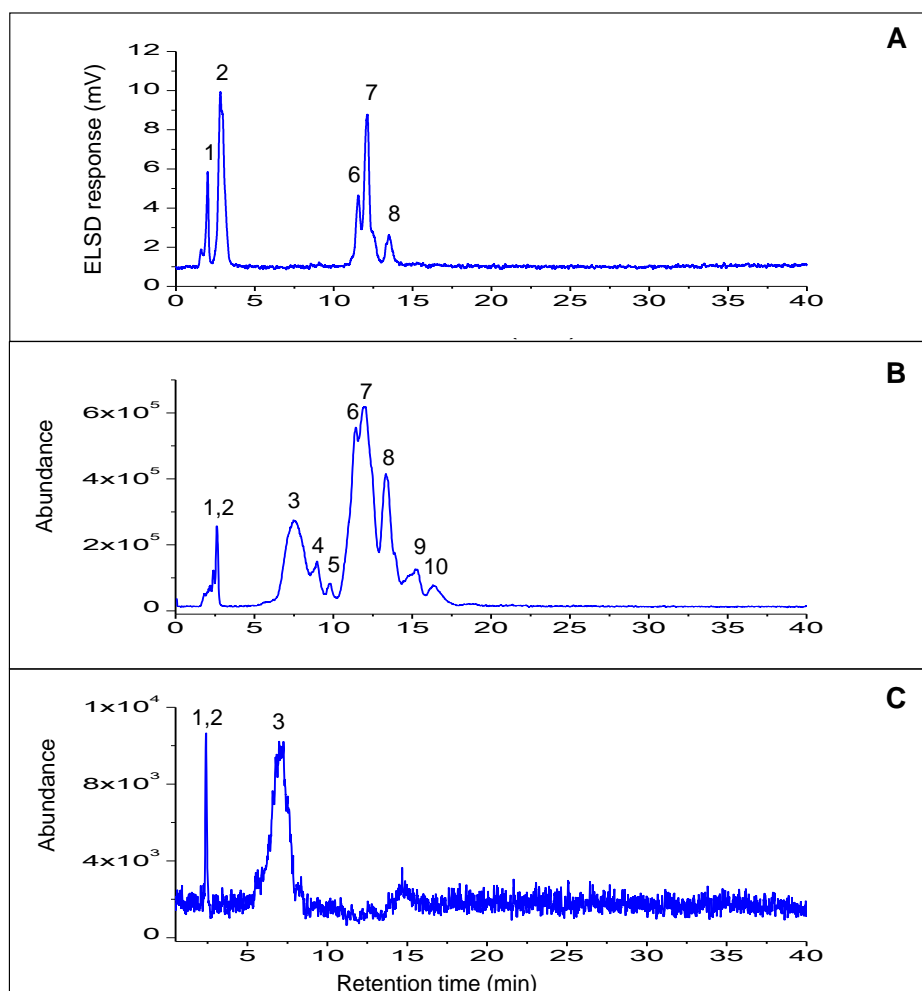


Figure 4.43: LC-ELSD (A), positive (B) and negative (C) TIC scans of additive C4 at critical conditions of adsorption of PEG.

The interpretation of additive C4 was performed by comparing the mass spectra acquired in the positive and negative modes for peaks 1 and 2. This was to investigate the types of chemical structures when the analyte was subjected to both ionization modes.

In Figure 4.44A, the positive scan mass spectra of peaks 1 and 2 were overlapped as shown by multiple molecular ion series arising from combinations of different cations. There was therefore no conclusive distinction between each of the series from various cations. However, the singly-charged green molecular ion series with peaks at  $m/z$  479, 523, 567 etc. was assigned to  $[\text{PEG} + \text{Na}]^+$ . The ion at  $m/z$  523 matched a PEG of average molar mass 502 g/mol and 11 EO repeat units.

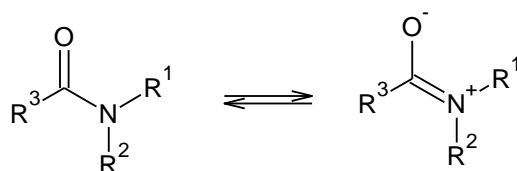
The component at peak 2 was identified using the information from the additive supplier's data sheet (Table 3.2) and the positive and negative spectra in Figure 4.44. On the negative scan, the  $[\text{M} - \text{H}]^-$  peaks at  $m/z$  71 and 115 were assigned to the components with molar masses of 72.06 g/mol and 116.01 g/mol, respectively.



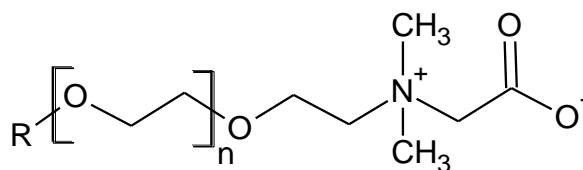
## Chapter 4: Results and discussion

Moreover, the black molecular ion series ( $m/z$  467, 511, 555, 599 etc.) from the positive mode was equivalent to the positively charged  $[M + 72 + 1]^+$ , where  $M$  is the precursor ion and 72 and 1 are the molar masses of the two end groups. This assignment suggested a component bearing both the positive and negative charges. According to the manufacturer's description in Table 3.2, one of the components of additive C4 consists of a polymer with a tertiary amine.

Studies have shown the ability of the amine- and amide-based surfactants to show zwitterionic behaviour due to the delocalisation of the lone pair on the nitrogen atom. In amides (Scheme 1), this phenomenon forms a partial double bond between the oxygen and nitrogen atoms, producing a negative and positive charge. In the tertiary amine surfactants based on betaines or sulfo betaines (Scheme 2), the components consist of cationic and anionic species which are not adjacent to one another<sup>20</sup>.



*Scheme 1: Delocalization of a lone pair on the nitrogen atom from an amide.*



*Scheme 2: Zwitterionic character of a betaine-based surfactant.*

The incorporation of the tertiary amine- or amide-based end groups in additives has been reported by various commercial additives suppliers. They claimed that the tertiary amine/amide hydrophilic head acts as an excellent anchoring group for the different types of organic and inorganic pigments in aqueous dispersions<sup>21–24</sup>. The presence of the tertiary amide-PEG will be confirmed by NMR spectroscopy later in this section.

## Chapter 4: Results and discussion

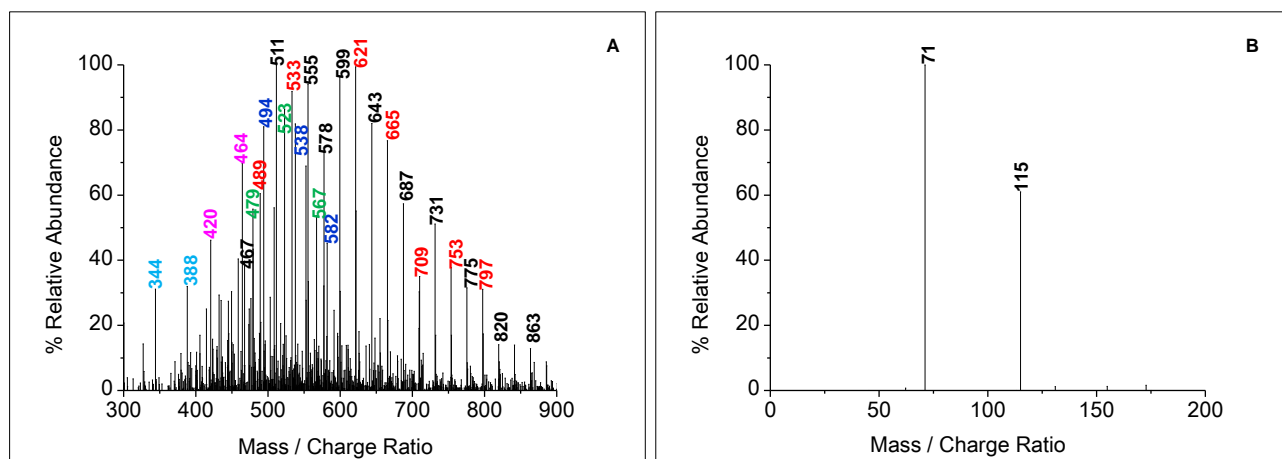


Figure 4.44: Positive scan LC-MS for peaks 1 and 2 (A) and negative scan LC-MS for peak 2 (B) in additive C4.

The mass spectra in Figure 4.45A and B for peak 3 were acquired in the positive and negative mode, indicating the anionic character of the component at peak 3. The assigned molecular ion series in spectra A and B were  $[M + \text{NH}_4]^+$  and  $[M - \text{H}]^-$ , respectively, where M is the same unidentified polymer as peak 2. Using the abundant ion at  $m/z$  494 (Figure 4.45A) and 72.06 g/mol as one of the polymer end groups (from peak 2), the molar mass of the second end group was calculated as 96 g/mol. This value is the approximate molar mass of the most common anions such as the sulphate ( $\text{OSO}_3^-$ , 96.06 g/mol) or phosphate ( $\text{PO}_4^{2-}$ , 94.97 g/mol). Due to the similarity in molar masses of these two anions, no conclusive assignment could be made on the identity of the second end group. Further analyses by elemental techniques are required to determine the presence of phosphorus or sulphur atoms in additive C4. However, some literature reported that the sulphated product is commonly used in surfactant systems<sup>19,25,26</sup>.

The synthesis of the sulphated products is typically achieved by the reaction of the amide ethoxylate product with sulphur trioxide ( $\text{SO}_3$ ) or chlorosulphuric acid ( $\text{HSO}_3\text{Cl}$ ). The resultant product is usually neutralized with a hydroxide base (typically NaOH or KOH) or amine-based neutralising agent<sup>19,26</sup>.

## Chapter 4: Results and discussion

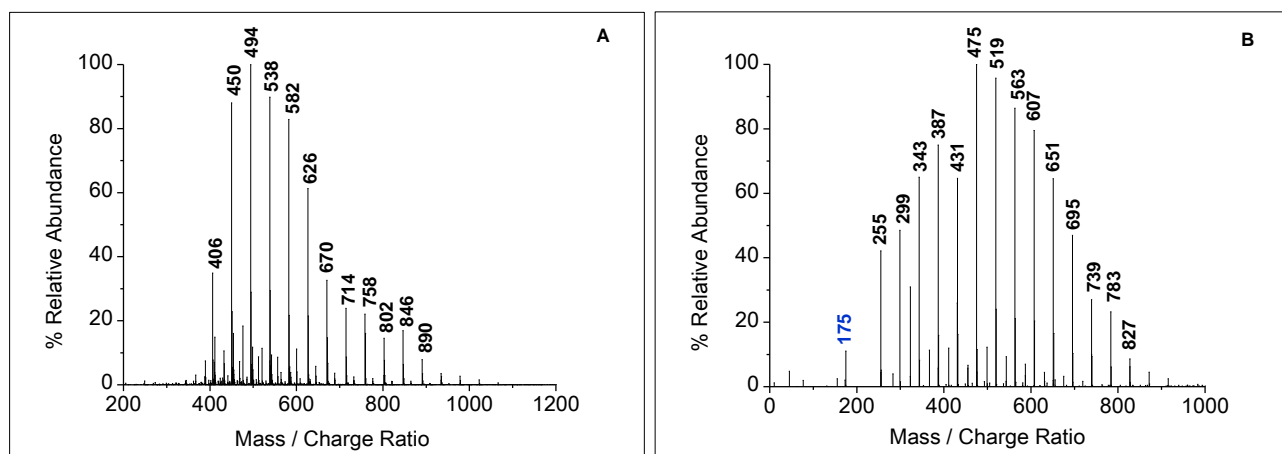


Figure 4.45: Positive (A) and negative (B) LC-MS of additive C4 for peak 3.

Figure 4.46A (peak 4) showed the  $[M + NH_4]^+$  series with peaks at  $m/z$  338, 382, 426, 470 etc. The mass spectrum of peak 5 was the similar to that of peak 4, hence it was not shown.

Both peaks 4 and 5 were assigned to a fatty acid-PEG:  $C_7H_{15}COO-(CH_2CH_2O)_n-H$ . The abundant ion at  $m/z$  426 showed six EO repeat units as shown:

$$(m/z)_{\text{experimental}} = 426.30$$

$$(m/z)_{\text{theoretical}} = 18.0385 + 6 \times 44.0526 + (143.2035 + 1.0079) = 426.57$$

In Figure 4.46B (peak 7), the  $[M + NH_4]^+$  series with peaks at  $m/z$  352, 396, 440 etc. showed a difference of 14 Da compared to the series at  $m/z$  338, 382 426 etc. (Figure 4.46A), confirming the presence of an additional  $-CH_2-$  group in the polymer chain. Peak 7 was thus assigned to the fatty acid-PEG:  $C_8H_{17}COO-(CH_2CH_2O)_n-H$ . The ion at  $m/z$  440 consisted of six repeat units:

$$(m/z)_{\text{experimental}} = 440.40$$

$$(m/z)_{\text{theoretical}} = 18.0385 + 6 \times 44.0526 + (157.2301 + 1.0079) = 440.59$$

The mass spectrum for peak 6 was similar to that of peak 7.

## Chapter 4: Results and discussion

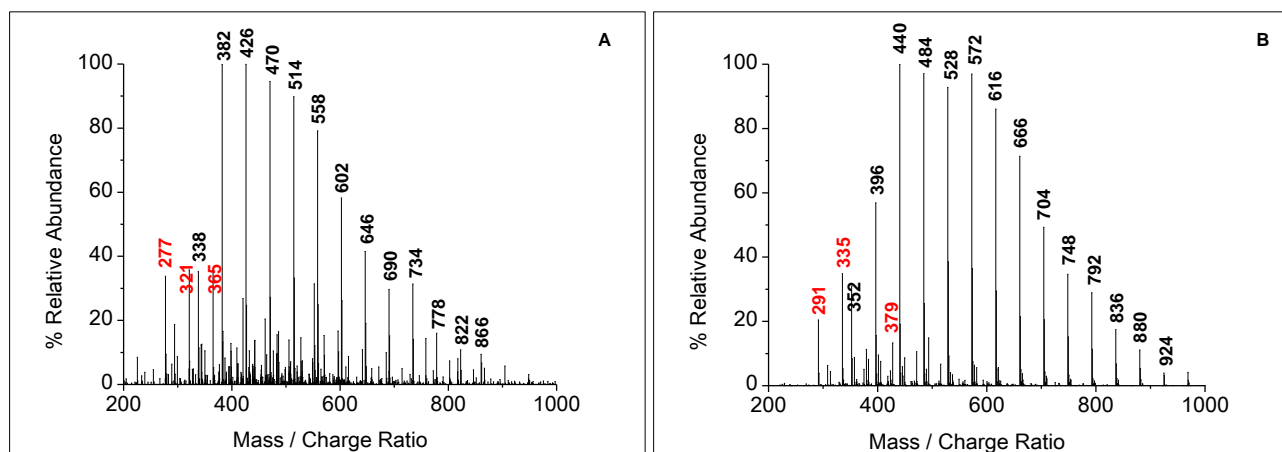


Figure 4.46: Positive scan LC-MS of additive C4 for peak 4 (A) and peak 7 (B).

Figure 4.47A (peak 8) showed the same molecular ion series ( $m/z$  352, 396, 440, 484 etc.) as discussed for peak 7. Similarly, the ion at  $m/z$  440 (peak 10) was assigned to a  $C_{10}$  fatty acid with six EO repeat units:  $C_9H_{19}COO-(CH_2CH_2O)_n-H$ :

$$(m/z)_{\text{experimental}} = 454.30$$

$$(m/z)_{\text{theoretical}} = 18.0385 + 6 \times 44.0526 + (171.2567 + 1.0079) = 454.62$$

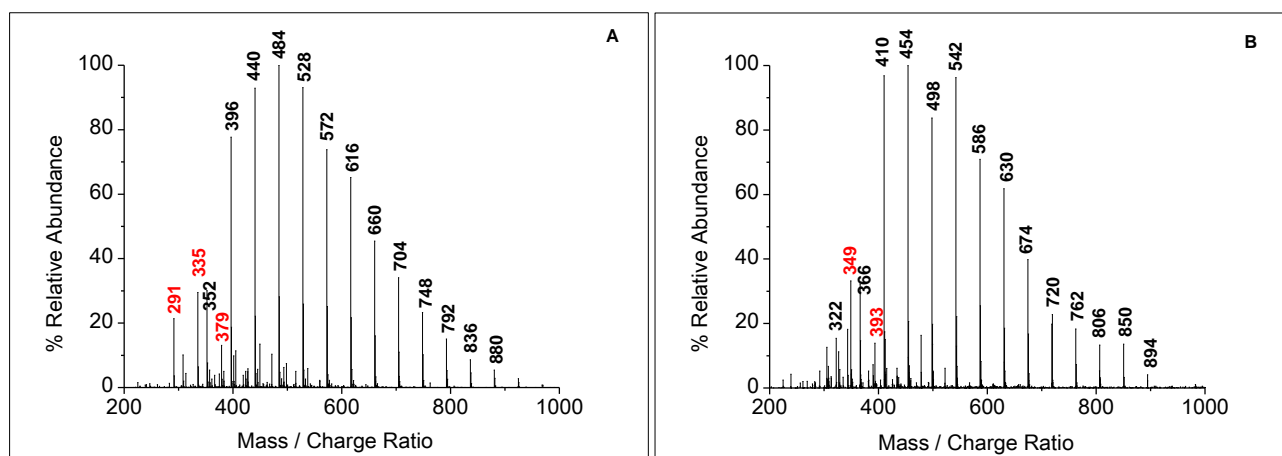


Figure 4.47: Positive scan LC-MS of additive C4 for peak 8(A) and peak 10 (B).

Further analyses were performed using solvent gradient elution, where the mobile phase composition was varied from critical conditions of PEG (79.9%/20.1% methanol/water) to 100% methanol. In this mode, the increase in the mobile phase strength enhanced the elution of the component at peak 11, which was not previously observed when only critical conditions of adsorption of PEG were employed in Figure 4.43. Moreover, pyrolysis GC-MS identified the component in peak 11 as a  $C_{18}$  polyunsaturated fatty acid-PEG with the chemical structure

## Chapter 4: Results and discussion

$C_{17}H_{29}COO-(CH_2CH_2O)_n-H$ . This polymer, which is derived from 9,12,15 octadecatrienoic acid, consists of three double bonded carbons on the alkyl chain, as shown in Figure 4.49.

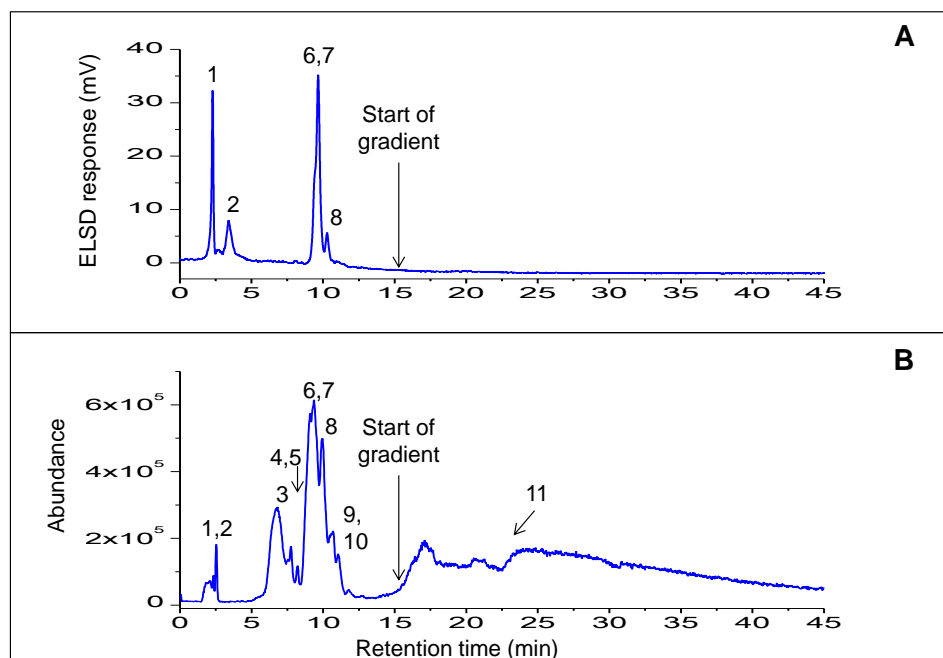


Figure 4.48: LC-ELSD (A) and positive scan TIC (B) of additive C4 acquired using a solvent gradient elution protocol.

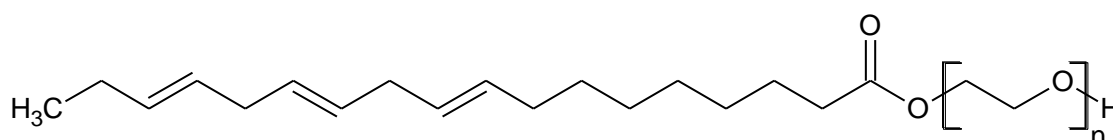


Figure 4.49: Structure of 9,12,15-octadecatrienoic acid detected by pyrolysis GC-MS.

In the  $^1H$  NMR spectrum (Figure 4.50), allylic protons were observed at 1.98 ppm while the vinyl protons were found at 5.31, 6.4 and 6.7 ppm confirming the tri-unsaturated alkyl chain. Furthermore, several double-bonded carbons were found at 128 to 135 ppm in the  $^{13}C$  NMR spectrum in Figure 4.51.

The presence of a fatty amide was confirmed by a large peak at 6.02 ppm. The higher peak intensity was attributed to the hydrogen-deuterium exchange. Methylene protons of the EO repeat unit were assigned at 3.51 ppm, while the methyl and methylene protons of the alkyl chain were observed by the peaks centered at 0.83 and 1.23 ppm, respectively.

## Chapter 4: Results and discussion

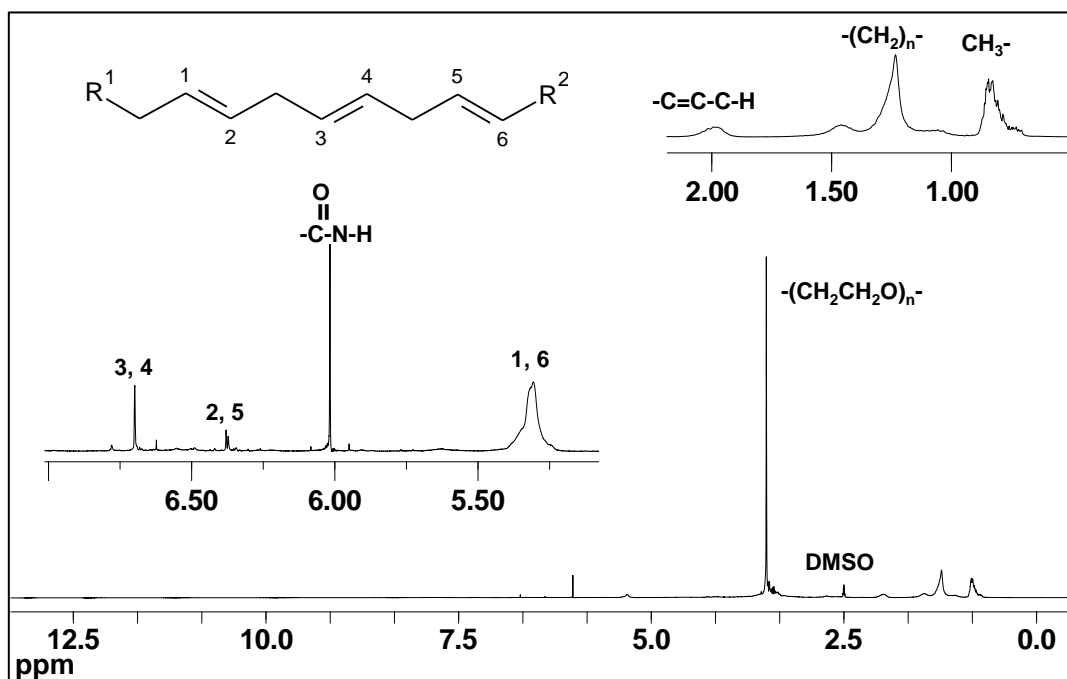


Figure 4.50:  $^1\text{H}$  NMR of additive C4 in DMSO, 25°C and 600 MHz.

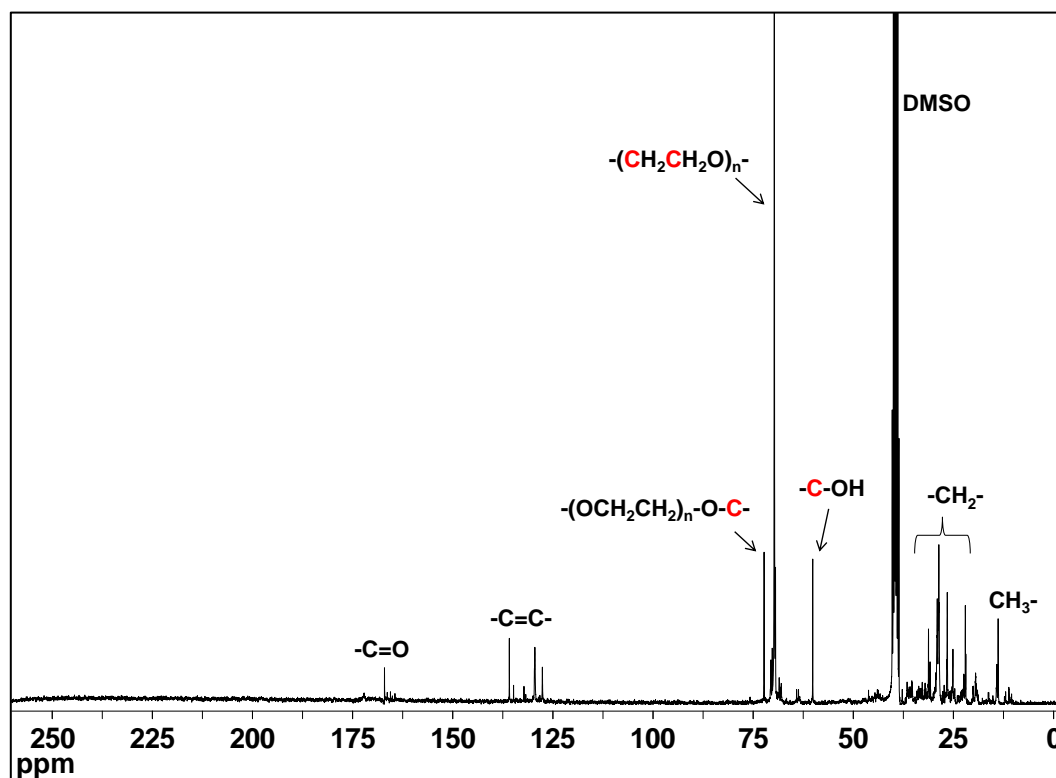


Figure 4.51:  $^{13}\text{C}$  NMR of additive C4 in DMSO, 25°C and 300 MHz.

## Chapter 4: Results and discussion

The chemical structures of the components of additive C4 were further confirmed by the FTIR-ATR spectrum of the unmodified sample in Figure 4.52. The assigned groups of the amine/amide (1542  $\text{cm}^{-1}$ , 1033  $\text{cm}^{-1}$ , 1647  $\text{cm}^{-1}$ ), carboxylic acid (1724  $\text{cm}^{-1}$ ), alkene (3002  $\text{cm}^{-1}$  and 1601  $\text{cm}^{-1}$ ) and ether (1104  $\text{cm}^{-1}$ ) all correlated to the LC-MS, NMR and pyrolysis-GC-MS results for additive C4.

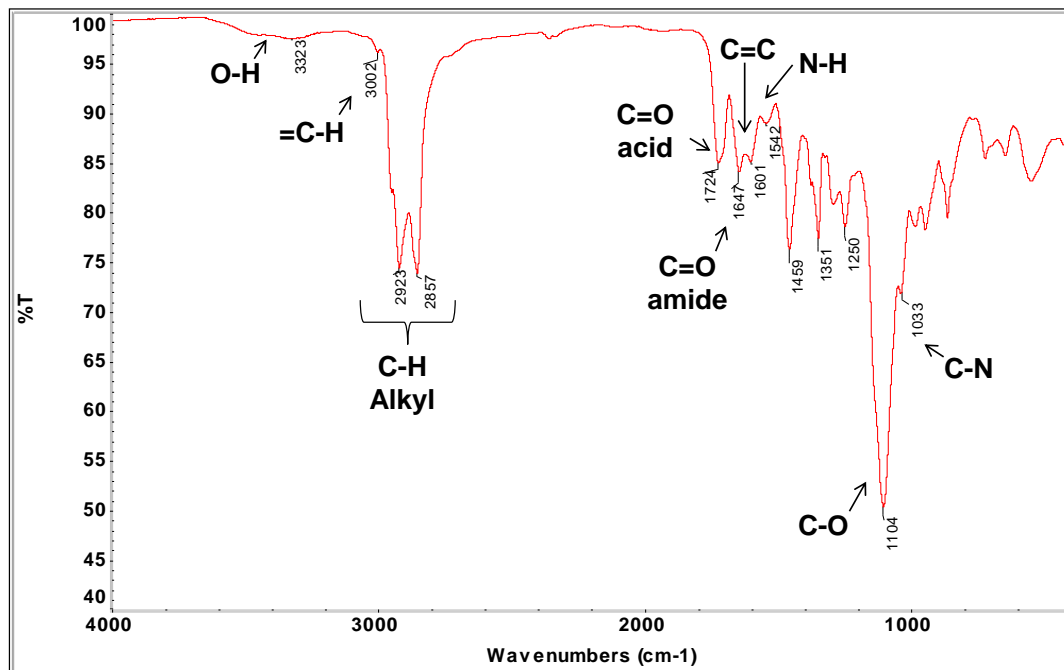


Figure 4.52: FTIR-ATR spectrum of additive C4.

Table 4.9 shows a summary of the components detected in additive C4, which consisted of PEG, the C<sub>8</sub>-, C<sub>9</sub>- and C<sub>10</sub>-fatty acid-PEGs as well as the C<sub>18</sub> polyunsaturated fatty acid-PEG. Peaks 2 and 3 (tertiary amine/amide based polymers) were excluded from the table as their end groups were not conclusively identified.

*Table 4.9: Components of additive C4, showing the molar mass of the most abundant ion.*

Peak No.	Molar mass (g/mol)	Average repeat units (n)	Molecular structures
1	502	11	
4	408	6	
7	422	6	
10	436	6	
11	Detected by py- GC-MS		

#### 4.3.3.4. Analyses of additive C5

Figures 4.53 to 4.56 show the results for additive C5 analysed by LC-MS at critical conditions and  $^1\text{H}$  NMR. According to the known chemical structures in Table 3.2, additive C5 is derived from nonyl phenol ethoxylates, hence the analysis by UV detection at 230 nm versus LC-MS is presented in Figure 4.53. The LC-MS results are reported in the negative scan mode as it showed the presence of anionic components. Several oligomers were observed in the UV chromatogram and the corresponding peaks were further detected by the negative scan TIC.

The mass spectrum for peak 1 (Figure 4.54A) shows a single abundant ion at  $m/z$  97. This value is the approximate molar mass of common anionic compounds such as  $\text{PO}_4^{2-}$  or  $\text{SO}_4^{2-}$ . Peaks 2 to 10 were all integrated simultaneously, to give the mass spectrum in Figure 4.54B. The  $[\text{M}-\text{H}]^-$  molecular ions at  $m/z$  283, 297, 311, 325 and 339 showed a peak-to-peak difference of 14 Da, suggesting an alkyl chain with increasing numbers of  $-\text{CH}_2-$  groups. The predominant ion at  $m/z$  325 matched dodecylbenzene sulfonate,  $\text{C}_{12}\text{H}_{25}-\text{C}_6\text{H}_4-\text{SO}_3^-$ . This surfactant is available commercially as a salt of various cations such as  $\text{Na}^+$ ,  $\text{K}^+$ ,  $\text{Ca}^+$  or as an amine salt. The alkylbenzene sulfonate surfactants are among the most popular anionic surfactants, commonly used in cosmetics, detergents and coatings<sup>27–29</sup>.



## Chapter 4: Results and discussion

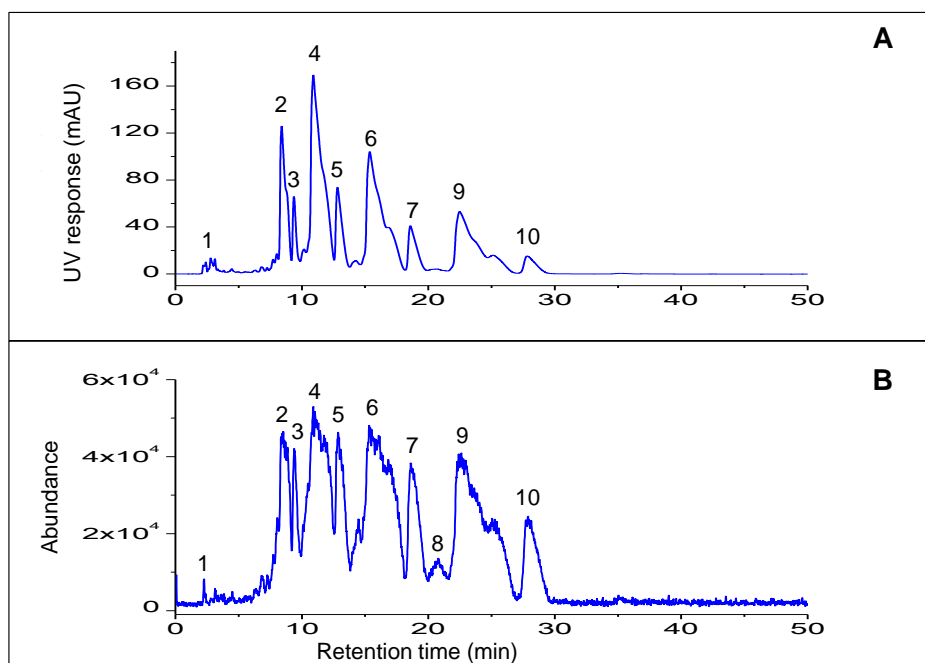


Figure 4.53: LC-UV at 230 nm (A) and negative scan TIC (B) of additive C5.

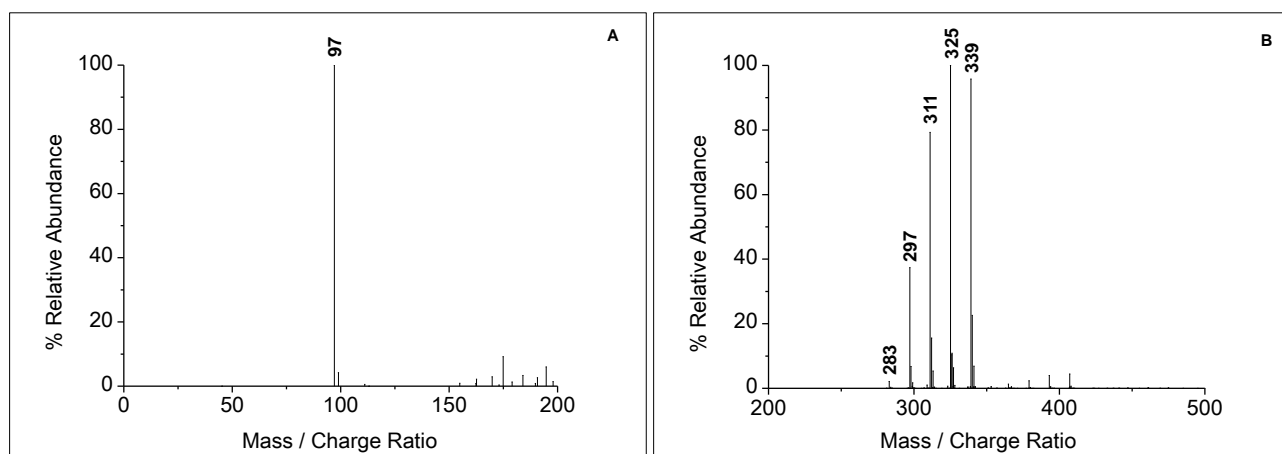


Figure 4.54: Negative scan TIC of additive C5 for peak 1(A) and peaks 2 to 10 (B).

The FTIR-ATR and  $^1\text{H}$  NMR spectra in Figures 4.55 and 4.56, respectively, were used to confirm the components of additive C5. The presence of the aromatic ring was shown by the  $=\text{C}-\text{H}$  stretch at  $3056\text{ cm}^{-1}$  as well as the  $=\text{C}-\text{H}$  out of plane bend at  $832\text{ cm}^{-1}$ . The aromatic sulfonates were indicated by the strong asymmetric stretches at  $1126$  to  $1200\text{ cm}^{-1}$ . This observation correlated to the structure of dodecylbenzene sulfonate identified by LC-MS.

The peak at  $1632\text{ cm}^{-1}$  was attributed to the broad N-H bend arising from the primary amine group.

## Chapter 4: Results and discussion

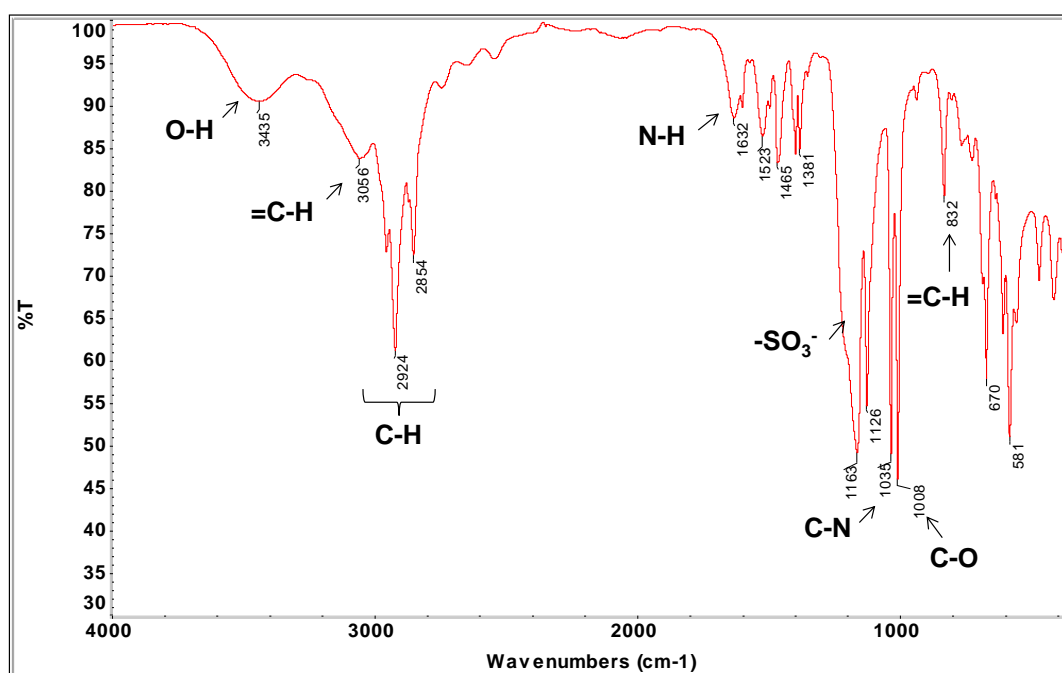


Figure 4.55: FTIR-ATR spectrum of additive C5.

The  $^1\text{H}$  NMR (Figure 4.56) showed aromatic protons at 7.10 to 7.53 ppm, confirming the alkylbenzene sulfonate component. Further evidence of the presence of the amine-type components was indicated by a doublet at 1.15 ppm. This doublet was assigned to the two methyl groups from isopropyl amine,  $\text{H}_2\text{N}-\text{CH}-(\text{CH}_3)_2$ . The methine proton from  $\text{H}_2\text{N}-\text{CH}-(\text{CH}_3)_2$  was assigned to a septuplet centred at 3.27 ppm. These assignments confirmed the presence of isopropyl amine dodecylbenzene sulfonate, which is commonly used as a dispersant in coatings. A singlet at 3.17 ppm in the  $^1\text{H}$  NMR was assigned to the methyl groups of dimethyl amine ( $-\text{N}-(\text{CH}_3)_2$ ), which was possibly the second component of the additive blend.

The  $^1\text{H}$  NMR showed two types of  $\text{CH}_3$ - groups at 0.68 to 0.84 ppm. A triplet centred at 0.69 ppm was attributed to a  $\text{CH}_3$ - group from a linear hydrocarbon chain while the multiplet centred at 0.81 ppm was assigned to a  $\text{CH}_3$ - group on a branched hydrocarbon chain. The synthesis of alkylbenzene from alpha-olefins is associated with the formation of branched hydrocarbon products<sup>19</sup>. The other two peaks centred at 2.40 ppm and 2.66 ppm could not be accurately assigned. These peaks were attributed to a second amine-type component of additive C5, in addition to isopropyl amine alkylbenzene sulfonate.

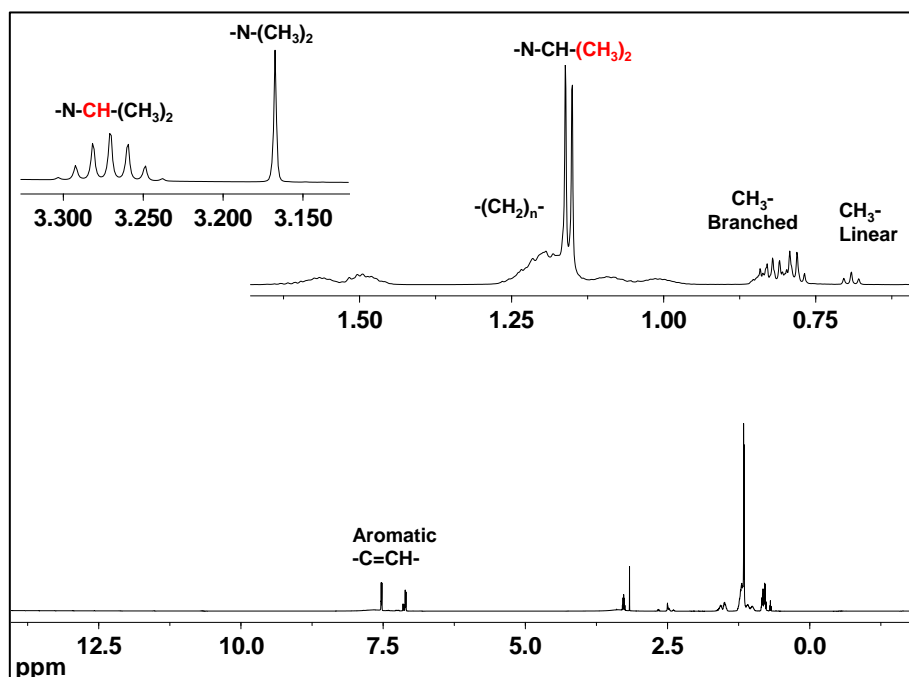


Figure 4.56:  $^1\text{H}$  NMR of additive C5 in DMSO, 25°C and 600 MHz.

The results showed that additive C5 is an anionic surfactant that consists of isopropylamine and another component based on dimethyl amine. The additive also contains a mixture of linear and branched alkylbenzene sulfonates. The abundant ion from LC-MS was assigned to dodecylbenzene sulfonate with 10 methylene repeat units and a molar mass of 326 g/mol.

#### 4.3.3.5. Analyses of additive C6

Figure 4.57 was acquired from the analysis of additive C6 at critical conditions of adsorption of PEG in the positive and negative scan modes. The chemistry of this additive was unknown, hence the characterization was performed by comparing it to the identified components in other additives. In the positive scan TIC (A), multiple peaks were detected, some with poor resolution and no baseline separation. The negative TIC scan (B) showed various oligomers with little correlation to the positive scan in terms of the elution of the corresponding peaks at the same retention times. The negative scan mass spectrum (Figure 4.62) showed that all the peaks from the negative scan TIC were from oligomers of a single, anionic component.

## Chapter 4: Results and discussion

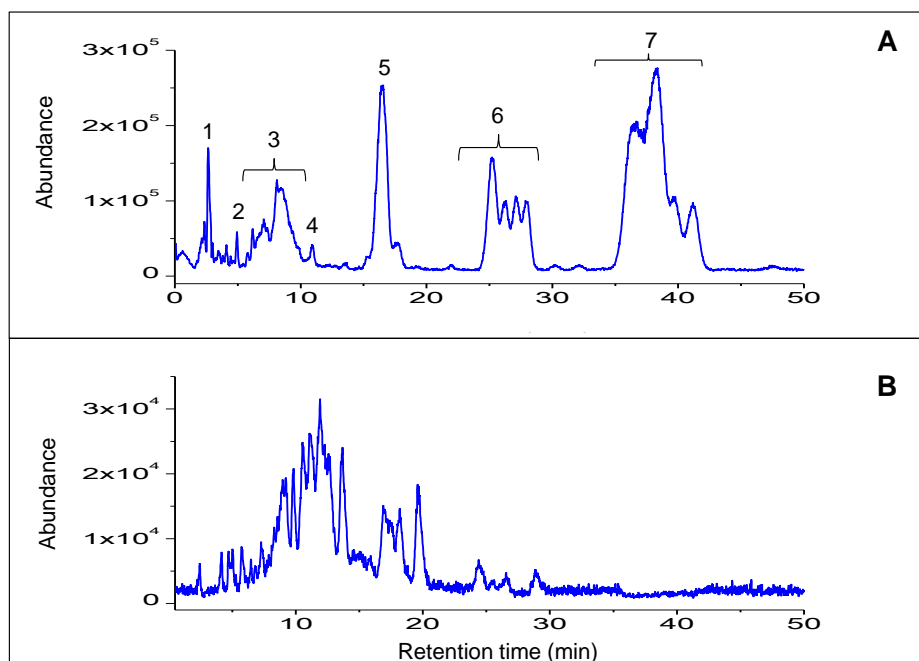


Figure 4.57: Positive (A) and negative (B) TIC scans of additive C6.

The mass spectra of peaks 1 and 2 are shown in Figures 4.58A and B. In spectrum A, two molecular ion series were observed, with predominant ions at  $m/z$  489 and 564 in the red and black series, respectively. The  $[M + \text{NH}_4]^+$  ion at  $m/z$  564 in the black series corresponded to a PEG with 12 EO repeat units, as already discussed for additive C1. The red series was a result of multiple charges at the PEG precursor ion:  $[\text{PEG} + z_1 + z_2]^{2+}$ , where  $z_1$  and  $z_2$  are the two different cations.

The mass spectrum for peak 2 in Figure 4.58B showed the doubly charged species ( $m/z$  377, 399, 421 etc.) while the series at  $m/z$  429, 472, 516, 560, 605 etc. was attributed to  $[M + \text{NH}_4]^+$ . The identity of M will be discussed later in the section.

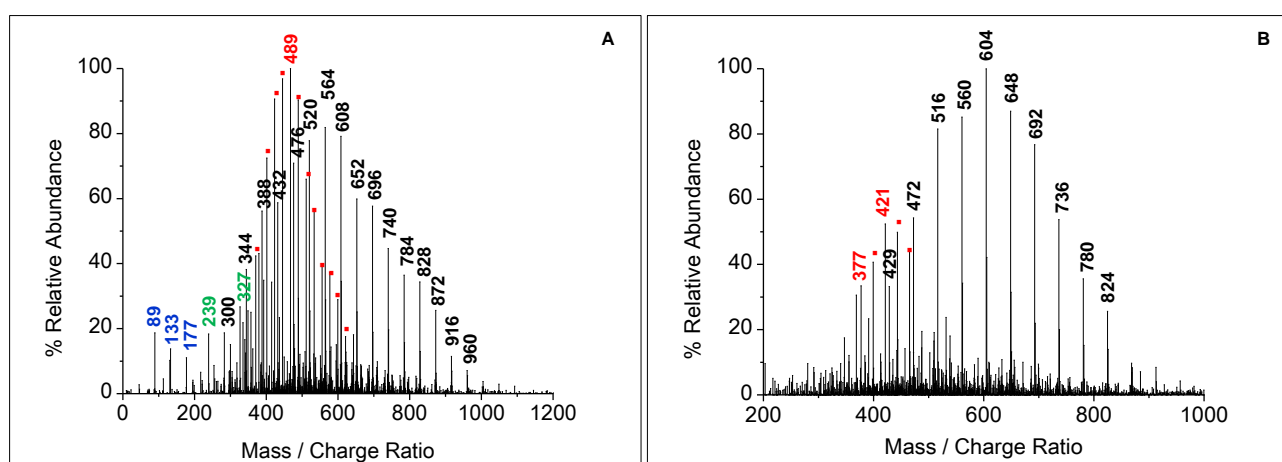


Figure 4.58: Positive scan LC-MS of additive C6 for peak 1 (A) and peak 2 (B).

## Chapter 4: Results and discussion

In Figure 4.59A and B, a difference of 28 Da was observed between the ion for peak 2 ( $m/z$  604) and peak 3 ( $m/z$  632), for the same number of repeat units. This suggested the presence of an additional  $\text{CH}_3\text{CH}_2$ - group to the alkyl chain of peak 3. Similarly, the ion at  $m/z$  646 (peak 4) showed an additional  $\text{CH}_3$ - compared to the ion at  $m/z$  632 (peak 3). These data indicated oligomer separation by the differences in the length of the polymer chain.

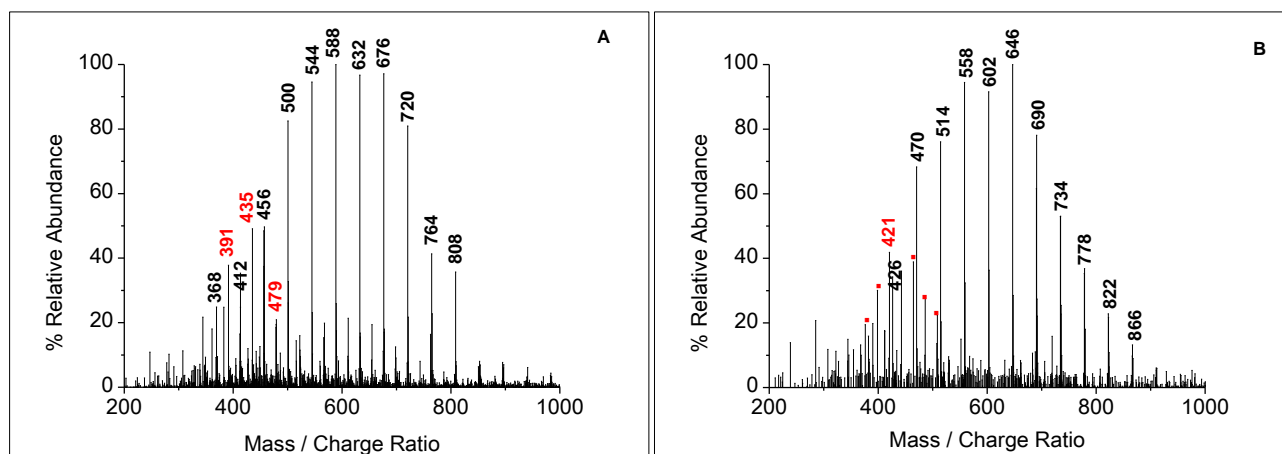


Figure 4.59: Positive scan LC-MS of additive C6 for peak 3 (A) and peak 4 (B).

The positive scan TIC indicated peak 5 as the oligomer with the second largest peak area (27%), hence it was expected as one of the main constituents of the additive. The abundant ion at  $m/z$  716 (peak 5) in Figure 4.60 showed a difference of 26 Da compared to  $m/z$  690 (peak 4). A value of 26 Da suggested an additional  $-\text{CH}=\text{CH}-$  group, which was attributed to some unsaturation in the alkyl chain of the polymer end group. Further analyses by NMR and FTIR later in the section will confirm this. Moreover, based on the elution behaviour of additives C1 and C4 from an earlier discussion, components having a  $\text{C}_8$  to  $\text{C}_{10}$  alkyl chain were detected at the elution region of 10 to 20 minutes. Peak 5 of additive C6 was centered at a retention time of 16 minutes; hence a  $\text{C}_8$  to  $\text{C}_{10}$  alkyl chain chemical structure was expected.

## Chapter 4: Results and discussion

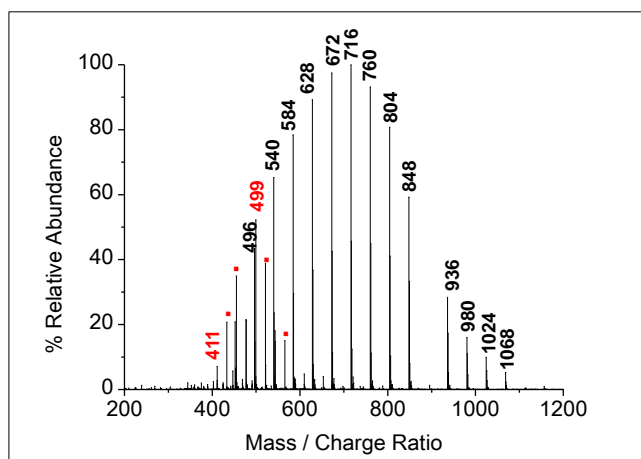


Figure 4.60: Positive scan LC-MS of additive C6 for peak 5.

Peaks 6 and 7 showed various oligomer separations in each of the peaks; hence all the oligomers were integrated simultaneously as shown by the spectra in Figure 4.61. Both spectra consisted of the ammoniated ions with the EO repeat unit. The molecular ion distribution highlighted in blue in spectrum B ( $m/z$  556, 600, 644 etc.) was similar to spectrum A, but with the elution of some higher molar mass species. When the two spectra were compared; the ion at  $m/z$  556 (peak 6) was 14 Da less than the ion at  $m/z$  570 (peak 7). Hence these two components were separated from each other by a  $-\text{CH}_2-$  group. There was no distinct relation observed between peak 5 and the two components at peaks 6 and 7 in terms of the separation by the length of the polymer chain. This meant that peaks 6 and 7 consisted of different chemical compositions compared to peak 5.

Furthermore, these two components were observed in the elution region that was expected for  $\text{C}_{12}$  to  $\text{C}_{16}$  hydrocarbon chains. Literature studies were found on the analysis of fatty alcohol ethoxylates using the  $\text{C}_{18}$  column and methanol/water mobile phase<sup>30,31</sup>. They showed the elution of the  $\text{C}_{12}$  to  $\text{C}_{16}$  fatty alcohol ethoxylates in the region of 20 to 40 minutes, which correlated to the findings in this research. An alcohol such as tridecanol, which is a mixture of  $\text{C}_{12}$  to  $\text{C}_{16}$  alcohols, is commonly associated with the synthesis of these types of fatty alcohol-PEGs<sup>19</sup>.

## Chapter 4: Results and discussion

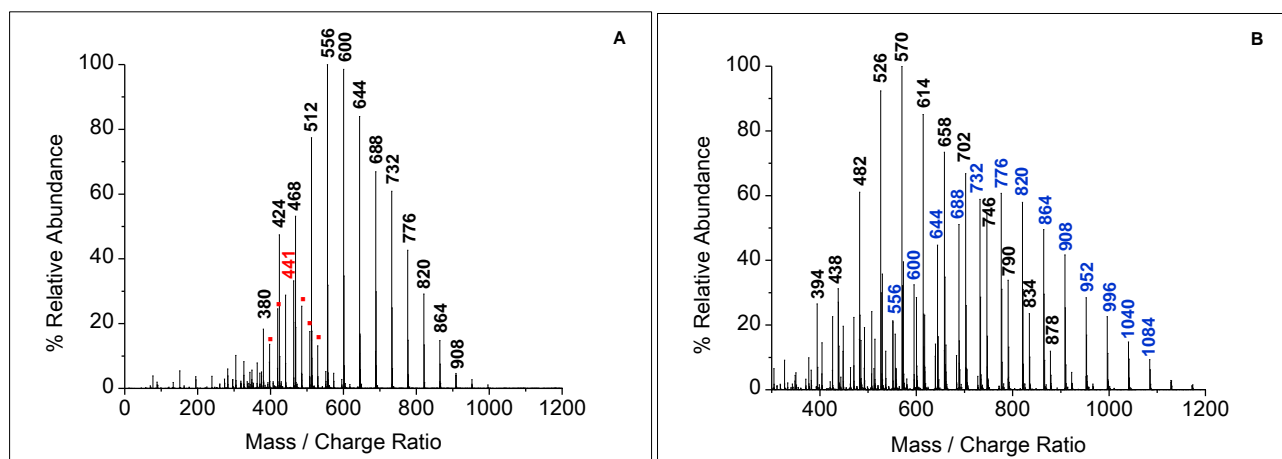


Figure 4.61: Positive scan LC-MS of additive C6 for peak 6 (A) and peak 7 (B).

A simultaneous integration of all the peaks from the negative scan TIC showed the mass spectrum in Figure 4.62. The  $[M-H]^-$  molecular ions at  $m/z$  269, 283, 297, 311, 325 etc. showed a peak-to-peak difference of 14 Da, suggesting an alkyl chain with increasing number of  $-CH_2-$  groups. The predominant ion at  $m/z$  325 matched dodecylbenzene sulfonate,  $C_{12}H_{25}-C_6H_4-SO_3^-$ . This assignment correlated to the characterization of additive C5 in section 4.3.3.4. The mass spectrum of dodecylbenzene sulfonate was also confirmed by Nishikawa *et al.*<sup>30</sup>.

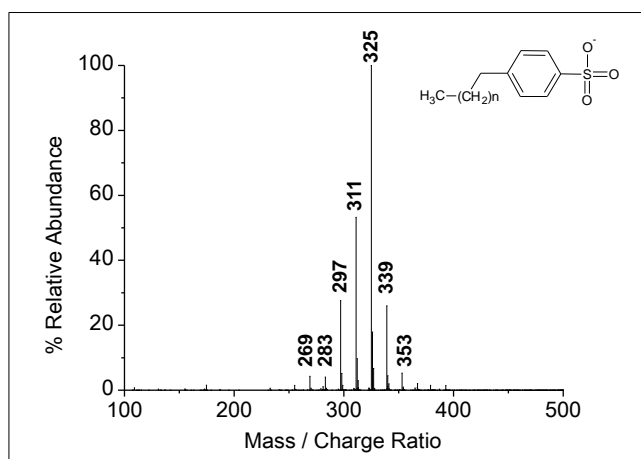


Figure 4.62: Negative scan LC-MS of additive C6.

The types of chemical groups in additive C6 were identified by FTIR-ATR (Figure 4.63) and these were correlated to both the LC-MS and NMR (Figure 4.64) data. FTIR-ATR spectrum confirmed the presence of unsaturated components as shown by several  $=C-H$  bending vibrations at 833, 759 and  $700\text{ cm}^{-1}$ . The  $C=C$  stretch of either an alkene chain or an aromatic ring was observed by a weak signal at  $1598\text{ cm}^{-1}$ . These results were further supported by the  $^1H$  NMR where the signals

## Chapter 4: Results and discussion

arising from the aromatic protons were observed at 7.03 to 7.52 ppm as well as the vinyl (5.32 ppm) and allylic (2.02 ppm) protons of the alkyl chain. The S=O stretch from an aromatic sulfonate was assigned at  $1174\text{ cm}^{-1}$  while the signals at  $2955$ ,  $2924$  and  $2855\text{ cm}^{-1}$  were due to the C-H stretch vibrations on a hydrocarbon chain. These results confirmed the presence of alkylbenzene sulfonate as well as the unsaturated hydrocarbon chain end group.

FTIR-ATR spectrum also showed the C=O stretch from an ester group at  $1742\text{ cm}^{-1}$ . This suggested that additive C6 was possibly an ester-based PEG, which is a type of surfactant that is commonly used in coatings. Moreover, some ester-type fragments were detected by pyrolysis GC-MS analyses. Fatty ester-PEGs are typically synthesized by esterification or ethoxylation of fatty acids. The types of products obtained from this synthesis route are often mixtures of monoesters, diesters and PEG, which makes it difficult to fully characterize these types of additives<sup>32,33</sup>.

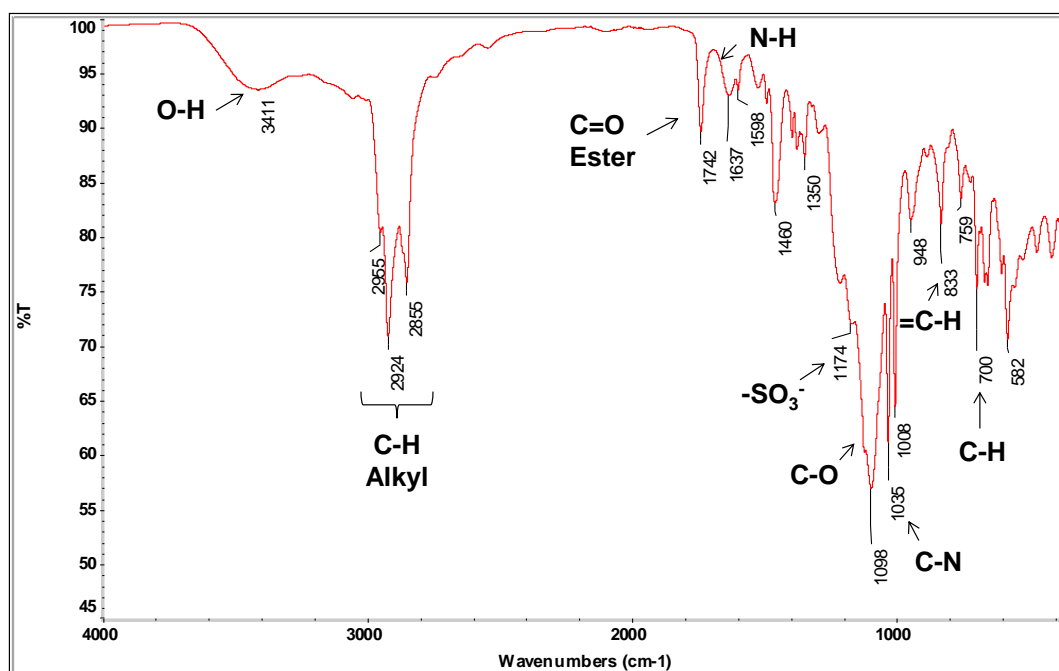


Figure 4.63: FTIR-ATR of additive C6.

The  $^1\text{H}$  NMR in Figure 4.64 showed the methylene protons of the EO repeat unit at 3.51 ppm while a peak at 3.33 ppm was due to the hydrogen-deuterium exchange. The peak at 4.6 ppm was assigned to the hydroxyl end group. The methylene protons from the alkyl chain repeat unit were assigned at 1.24 ppm. The complex multiplet at 0.7 to 0.9 ppm was due to branching on the alkylbenzene sulfonate as discussed for additive C5 in Section 4.3.3.4. A doublet centered at 1.16 ppm was attributed to the two methyl groups on the isopropyl amine structure:  $\text{H}_2\text{N}-\text{CH}-(\text{CH}_3)_2$ , as discussed for additive C5. The presence of isopropyl amine was further confirmed by the C-N ( $1035\text{ cm}^{-1}$ ) and N-H ( $1637\text{ cm}^{-1}$ ) stretches in the FTIR-ATR spectrum. The most common commercial



surfactant such as isopropyl amine dodecylbenzene sulfonate has a wide range of applications in cosmetics, detergents and coatings.

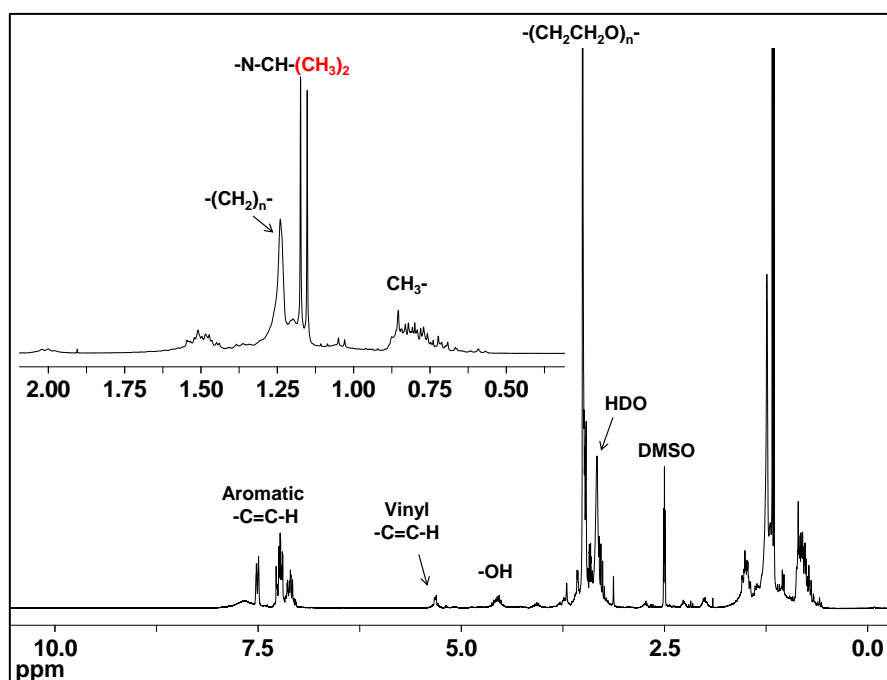


Figure 4.64:  $^1\text{H}$  NMR of additive C6 in DMSO,  $25^\circ\text{C}$  and 600 MHz.

The results showed that additive C6 consists of a PEG of 12 EO repeat units and an average molar mass of 546 g/mol. LC-MS data indicated the presence of the two main types of polymers with the EO repeat unit, bearing the alkyl hydrocarbon chain end groups. The information acquired from FTIR-ATR, pyrolysis GC-MS and  $^1\text{H}$  NMR suggested that one of the main components of additive C6 (peak 5) may be an unsaturated fatty ester-PEG with a chain length range of  $\text{C}_8$  to  $\text{C}_{10}$ . Several oligomers of decreasing chain length were observed to be related to peak 5. These components may be mixtures of mono- and diesters that are typically formed during the synthesis of fatty ester-PEGs.

The two related components at peaks 6 and 7 were separated by one methylene group, and these were possibly due to the long chain ( $\text{C}_{12}$  to  $\text{C}_{16}$ ) fatty alcohol-PEG. The fatty alcohol ethoxylates synthesized from tridecanol are common in surfactant industries, and these usually form a mixture of  $\text{C}_{12}$  to  $\text{C}_{16}$  products, as observed in this research. Analyses of additives that contain these types of components are required to confirm this. The negative scan LC-MS, FTIR-ATR and NMR confirmed isopropyl amine dodecylbenzene sulfonate as one of the components.

#### 4.3.3.6. Analyses of additive C7

The positive and negative TIC scans of additive C7 in Figure 4.65 were acquired at critical conditions of adsorption of PEG. Seven peaks were detected in the positive scan mode while three were observed in the negative mode. The absence of peaks 3 to 6 in the negative mode was attributed to either the weak anionic behaviour or the non-ionic character of the components.

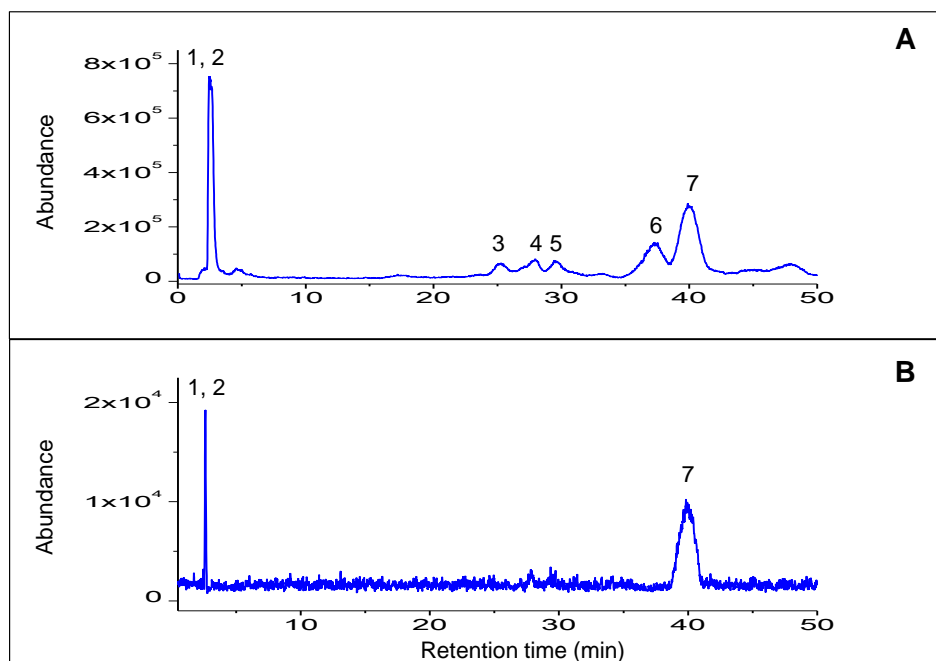


Figure 4.65: Positive (A) and negative (B) TIC scans of additive C7.

The positive scan mass spectra of the components at peaks 1 and 2 are presented in Figure 4.66. Figure 4.66A (peak 1) showed two molecular ion series at  $m/z$  326, 370, 414, 458 etc. (black) and at  $m/z$  392, 436, 480, 524 etc. (red). The black series was attributed to  $[M + \text{NH}_4]^+$  while the red series was  $[M + \text{K}]^+$ , where M is a cyclic PEO. The theoretical versus experimental values for the most abundant ion in the ammoniated series showed an average of 12 EO repeat units.

$$(m/z)_{\text{experimental}} = 546.45$$

$$(m/z)_{\text{theoretical}} = 18.0385 + 12 \times 44.0526 = 546.67$$

In Figure 4.66B (peak 2) the  $[M + \text{NH}_4]^+$  series at  $m/z$  300, 344, 388 etc. was similar to the mass spectrum of additive A1 in section 4.3.1.1. The most abundant ion at  $m/z$  388 was assigned to a PEG with eight EO repeat units.

## Chapter 4: Results and discussion

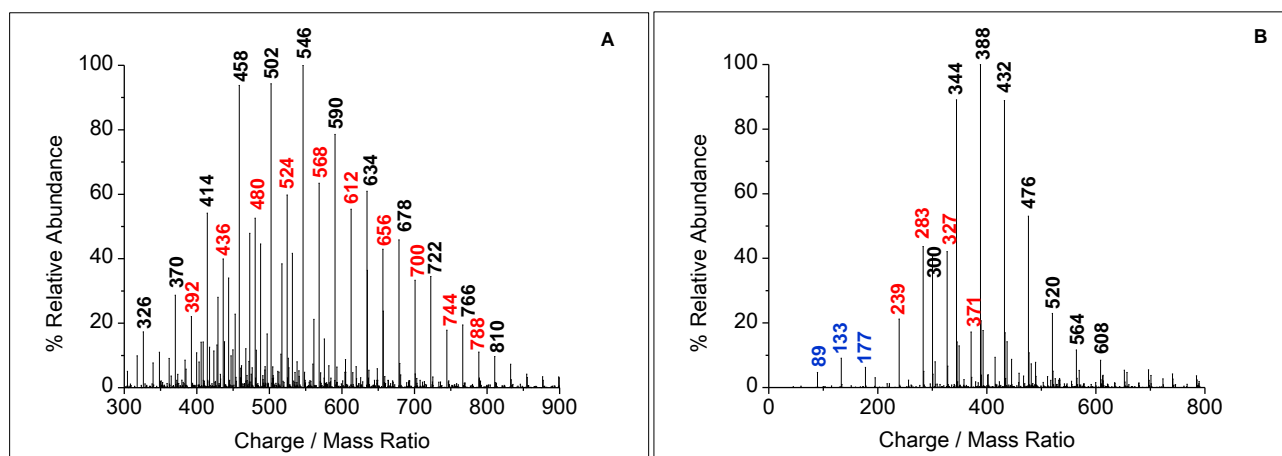


Figure 4.66: Positive LC-MS of additive C7 for peak 1 (A) and peak 2 (B).

The mass spectra acquired from peaks 3 and 4 were similar to that of peak 5 as presented in Figure 4.67A. Peak 5 showed the mass spectrum with the singly charged series ( $m/z$  586, 630, 674 etc.) as well as the doubly charged species at  $m/z$  368, 390, 412 etc. The mass spectrum of peak 6 (Figure 4.67B) consisted of only the doubly charged species at  $m/z$  457, 479, 501 etc. Both the components at peaks 5 and 6 components showed weak anionic behaviour compared to peaks 1, 2 and 7. Furthermore, based on the information from additives C1, C4 and C6; the presence of the alkyl chain ( $C_{10}$ - $C_{16}$ ) end group was expected in the elution region of 25 to 45 minutes. The FTIR-ATR and NMR analyses will later confirm the hydrocarbon chain.

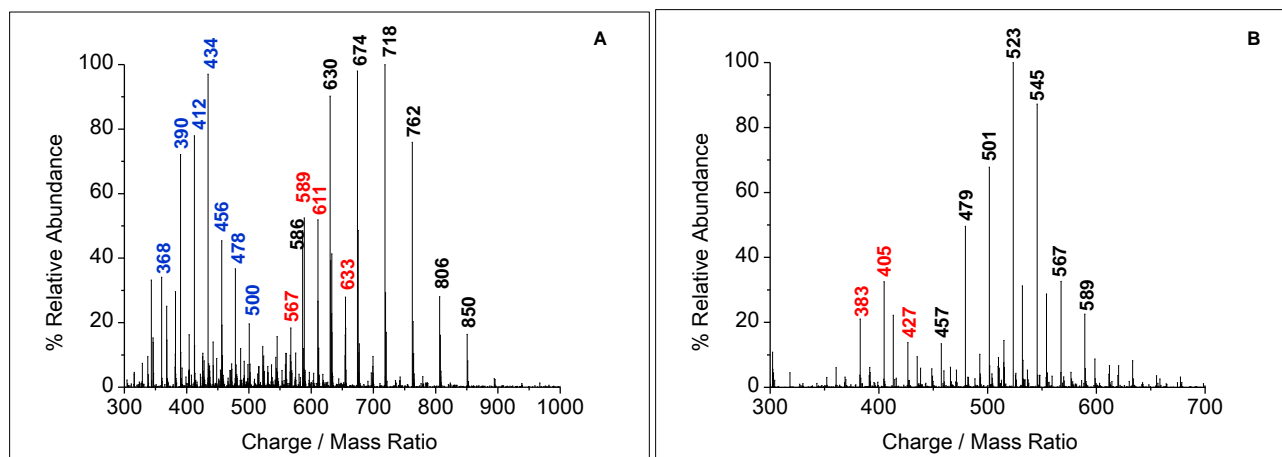


Figure 4.67: Positive scan LC-MS of additive C7 for peaks 5(A) and 6 (B).

In Figure 4.69, the mass spectrum acquired at peak 7 in the positive and negative modes showed the same series at  $m/z$  544, 588, 632 etc. The presence of the same series in the two scan modes suggested the presence of a component that consists of both the negative and positive charge in the

## Chapter 4: Results and discussion

same molecule. This phenomenon is commonly associated with zwitterionic surfactants. The source of the positive charge is mostly the ammonium ion while the negative charge may be a number of end groups; however, the carboxylate group is the most common source. The typical zwitterionic surfactants are derived from glycine, amino propionic acid or betaine<sup>26,34</sup>

The N-oxides of tertiary amines may also show the zwitterionic, cationic or non-ionic behavior depending on the pH of the solution or the presence of anionic components<sup>26,35</sup>. The other source of two charges on the same molecule may be the amide end group as discussed in Section 4.3.3.3. This occurs due to the delocalization of the electrons between the carbonyl group and the lone pair on the nitrogen atom<sup>35</sup>. Figure 4.68 shows examples of the most common EO-based zwitterionic surfactants that have been reported in literature<sup>25,26,30,36</sup>.

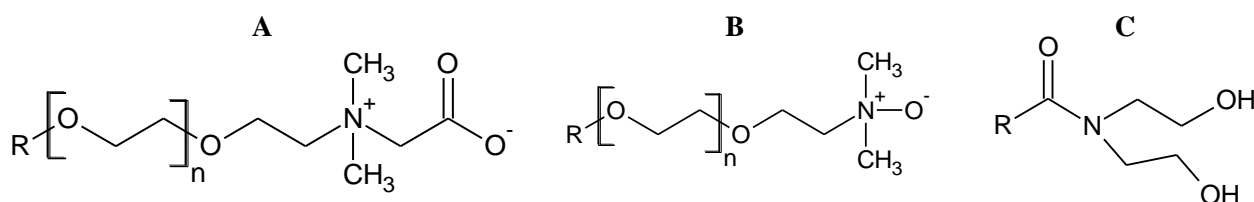


Figure 4.68: Examples of common zwitterionic surfactants.

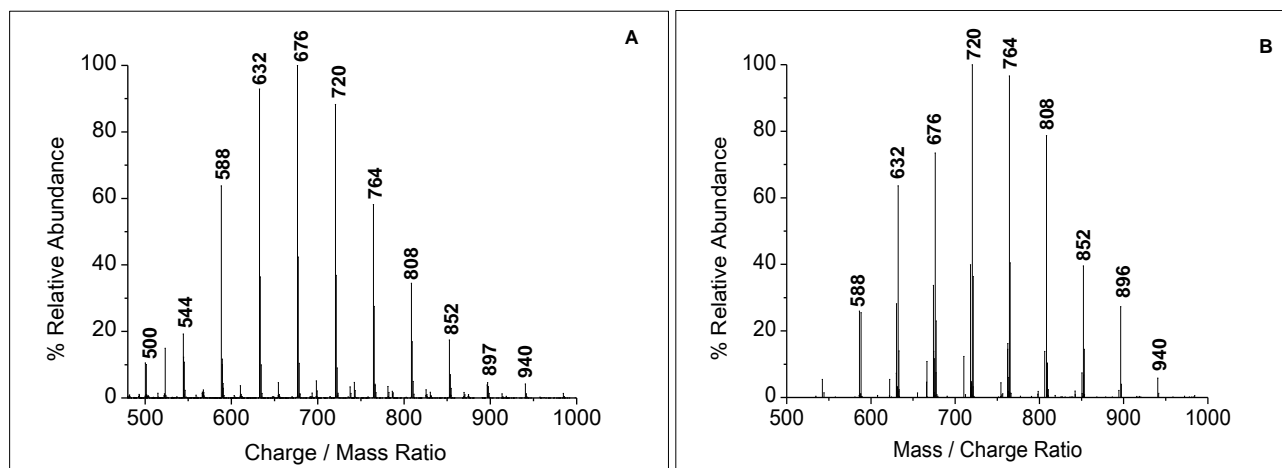


Figure 4.69: Positive (A) and negative (B) LC-MS of additive C7 for peak 7.

The  $^1H$  NMR,  $^{13}C$  NMR and FTIR-ATR spectra in Figures 4.70 to 4.72 were used to identify the chemical structures of the end groups. The  $^1H$  NMR in Figure 4.70 (0 to 3 ppm) and Figure 4.71 (3 to 11 ppm) indicated the presence of a polyunsaturated hydrocarbon chain. This was confirmed by several signals arising from the allylic (1.9 to 2.3 ppm) and vinyl (5.3 to 6.2 ppm) protons.

## Chapter 4: Results and discussion

The  $^{13}\text{C}$  NMR (Figure 4.72) also showed multiple signals of the  $-\text{C}=\text{C}-$  groups at 125 to 134 ppm. The peak area integration in the  $^1\text{H}$  NMR indicated four vinyl protons in the region of 5.3 to 6.2 ppm. Based on this information and the number of  $-\text{C}=\text{C}-$  signals in the  $^{13}\text{C}$  NMR, it was estimated that the unsaturated hydrocarbon chain end group consisted of at least three double bonds. The methyl (0.848 ppm) and methylene (1.2 to 1.5 ppm) protons further confirmed the presence of a polyunsaturated hydrocarbon chain as one of the end groups.

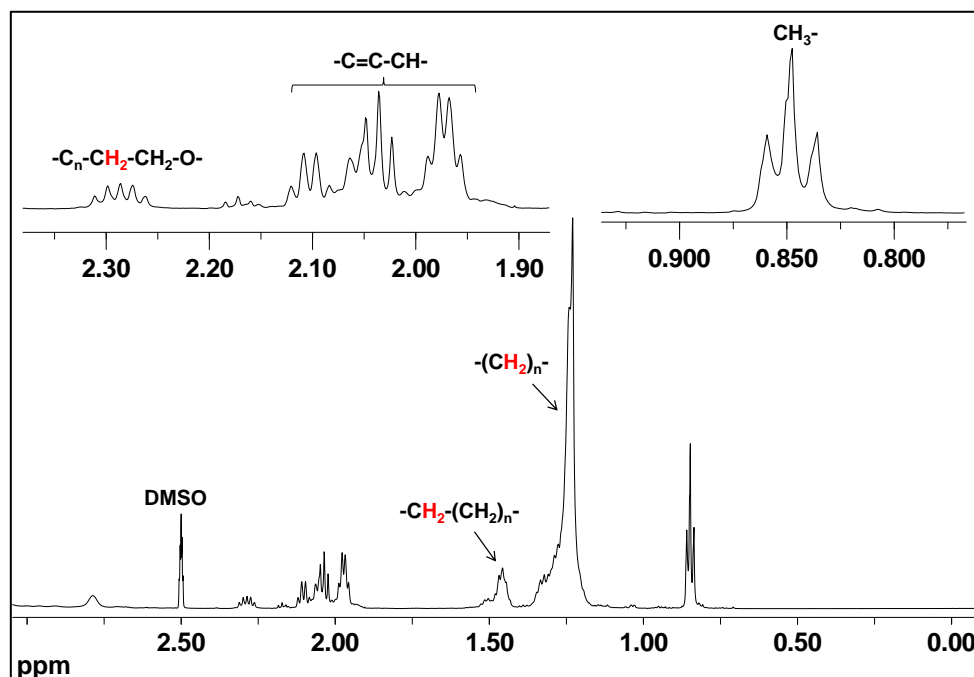


Figure 4.70:  $^1\text{H}$  NMR of additive C7 in DMSO, 25°C and 600 MHz, at 0 to 3 ppm.

In Figure 4.71, the methylene protons of the EO oxide repeat unit were assigned at 3.51 ppm. A quartet centered at 3.18 ppm was attributed to the  $-\text{CH}_2-$  group that was in the proximity of an electronegative atom such as oxygen or nitrogen. The amide group ( $\text{HN}-\text{CO}-\text{R}$ ) was observed by the hydrogen-deuterium exchange triplet at 7.80 ppm as well as the carbonyl ( $\text{C}=\text{O}$ ) signal at 172 ppm on the  $^{13}\text{C}$  NMR in Figure 4.72. The FTIR-ATR spectrum (Figure 4.73) also showed a strong signal of the  $\text{C}=\text{O}$  stretch ( $1646\text{ cm}^{-1}$ ), arising from the amide compound.

## Chapter 4: Results and discussion

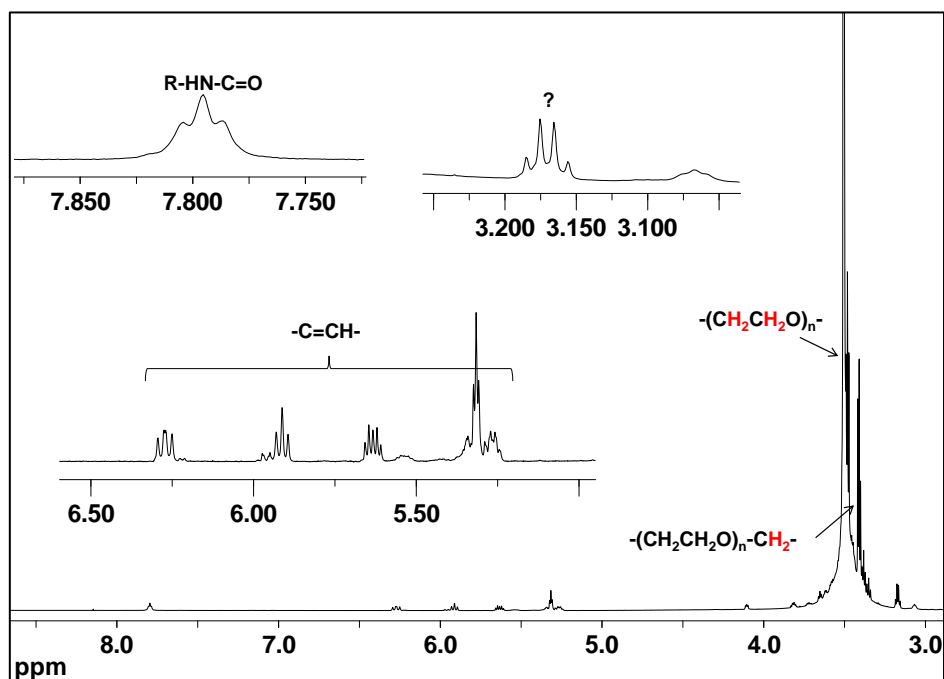


Figure 4.71:  $^1\text{H}$  NMR of additive C7 in DMSO,  $25^\circ\text{C}$  and 600 MHz, at 3 to 9 ppm.

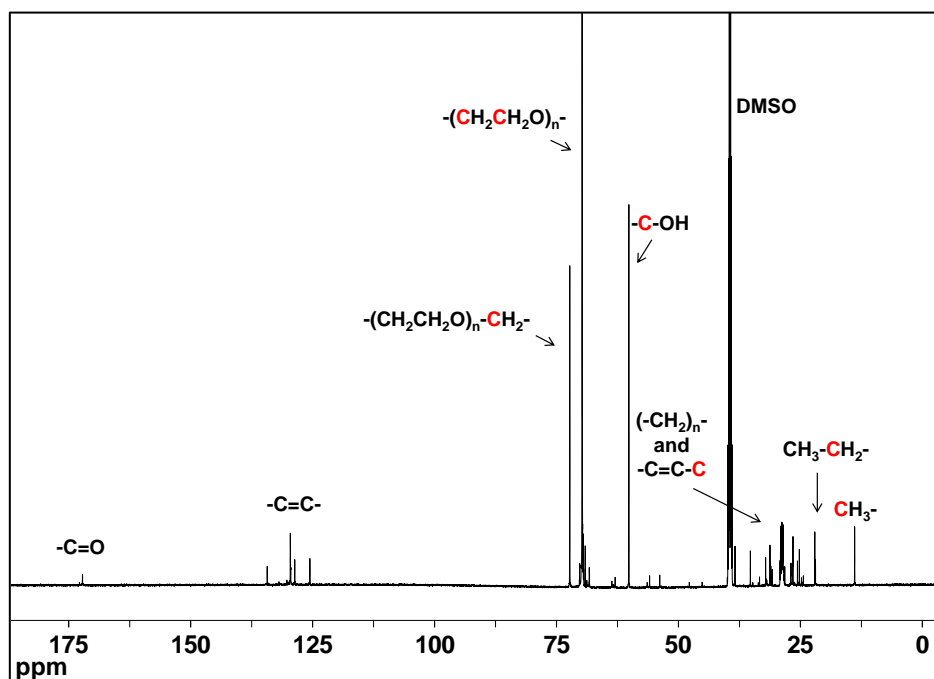


Figure 4.72:  $^{13}\text{C}$  NMR of additive C7 in DMSO,  $25^\circ\text{C}$  and 300 MHz.

## Chapter 4: Results and discussion

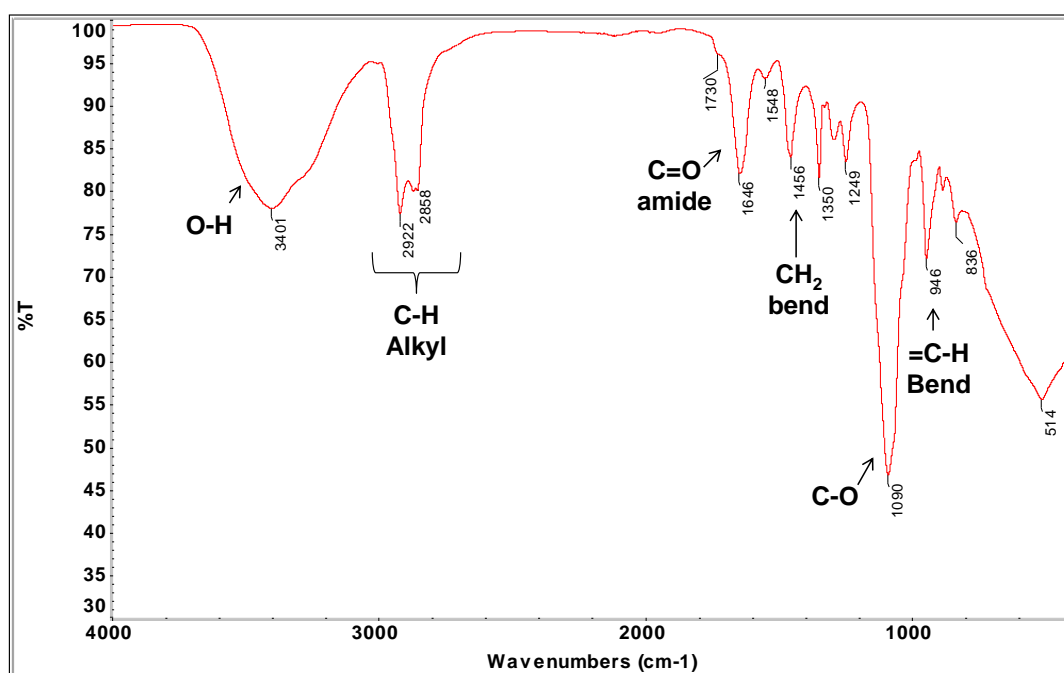


Figure 4.73: FTIR-ATR spectrum of additive C7.

The LC-MS results showed that additive C7 consists of a cyclic PEO ( $M_p$  528 g/mol,  $n = 12$ ) and a PEG ( $M_p$  370,  $n = 8$ ). LC-MS also indicated that the additive contains a PEG-based component that has a zwitterionic end group. The  $^1\text{H}$  and  $^{13}\text{C}$  NMR showed the presence of a polyunsaturated hydrocarbon chain with at least three double bonds and a chain length range of  $\text{C}_{10}$  to  $\text{C}_{16}$ . Both the NMR and FTIR-ATR showed prominent signals of an amide-type end group. These data suggested that the other component of the additive has the EO repeat unit with a polyunsaturated chain and an amide-based end group.

#### 4.4. Identification of additives in colourants

The two formulations in Tables 4.10 and 4.11 were prepared according to realistic recipes of commercial colourants. Each of the colourants was made up of a solvent (water), organic and inorganic pigments, additives, and other colourants. The types of additives were glycols, wetting and dispersing agents, biocides, acticides, thickeners, and defoamers. The additives were extracted from the colourant by centrifugation and analysed by LC-UV and LC-MS at critical conditions of adsorption of PEG. All the targeted additives in the formulations were characterized as discussed in Sections 4.3.1 to 4.3.3.

## Chapter 4: Results and discussion

According to Table 4.10, the reddish-brown colourant formulation consisted of additives A3, C1, C2 and C5. The formulation also contained the red, yellow, and black colourants; which were added to obtain the reddish-brown colour.

*Table 4.10: Formulation of a reddish-brown colourant.*

Raw Materials	% Mass	Additives identified by LC-MS and LC-UV
Water	9.67	
Additive A3	8.99	✓
Filler	0.14	
Defoamer 1	0.49	
Emulsifier 1	0.90	
Additive C1	2.95	✓
Additive C2	0.48	✓
Additive C5	0.48	✓
Inorganic extender	26.69	
Defoamer 2	0.19	
Yellow colourant	10.99	
Red oxide colourant	5.04	
Black colourant	20.51	
Yellow oxide colourant	12.49	
Total	100.00	

Figure 4.74 shows the LC-UV chromatograms of the additives extracted from the reddish-brown colourant, compared to the pure additives C1 and C5. The samples were all analysed at critical conditions of PEG with UV detection (230 nm) in order to show the UV active phenyl-based components of additives C1, C2 and C5. Additive C1 and C2 are both based on the alkylphenyl ethoxylate chemical structures; hence their peaks were expected to overlap at retention times 1, 5, 6 and 7. Additive C5 was identified by several oligomers, all labelled by 4.

Moreover, the identification of additives A3 (ethylene glycol), C1, C2 and C5 was also achieved by MS detection. The mass spectra acquired for peak 4 (additive C5) and peak 6 (additive C1) of the pure versus extracted additives are presented in Figures 4.75 and 4.76. These spectra were identical, confirming the efficient extraction and identification of the additives in the colourant.



## Chapter 4: Results and discussion

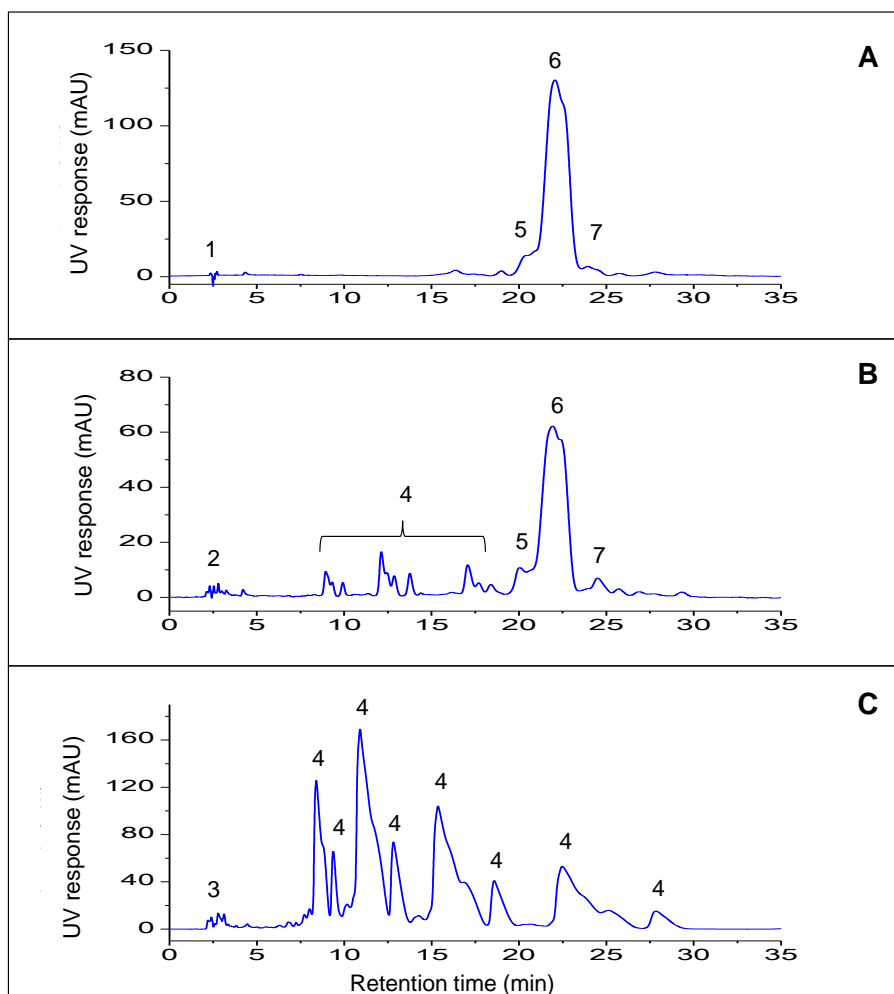


Figure 4.74: LC-UV chromatograms at 230 nm for additive C1 (A), extracted additives from the reddish-brown colourant (B) and additive C5 (C).

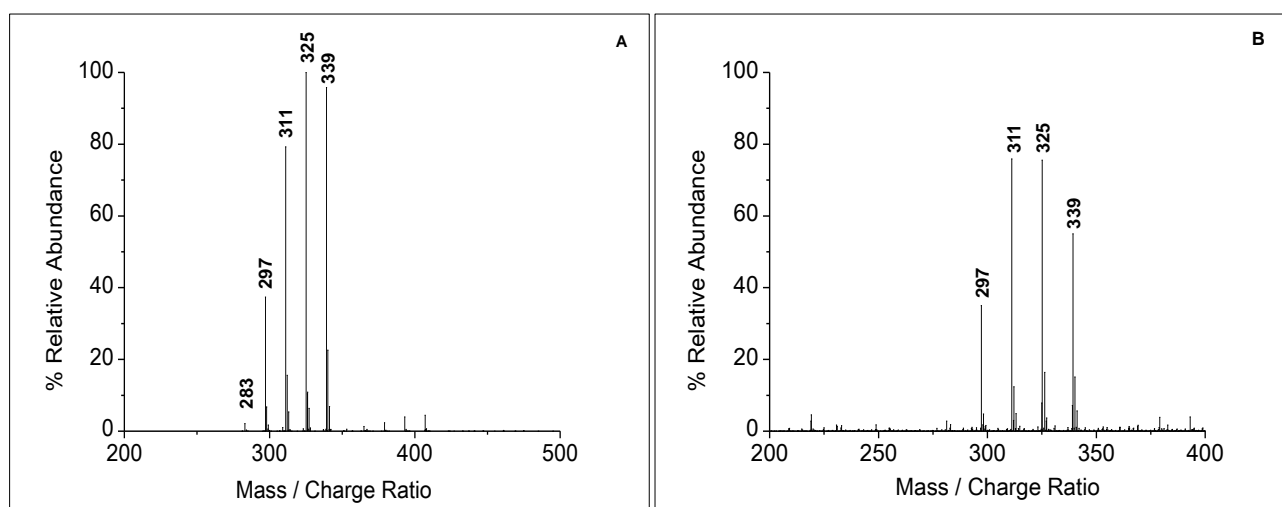


Figure 4.75: Negative scan LC-MS of peak 4 for the pure (A) and extracted (B) additive C5.

## Chapter 4: Results and discussion

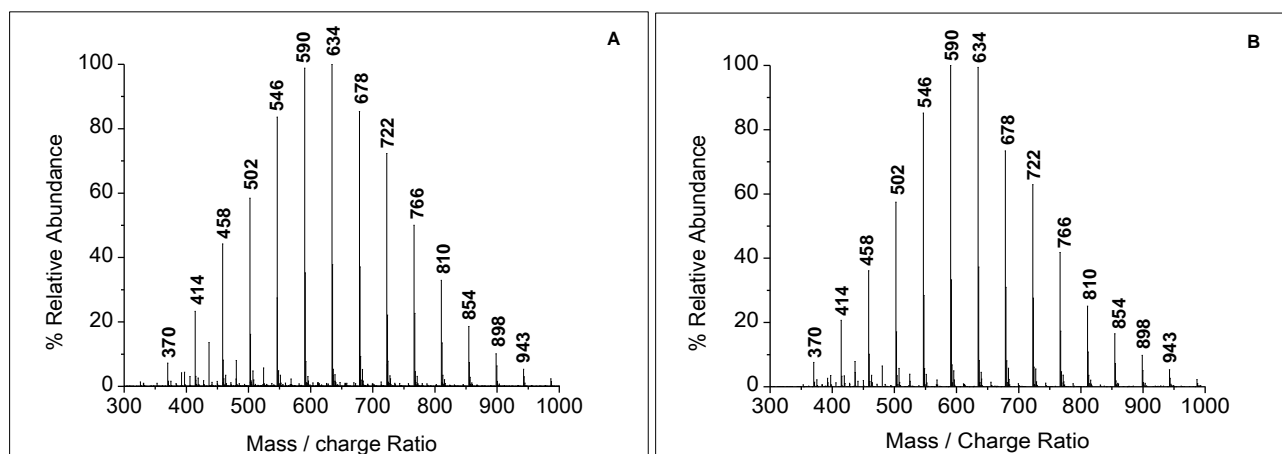


Figure 4.76: Positive scan LC-MS of peak 6 for the pure (A) and extracted (B) additive C1.

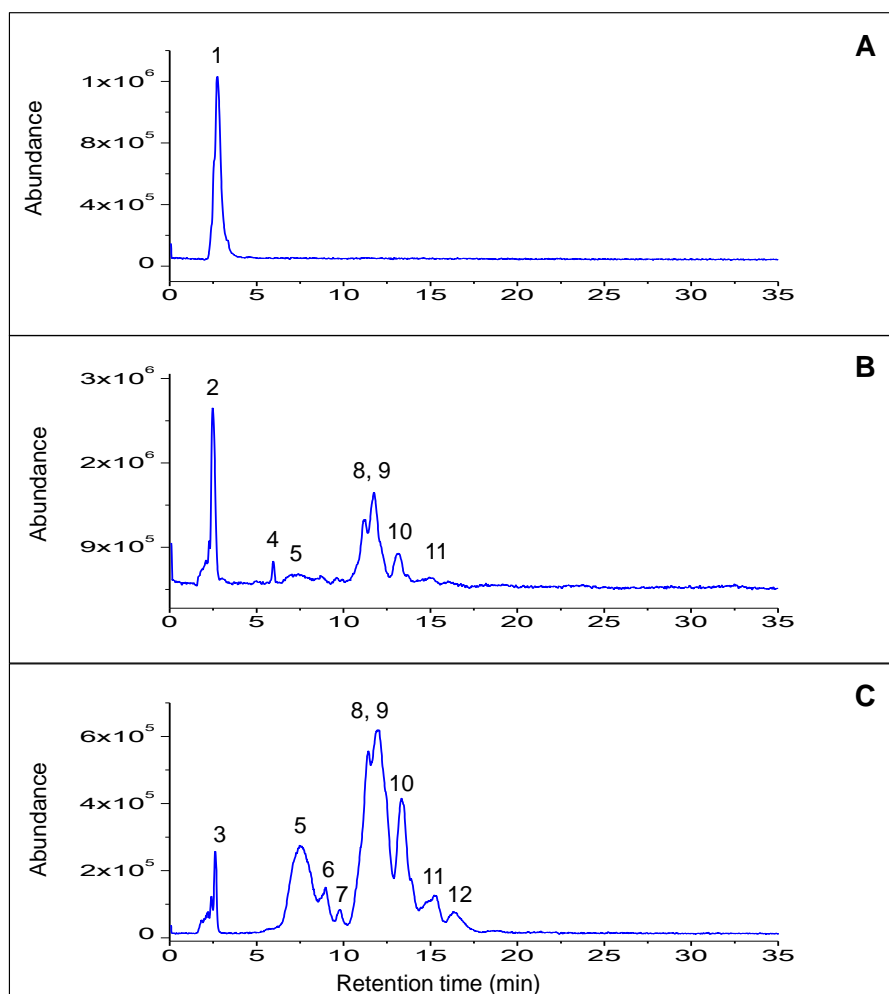
Table 4.11 shows the formulation of a bright yellow colourant, which consisted of water, additives B3 and C4, thickeners, biocide and acticides. The yellow pigments, extender paste and a white colourant were also added to make the bright yellow colourant.

Table 4.11: Formulation of a bright yellow colourant.

Raw Materials	% Mass	Additives identified by LC-MS and LC-UV
Water	40.00	
Additive B3	10.00	✓
Additive C4	5.00	✓
Base solution	0.76	
Defoamer	0.80	
Thickener 1	0.60	
Acticide 1	0.32	
Inorganic extender paste	19.78	
Yellow pigments	8.03	
Water	9.45	
Biocide	0.20	
Acticide 2	0.35	
Thickener 2	1.00	
White colourant	3.71	
Total	100.00	

The extracted additives were analysed at critical conditions of PEG and both additive B3 and C4 were identified by LC-MS as presented in Figure 4.77. The elution of additive B3 and the two components of additive C4 were overlapped at peaks 3. The other components of additive C4 were identified at peaks 5 to 11. Peak 4 was attributed to 2-octyl-2H-isothiazol-3-one, which is a

component of an anti-fungal agent (acticide 2) in the colourant formulation shown in Table 4.11. The method's sensitivity and selectivity can be evaluated by incorporating various concentrations of the additives in the original formulation followed by extraction and LC-MS analyses.



*Figure 4.77: TIC scans of additive B3 (A), extracted additives of the bright yellow colourant (B) and additive C4 (C).*

The mass spectra of the pure versus extracted additives B3 and C4 (peak 6) are presented in Figures 4.78 and 4.79, respectively. The extraction and identification of the additives from the colourant was successfully achieved and confirmed by both the LC behaviour and LC-MS spectra.

## Chapter 4: Results and discussion

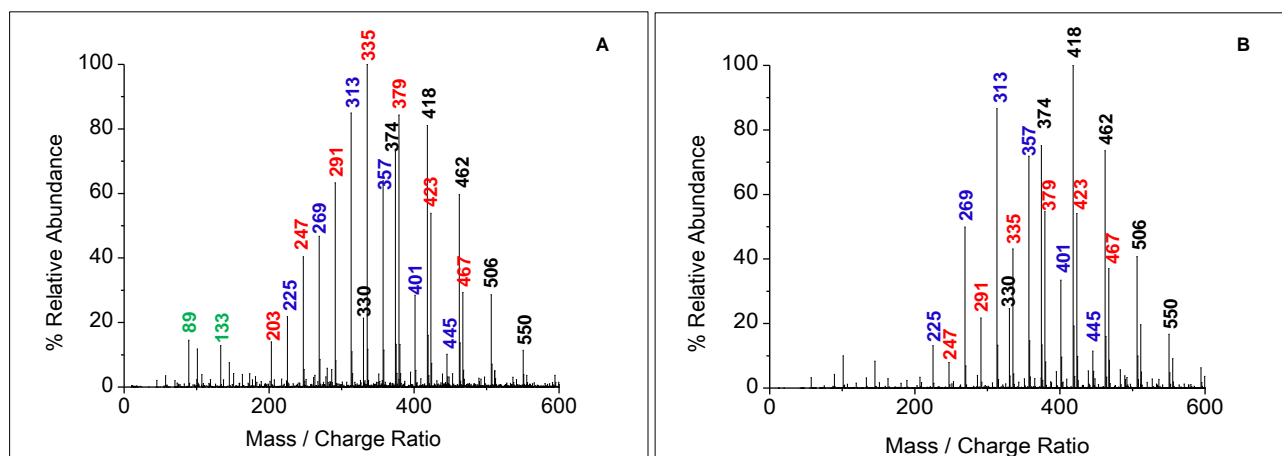


Figure 4.78: Positive scan LC-MS for the pure (A) and extracted (B) additive B3.

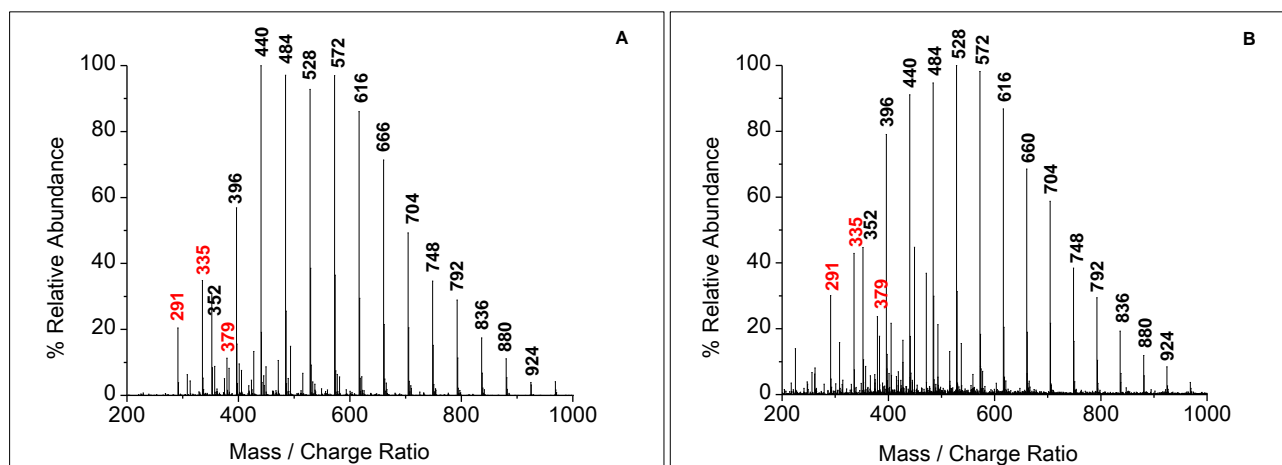


Figure 4.79: Positive scan LC-MS of peak 6 for the pure (A) and extracted (B) additive C4.

## 4.5. Conclusions

Liquid chromatography, NMR, FTIR-ATR and pyrolysis GC-MS analyses were successfully conducted on commercial additives that are used in colourants. In particular, liquid chromatography at critical conditions of adsorption of PEG and solvent gradient elution allowed for the separation of the additives' components according to the differences in functional end groups.

### The search for the critical point of adsorption of PEG

Liquid chromatography at critical conditions was identified as a powerful technique for the separation of PEG-based polymers. The ELS and UV detectors were used to determine the critical point of adsorption of PEG standards. The technique was applied to commercial additives in order

to exclude the molar mass effects while separating according to the differences in functional end groups and polymer blends.

### **Characterization of type A additives**

The three types of additives such as poly(ethylene glycol), poly(propylene glycol) and ethylene glycol were successfully characterized by LC-MS and NMR.

### **Characterization of type B additives**

The chemical structures of the three types of humectants were successfully identified by LC-MS and NMR. The results showed that in all of these additives; at least one of the components was a polymer with multiple hydroxyl end groups. This correlated with the properties of these types of additives to act as hydrophilic moisturizing agents in colourants.

In additive B1, the glucose-based components such as alkyl glucosides and alkyl oligoglucosides were characterized by LC-MS in the negative scan mode. The long chain, non-polar components such as PEG monooleyl ether ( $C_{18}$ , unsaturated) and PEG decyl ether phosphate ( $C_{13}$ , saturated) required a combination of LCCC and solvent gradient separation modes, for the enhancement of the elution. All the identified components correlated to the manufacture's data sheet for additive B1.

LC-MS analyses in the negative mode and NMR showed that additive B2 consisted of PEG monomethyl ether ( $M_p$  502 g/mol,  $n=11$ ) and an oligoglucoside with four glucose units. The negative mode LC-MS confirmed that the fragmentation of oligoglucoside in this additive was as a result of the cross-ring and glycosidic bond cleavages.

In additive B3, the three-arm star PEG ( $M_p$  400g/mol,  $n=7$ ) was identified by both LC-MS and NMR. The additive showed a trimodal molecular ion distribution in LC-MS, suggesting various affinities for the types of cations in solution.

### **Characterization of type C additives**

The type C additives (C1 to C7) all showed the presence of three or more components which were either PEG-based and/or non-polymeric. PEG ( $M_p$  502 and 546 g/mol,  $n=11$  and 12) was identified in additives C1, C2, C4 and C6 while additive C7 showed the presence of a PEG with average molar mass of 370 g/mol and eight EO repeat units.

Additives C1 and C2 were based on the octyl-, nonyl- and decylphenyl ethoxylates. NMR data confirmed the presence of branching at the hydrocarbon chain of these additives. The phenyl-based

chemical structure was further identified in additives C5 and C6, which consisted of alkylbenzene sulfonate. NMR and FTIR-ATR indicated isopropyl amine as the neutralising agent of alkylbenzene sulfonate.

The fatty acid and fatty ester based polymers were identified in additives C4 and C6, respectively. The fatty acid polymer in additive C4 was based on a mixture of caprylic ( $C_8$ ), perlagonic ( $C_9$ ), capric ( $C_{10}$ ) acid as well as alpha-linolenic ( $C_{18}$ ) polyunsaturated fatty acid. Additive C6 showed multiple oligomers of fatty ester-PEG, which were possibly mixtures of mono- and diesters.

Fatty alcohol ethoxylates were present in additive C6. The length of the alcohol chain length was estimated to be in the range of  $C_{12}$  to  $C_{16}$ . A  $C_{18}$  unsaturated fatty alcohol ethoxylate in the form of PEG monooleyl ether was identified in additive C3.

Zwitterionic behaviour was observed in additives C4 and C7. FTIR-ATR analyses showed the amine and amide end group types in these additives, which are commonly associated with this type of behaviour.

### **Identification of additives in colourants**

Two colourants were prepared with the characterized additives to evaluate the extraction efficiency and traceability of the extracted additives to the original formulation. The constituents of the colourant mixtures were water, organic and inorganic pigments, extenders, thickeners, acticides, biocides and defoamers. The targeted additives were successfully extracted, separated and identified from each of the two colourant formulations using LC-MS at critical conditions of PEG. Assignments of the extracted additives could be performed based on the LC behaviour as well as the LC-MS spectra for the chromatographic peaks.

## 4.6. References

- (1) Pasch, H.; Trathnigg, B. *Multidimensional HPLC of Polymers*; Springer: New York, 2013; pp 17–34.
- (2) Pasch, H.; Trathnigg, B. *HPLC of Polymers*; Springer: Heidelberg, 1999; pp 128–137.
- (3) Koster, S.; Duursma, M. C.; Boon, J. J.; Heeren, R. M. A. *J. Am. Soc. Mass Spectrom.* **2000**, *11*, 536–543.
- (4) Izunobi, J. U.; Higginbotham, C. L. *J. Chem. Educ.* **2011**, *88*, 1098–1104.
- (5) Dauner, B. R.; Pringle, D. L. *J. Chem. Educ.* **2014**, *91*, 743–746.
- (6) Taylor, V. F.; March, R. E.; Longerich, H. P.; Stadey, C. J. *Int. J. Mass Spectrom.* **2005**, *243*, 71–84.
- (7) O'Brien, R. D.; Farr, W. E.; Wan, P. J. *Introduction to fats and oils technology*; AOCS Press: Champaign, Illinois, 2000; pp 515–541.
- (8) Domon, B.; Costello, C. E. *Glycoconj. J.* **1988**, *5*, 397–409.
- (9) Lemoine, J.; Fournet, B.; Despeyroux, D.; Jennings, K. R.; Rosenberg, R. *J. Am. Soc. Mass Spectrom.* **1993**, *4*, 197–203.
- (10) Harvey, D. J. *J. Mass Spectrom.* **2000**, *35*, 1178–1190.
- (11) Garozzo, D.; Giuffrida, M.; Impallomeni, G.; Ballistreri, A.; Montaudo, G. *Anal. Chem.* **1990**, *62*, 279–286.
- (12) Chai, W.; Piskarev, V.; Lawson, A. M. *Anal. Chem.* **2001**, *73*, 651–657.
- (13) Cui, S. W. *Food Carbohydrates: Chemistry, Physical Properties and Applications*; Taylor & Francis Group: Boca Raton, USA, 2005; pp 112–167.
- (14) Prozil, S. O.; Costa, E. V.; Evtuguin, D. V.; Popez, L. P.; Domingues, M. R. M. *Carbohydr. Res.* **2012**, *356*, 252–259.
- (15) Sanghi, R.; Dhar, D. N. *J. Sci. Ind. Res.* **2001**, *60*, 463–492.
- (16) Bubbb, W. A. *Concepts Magn. Reson. Part A* **2003**, *19A*, 1–19.
- (17) Lapienis, G. *Prog. Polym. Sci.* **2009**, *34*, 852–892.
- (18) Merrill, E. W. *J. Biomater. Sci.* **1993**, *5*, 1–11.
- (19) Salager, J.-L. *Surfactants types and uses*, Second Edn.; Universidad de Los Andes: Merida-Venezuela, 2002, pp 3–47.
- (20) Falbe, J. *Synthesis of surfactants*; Springer Science and Business Media: Berlin, 2012, pp 1–100.

Chapter 4: Results and discussion

- (21) Ma, S.-H. Polymeric pigment dispersants having multiple pigment anchoring groups. US Patent 6451950 B1, 2002.
- (22) Mößmer, S.; Roch, M.; Göbelt, B.; Johann, S. *Eur. Coatings J.* **2010**, 2, 28–31.
- (23) The role of Fatty Acid Modified Emulsifiers (FAME) <https://www.dispersions-pigments.basf.com/portal/basf/> (accessed Jul 11, 2015).
- (24) Specialty Additives product selection guide <http://www.pcimag.com/ext/resources/> (accessed Jul 11, 2015).
- (25) Hou, L.; Zhang, H.; Chen, H.; Xia, Q. *J. Surfactants Deterg.* **2014**, 17, 403–408.
- (26) Holmberg, K.; Bo, J.; Kronberg, B.; Lindman, B. *Surfactants and polymers in aqueous solutions*; J. Wiley & Sons, LTD: England, 2003; pp 7–23.
- (27) Molever, K. *J. Surfactants Deterg.* **2005**, 8, 199–202.
- (28) Texter, J. *Reactions and synthesis in surfactant systems: Surfactant Science*; CRC Press: New York, 2001; pp 1–44.
- (29) Zoller, U.; Sosis, P. *Handbook of Detergents, Part F: Production (Surfactant Science)*; CRC Press: Boca Raton, FL, USA, 2008; pp 83–115.
- (30) Nishikawa, M.; Katagi, M.; Miki, A.; Tsuchihashi, H. *J. Heal. Sci.* **2003**, 49, 138–148.
- (31) Cretier, G.; Podevin, C.; Rocca, J. *J. Chromatogr. A* **2000**, 874, 305–310.
- (32) Trathnigg, B.; Rappel, C.; Raml, R.; Gorbunov, A. *J. Chromatogr. A* **2002**, 953, 89–99.
- (33) Abrar, S.; Trathnigg, B. *J. Chromatogr. A* **2010**, 1217, 8222–8229.
- (34) Gursel, Y. H.; Sarac, A.; Senkal, B. F. *Am. J. Anal. Chem.* **2014**, 5, 39–44.
- (35) Lim, J.; Han, D. *Colloids Surfaces A Physicochem. Eng. Asp.* **2011**, 389, 166–174.
- (36) Salvador, A.; Chisvert, A. *Analysis of cosmetic products*; Elsevier B.V.: Spain, 2007; pp 291–322.



## **Chapter 5**

### **Summary, conclusions and recommendations**

#### **5.1. Summary**

The development of colourants in the coating's industry involves the use of various commercial additives that offer properties such as: the improvement of pigment dispersions, compatibility and drying-out resistance. However, the information on the chemical composition of these additives is often incomplete or missing in the manufacturer's data sheets. The shortage of this information presents limitations for the developments of new colourants.

The main focus of this research was to develop a method of identifying and characterizing PEG-based commercial additives that are used as moisturizing, wetting and dispersing agents in colourants. The molar mass distributions and chemical compositions of the additives were determined through the use of a combination of LCCC and solvent gradient separation modes with ELSD, MS and UV detectors. Techniques such as NMR, pyrolysis-GC-MS and FTIR-ATR were used to identify the types of end groups in the additives' blend. The method used in this research will be useful for the analyses and understanding of the composition of the additives that are used in the development of paints and colourants in the coatings industry.

#### **5.2. Overall conclusions**

Below are the conclusions to the objectives of the research:

The different types of commercial additives (glycols, moisturizing and wetting and dispersing agents) that are used in colourants were successfully characterized by various analytical techniques. The additive components were based on various chemical structures namely: linear PEG, PPG, star-shaped PEG, alkyl glucosides and oligoglucosides. Other compounds such as alcohol ethoxylates, alkylphenyl ethoxylates, alkylbenzene sulfonates, fatty acid- and fatty ester-PEG were also identified.

The identification of linear PEG, PPG and star-shaped PEG was achieved by LCCC coupled to MS in the positive mode and  $^1\text{H}$  NMR. Linear PEG was identified in most additives with average molar masses ranging from 370 to 546 g/mol at 8 to 12 EO repeat units. Glycerol ethoxylate, which is a three-arm star-shaped PEG, was detected in two of the additives at an average molar mass of 400

## Chapter 5: Summary, conclusions and recommendations

g/mol and seven EO repeat units while PPG ( $M_p$  600 g/mol,  $n = 10$ ) was observed in one of the additives.

LC-MS in the negative mode and  $^1\text{H}$  NMR were the suitable techniques for the identification of alkyl glucosides and oligoglucosides in two additives. In this mode, the fragmentation of glucose was observed and oligoglucoside was subjected to the cross-ring and glycosidic bond cleavages. The glucose-based additives were made up of ethyl-, octyl-, and decyl glucosides while oligoglucosides of up to four glucose units were also identified.

The combination of LCCC and solvent gradient elution with UV, ELS and MS detectors enhanced the elution of the wetting and dispersing agents. These additives consisted of mixtures of anionic, non-ionic and zwitterionic components with polymer chain lengths of up to  $C_{18}$ . LCCC demonstrated the separation of polymers due to differences in polarity, hydrophobicity, and length of the polymer chain. This was observed in additives that consisted of alkylphenyl ethoxylates, fatty acid-PEG, fatty ester-PEG and fatty alcohol ethoxylate components. In alkylphenyl ethoxylates, the octyl- ( $C_8$ ), nonyl- ( $C_9$ ) and decylphenyl ( $C_{10}$ ) products were clearly separated and identified by LC-MS. The presence of branched isomers in alkylphenyl hydrocarbon chain was confirmed by  $^1\text{H}$  NMR. The fatty acid-based polymers contained mixtures of saturated and unsaturated fatty acid end groups with chain lengths of  $C_8$ ,  $C_9$ ,  $C_{10}$  and  $C_{18}$ . Solvent gradient elution was required for the identification of the  $C_{18}$  components while FTIR-ATR and pyrolysis GC-MS were used to confirm these types of end groups. One of the additives showed evidence of the presence of mixtures of mono- and diester components which is a phenomenon commonly associated with these types of polymers.

Different types of fatty alcohol ethoxylates were identified in some additives by liquid chromatography using a gradient elution protocol. The presence of saturated and unsaturated alkylether ethoxylates with chain lengths of  $C_{12}$  to  $C_{18}$  was confirmed by LC-MS,  $^1\text{H}$ , and  $^{13}\text{C}$  NMR. Evidence of either the sulphated or phosphated species was also obtained.

LC-MS analyses in the positive and negative scan modes as well as FTIR-ATR showed evidence of zwitterionic end groups in some additives. This behaviour is indicative of compounds bearing both a positive and negative charge on the same molecule. The nitrogen atom of the tertiary amine or amide was confirmed as the source of the positive charge while the negative charge was due to a

## Chapter 5: Summary, conclusions and recommendations

carboxyl or sulphate groups. These types of end groups have been reported in literature as excellent anchoring moieties for organic and inorganic pigments.

The non-polymeric components in two of the additives were based on alkylbenzene sulfonate with a mixture of linear and branched isomers. In both additives, LC-MS (negative mode) confirmed decylbenzene sulfonate as the most abundant oligomer while  $^1\text{H}$  NMR showed isopropyl amine as a neutralizing agent.

The incorporation of the different types of additives in multi-component colourant formulations followed by extraction (centrifugation) and separation by LCCC was achieved. The identification of the extracted additives by LC-MS was also successfully achieved. The additives incorporated in colourants could be traced to the original formulation and the chemical structures of the extracted versus pure additives was matched.

Overall, the combination of LCCC, solvent gradient, LC-MS and NMR are powerful techniques for the separation and identification of the number and type of end groups in PEG-based additives. Moreover, additional techniques such as FTIR-ATR and pyrolysis GC-MS can be used to fully characterize the components of commercial additives that are used in colourants.

### 5.3. Recommendations for future work

The recommendations for future work are as follows:

The ionizability of various components of the additives may be evaluated by using other ionizing agents such as ammonium acetate, formic acid etc. This can assist in evaluating the response of the non-ionizable and non-detectable components in additive blends.

Liquid chromatography with fraction collection followed by NMR analyses is required for the characterization of the unidentified components.

## Chapter 5: Summary, conclusions and recommendations

This research has identified the behaviour of zwitterionic surfactants in LC-MS analyses. The analysis of standard solutions of tertiary amines, amides or amine oxide-based polymers at various pH ranges may assist in understanding and characterizing these polymers in solutions.

The additives' technology is always changing and manufacturers always find more innovative and improved surfactant systems. The additives based on PEG and PPG block copolymers are popular in the additives industry. By performing continuous method developments for the identification and characterization of commercial additives from various manufacturers, other types of block copolymer technologies may be identified.

Quantification can be performed to determine the purity or the concentration of each of the components of various additives.

In colourant formulations, additives of certain chemical functionality at a certain concentration are required to provide specific properties. The method developed in this research can be used for the analysis of more commercial additives. In doing so, various additive blends of various chemical compositions can be incorporated in colourants to evaluate the optimum blend for the best performance. This can assist formulators with improved product developments and cost reductions.